K. Aydin[1]
C. Cokluk[1]
E. Kuruoglu[1]
S. Gelmez[2]
B. Diren[2]
C. Rakunt[1]
F. Çelik[1]

Using the Magnetic Resonance Three-Dimensional Volume Rendering for Tissues Technique in the Planning of Craniotomy Flaps with Linear Scalp Incision

Original Article

Abstract

Preoperative three-dimensional images with surface venous anatomy may be used in the planning of a linear scalp incision and the opening site of the dura mater for protection of surface veins during surgical dissection, and to find the splitting site of the brain according to the lesion. In 45 patients who had a brain tumor, linear scalp incision planning was done by regarding the three-dimensional images derived from post-contrast time-of-flight (TOF) sequence raw data. The findings of correspondence and the quality of routine contrast-enhanced magnetic resonance imaging (MRI) and three-dimensional volume rendering for tissues (VRT) images were analyzed separately with the surgical findings according to a visual grading system. Our experience revealed that the surgical findings correlated well with the three-dimensional VRT images. According to a visual surgical grading system, a grade III correlation was found in 20 (45 %), grade II in 15 (33 %), grade I in 7 (15 %), and grade 0 in 3 (7 %) patients in our study population. At the end of our research we conclude that this method is useful in terms of the preoperative determination of brain surface anatomy and may be used in the determination of the site of a linear scalp incision according to the localization of an intracranial lesion.

Key words

Three-dimensional images · venous anatomy · post-contrast time-of-flight (TOF) sequence data · linear scalp incision · intracranial lesion

Introduction

Recent developments in MRI and post-processing techniques permit the direct and non-invasive depiction of superficial structures of the brain. At the same time, they allow the visualization of pathologic tissues and their relationship with nearby neurovascular structures. There are so many imaging methods that have been presented in the literature to identify cerebral surface anatomy in relation to intracranial lesions in patients who have intracranial tumors [1, 2].

In routine practice, cortical and vascular imaging is performed by specific sequences based on TOF or phase-contrast (PC) techniques [3–8]. Imaging techniques after contrast medium administration have been tried for a better visualization of cortical and vascular tissues [3, 4, 7, 8]. The present study was carried out in order to apply a contrast-enhanced imaging technique and a new post-processing algorithm, namely, the VRT technique for demonstrating cortical and venous structures together with a better depiction of tumor tissue and its relationships.

These images may be used in preoperative planning of a linear scalp incision and the craniotomy location. In this study, we describe our experience with this technique, and assess the correlation of the data obtained from this technique with the surgical observations in 45 patients.

Affiliation
[1]Department of Neurosurgery, Medical Faculty, Ondokuzmayıs University, Samsun, Turkey
[2]Department of Radiology, Medical Faculty, Ondokuzmayıs University, Samsun, Turkey

Correspondence
Kerametti̇n Aydin, M.D. · Department of Neurosurgery · Medical Faculty · Ondokuzmayıs University · 55139 Samsun · Turkey · Tel.: + 90/362/312/19 19/36 52 int · Fax: + 90/362/457/60 41 · E-mail: kaydin@omu.edu.tr

Bibliography
Minim Invas Neurosurg 2006; 49: 189–193 © Georg Thieme Verlag KG · Stuttgart · New York
DOI 10.1055/s-2006-948300
ISSN 0946-7211

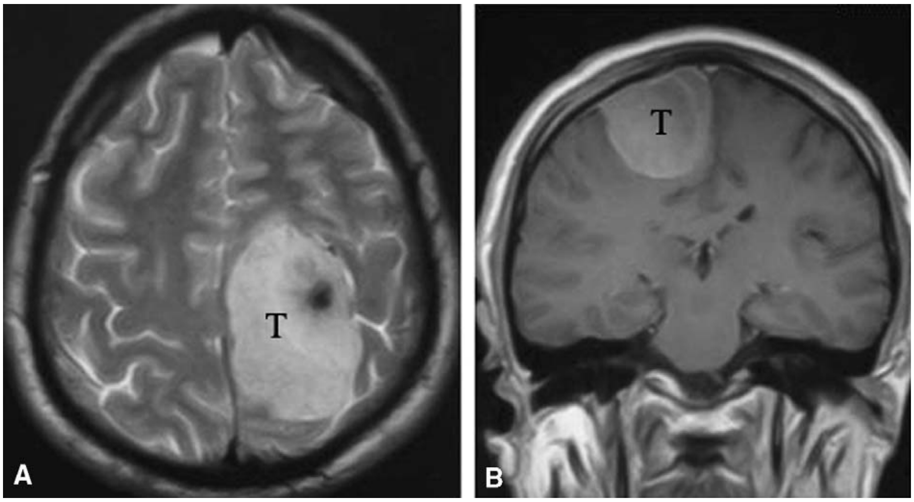

Fig. 1 **A** T_2-weighted axial, and **B** T_1-weighted with contrast coronal images. T = tumor.

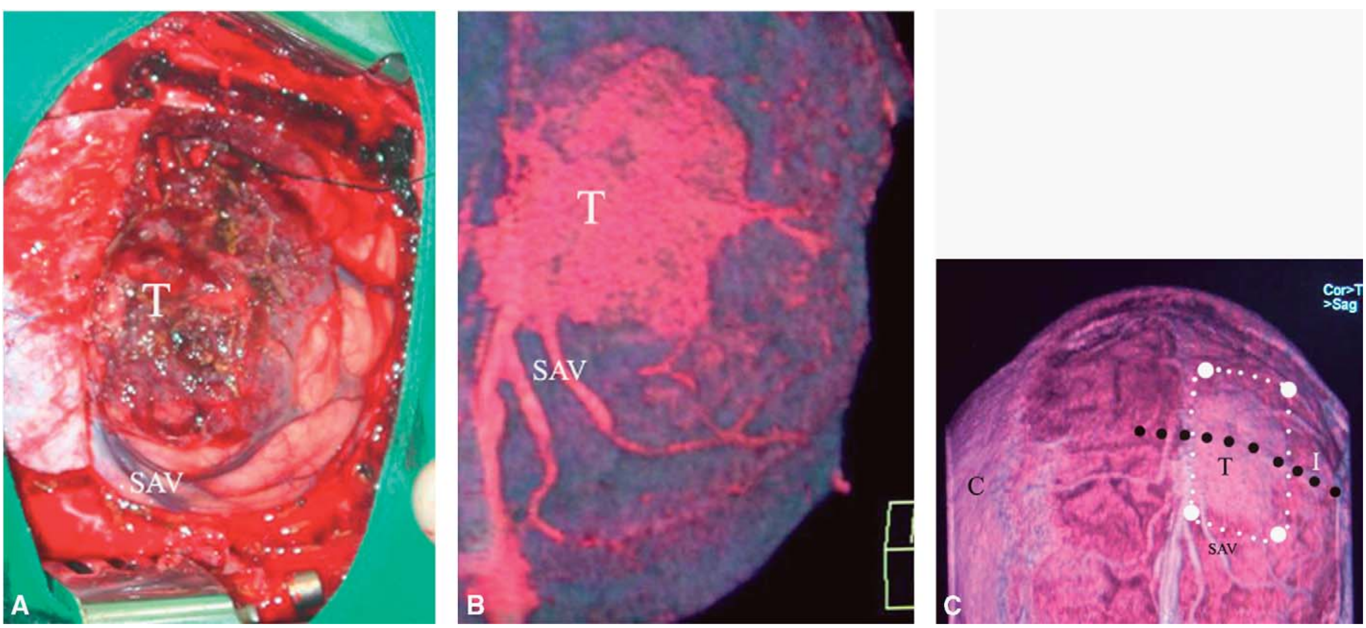

Fig. 2 **A** and **B** Tumor tissue and its relationship with nearby cortical and vascular structures were well demonstrated by three-dimensional imaging techniques and surgical observation. T = tumor, SAV = superior anastomotic vein. **C** The incision site was marked at the workstation. C = calvarium, T = tumor, I = incision site.

Materials and Method

This study included 45 patients (aged between 26 and 76 years) who had suffered from a cortical or a subcortical brain tumor between 2002 and 2004. Before operation, all patients underwent standard MRI examinations (T_1-weighted with contrast and non-contrast axial, coronal, sagittal, and T_2-weighted axial, coronal, and sagittal images) (Figs. **1** and **3**).

Imaging technique

We performed VRT-based, three-dimensional imaging from suitable raw data. After injection of 0.1 mmol/kg contrast material (Magnevist, 0.5 mmol/mL, Schering, Germany) we planned flash-three-dimensional TOF sequences (TR/TE: 36/4. 6 FA: 25 slice thickness: 1.5 mm interval: 0 mm; matrix: 256 × 384; field of view [FOV]: 150 × 200 cm; number of slabs: 4 partition: 64) in a 1.5 Tesla active super-conducting magnet system (Magnetom Symphony-Quantum, Siemens, Erlangen, Germany).

The FOV was planned to include the brain, calvarium and extracranial soft tissues in axial, coronal and sagittal planes in all patients. We use this sequence primarily as an intracranial imaging method with no contrast for venous or arterial angiography in routine practice. The mean acquisition time was about 7 minutes. After scanning, all raw data were transferred to the workstation (LEONARDO, the syngo post-processing unit, Erlangen, Siemens). Firstly, three-dimensional images were produced in the unit by using surface-shaded display (SSD). After manual removal of extracerebral tissues on three-dimensional SSD images by the crop technique provided by the software, maximum intensity projection (MIP) and VRT techniques were applied on the imaged data. The reconstructions were interactively

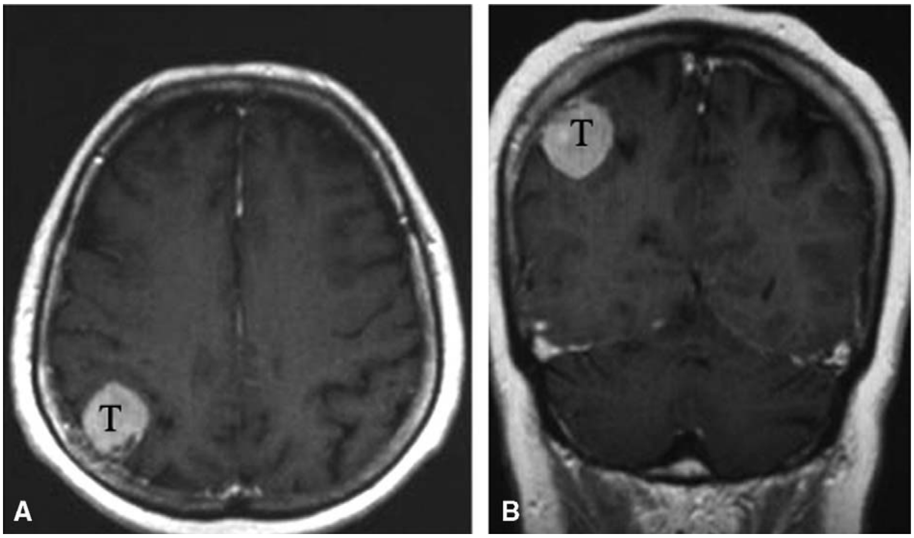

Fig. 3 **A** T_1-weighted with contrast axial, and **B** T_1-weighted coronal images. T = tumor.

Table **1** Grading of the correlation between three-dimensional VRT images and surgical observation

Grades	*Description*
Grade 0	There is no correlation between three-dimensional VRT images and surgical observation.
Grade I	There is some correlation between three-dimensional VRT images and surgical observation, but this correlation is not optimal with respect to the cortical venous system, gyral, sulcal and fissure formation, and tumor morphology and relationships with nearby cortical and venous structures.
Grade II	Although the correlation between three-dimensional VRT images and surgical observation is optimal in the aspect of lesion location on the brain surface, there is no complete correlation regarding cortical venous structures, gyral, sulcal and fissure formation.
Grade III	There is a complete correlation between three-dimensional VRT images and surgical observation.

Table **2** Summary of results with respect to the correlation between three-dimensional VRT images and surgical observation

Grades	*Results*	
	N	*%*
Grade 0	3	7
Grade I	7	15
Grade II	15	33
Grade III	20	45
Total	45	100

post-processed at the workstation and could be viewed from any chosen angle (Figs. **2, 4** and **5**).

All data derived from preoperative routine MRI with contrast and three-dimensional images were analyzed regarding the depiction of the cortical venous system, cortical formation, tumor morphology and tumor relationships with nearby cortical and venous structures.

We used a grading system for assessment of the correlation of the data obtained from this technique with the surgical observations. According to this system results were divided into four grades. These grades are shown in Table **1**. Student's t test was used for statistical analysis.

Results

Forty-five patients with intracranial tumors (twenty-five females and 20 males, aged between 26 and 76 years) were operated between 2002 and 2004 after the performance of the three-dimensional VRT imaging technique. All tumors were located in cortical and subcortical regions of the brain. Twenty of them were meningiomas (45 %), 15 (33 %) were metastasis, and the remainder (22 %) were primary glial tumors.

Tumor tissue and its relationship with nearby cortical and vascular structures were well demonstrated by three-dimensional imaging techniques in all patients.

Grade III correlations were found in 20 (45 %), grade II in 15 (33 %), grade I in 7 (15 %), and grade 0 in 3 (7 %) patients in our study population. Table **2** shows a summary of the results with respect to the correlation between three-dimensional VRT images and surgical observations.

We regarded grade 0 and I correlations as poor, and grade II and III correlations as good results. Good results were clearly better than poor results. The differences between poor and good results were statistically significant ($p < 0.001$).

Discussion

The relationship of tumor tissue with nearby normal cortical and vascular tissues is an important factor in the planning of a surgical intervention. Cortical venous structures, for example,

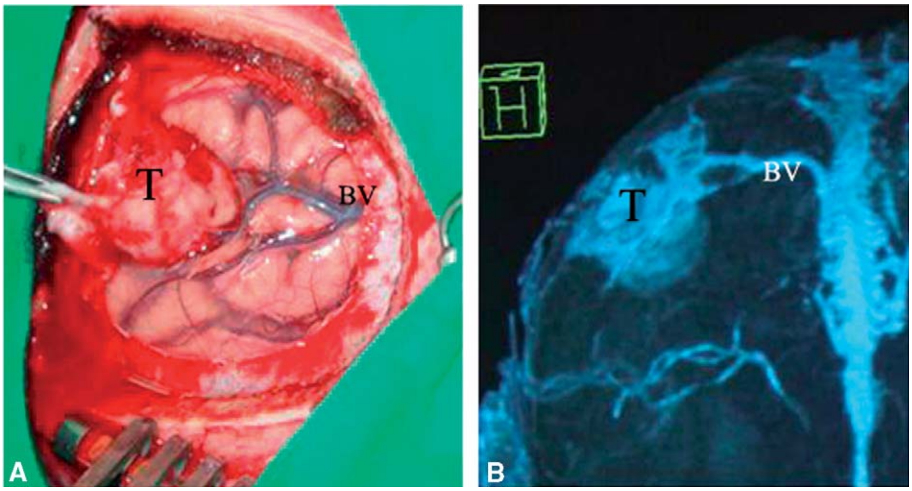

Fig. 4 **A** and **B** Tumor tissue and its relationship with nearby cortical and vascular structures were well demonstrated by three-dimensional imaging techniques and surgical observation. T = tumor, BV = bridging vein.

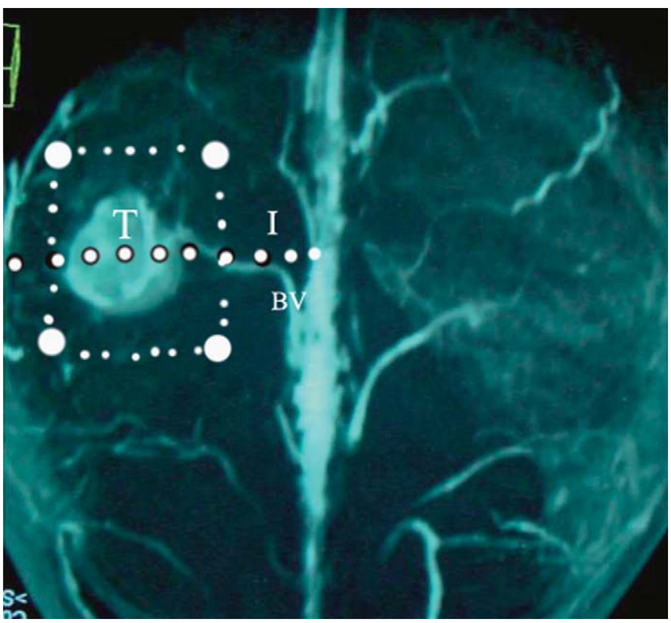

Fig. 5 The incision site of some case in Fig. **4** was marked at workstation. T = tumor, BV = bridging vein, I = incision site.

should be protected as much as possible during the surgical intervention for the complete removal of a brain lesion to avoid a devastating complication. Before starting a surgical intervention, knowledge about the location and the relationship of these structures to brain lesions not only may enhance the orientation of a surgeon to a surgical field but also may facilitate the planning of a proper linear scalp incision and a small but sufficiently large craniotomy as far distant as possible from venous structures.

In this study, we mainly hypothesized that three-dimensional VRT images may show the relationship between tumors and brain structures such as the cortical venous system, gyral, sulcal and fissure formation, and tumor morphology. This knowledge may enhance surgical orientation to a lesion seated in the brain. Three-dimensional images showing gyri, sulci, fissures and cortical venous structures may make it easier to approach the lesion and at the same time can prevent possible cortical venous damage [1,2].

The T_1 shortening effect of a contrast agent reduces the effect of spin saturation, and also compensates slow flow and in-plane flow, which is typical in the distal branch of intracranial vessels, resulting in better visualization of cortical venous structures. In this way, both decreasing the flip angle and decreasing TR levels are possible. Contrast-enhanced magnetic resonance angiography (MRA) can be useful in evaluating intracranial vascular lesions, particularly those with slow flow [7,8]. There are some studies in which phase contrast angiography sequences have been used for the depiction of intracranial vascular structures in the literature [1,3,5].

VRT, which was the primary post-processing technique, used for three-dimensional imaging in this study is a relatively new technique. Its algorithm is more complex than the other techniques and it requires expensive computation techniques and software. In this technique, all voxels in the volume are analyzed under four subgroups.

It includes all of the relevant data into the final three-dimensional image and overcomes many of the problems seen with MIP and SSD. Accordingly signal intensity levels, which have different colors and transparency, can be applied to different volumes. By using this technique one or more volumes can be made invisible to demonstrate underlying structures. The relationship of a volume with other structures can be imaged and demonstrated. This is a routine and widely using technique like SSD and MIP, which produces images by the use of preselected volumes. The primary reasons for using of volume rendering over MIP and SSD are the improvements of image accuracy and quality [9,10].

In 78 % of the cases, the correlation between software images and direct surgical observation was satisfactorily sufficient. Among these cases, 45 % of them were grouped into a grade III correlation. In this group, we found that the correlation between software images and surgical observation was excellent.

In 22 % of the cases, the correlation between images and direct observation was insufficient. Among these cases, 15 % of them showed some correlation between three-dimensional VRT images and surgical observation, but this correlation is not optimal with respect to the cortical venous system, gyral, sulcal and fissure formation, and tumor morphology and relationships with nearby cortical and venous structures. In 7 % of the cases (3 patients), the correlation was poor and insufficient. But in comparison with routine MRI, these data may give some information about the lesion to enhance the orientation of a surgeon to the surgical field.

Conclusion

Three-dimensional image generating software programs are useful in the demonstration of cortical and subcortical lesions and their anatomical relationship with nearby venous structures, gyri, sulci, and fissures formation. These data may be used to localize a linear skin incision on the scalp surface in accordance to the location of the lesion. At the same time, a small but sufficiently large craniotomy may be done on the cranium in accord with the lesion and perilesional structures such as drainage veins and sulci. These computer-generated software images may enhance the surgical orientation to a surgical field, and may also facilitate the protection of venous vessels nearby a lesion. This imaging technique may be useful in surgical interventions for cortical and subcortical brain tumors.

References

1 Tsuchiya K, Katase S, Hachiya J, Hiyama T, Shiokawa Y. A new technique of surface anatomy MR scanning of the brain: its application to scalp incision planning. AJNR Am J Neuroradiol 1999; 20: 515–518

2 Katada K. MR imaging of brain surface structures: surface anatomy scanning (SAS). Neuroradiology 1990; 32: 439–448

3 Liang L, Korogi Y, Sugahara T, Onomichi M, Shigematsu Y, Yang D, Kitajima M, Hiai Y, Takahashi M. Evaluation of the intracranial dural sinuses with a 3D contrast-enhanced MP-RAGE sequence: prospective comparison with 2D-TOF MR venography and digital subtraction angiography. AJNR Am J Neuroradiol 2001; 22: 481–492

4 Kirchhof K, Welzel T, Jansen O, Sartor K. More reliable noninvasive visualization of the cerebral veins and dural sinuses: comparison of three MR angiographic techniques. Radiology 2002; 224: 804–810

5 Liauw L, van Buchem MA, Spilt A, de Bruïne FT, van den Berg R, Hermans J, Wasser MNJM. MR angiography of the intracranial venous system. Radiology 2000; 214: 678–682

6 Lewin JS, Laub G. Intracranial MR angiography: a direct comparison of three time-of-flight techniques. AJNR Am J Neuroradiol 1991; 12: 1133–1139

7 Yang J, Hill M, Morrish W, Hudon M, Barber P, Demchuk A, Sevick R, Frayne R. Comparison of pre- and postcontrast 3D time-of-flight MR angiography for the evaluation of distal intracranial branch occlusions in acute ischemic stroke. AJNR Am J Neuroradiol 2002; 23: 557–567

8 Jung HW, Chang KH, Choi DS, Han MH, Han MC. Contrast-enhanced MR angiography for the diagnosis of intracranial vascular disease: optimal dose of gadopentetate dimeglumine. AJR Am J Roentgenol 1995; 165: 1251–1255

9 Karamessini M, Kagadis GC, Petsas T, Karnabatidis D, Konstantinou D, Sakellaropoulos GC, Nikiforidis GC, Siablis D. CT angiography with three-dimensional techniques for the early diagnosis of intracranial aneurysms. Comparison with intra-arterial DSA and the surgical findings. Eur J Radiol 2004; 49: 212–223

10 Uchida M, Ishibashi M, Abe T, Nishimura H, Hayabuchi N. Three-dimensional imaging of liver tumors using helical CT during intravenous injection of contrast medium. J Comput Assist Tomogr 1999; 23: 435–440

Endoscopic Management of Thalamic Gliomas

S. Selvapandian

Original Article

Abstract

The management of thalamic gliomas is extremely variable, ranging from radical excision in some cases to more conservative therapy such as a biopsy and radiation. There is a high incidence of associated hydrocephalus. The principles of management are, therefore, histological diagnosis, CSF diversion and adjuvant therapy. Endoscopy appears to offer a new approach to achieve histology and CSF diversion. The various goals achieved with the use of endoscopy in the management of 4 patients with thalamic gliomas are described. With the endoscope we achieved histological diagnoses and CSF diversion was facilitated in all these cases. There were no complications. The advantages of endoscopy in the management of thalamic masses are discussed. Endoscopic intervention appears to offer a modular approach to these lesions.

Key words

Glioma · thalamic · endoscope · CSF diversion

Introduction

The management of thalamic gliomas is constantly evolving. It ranges from empirical radiotherapy to open microsurgical excision [1–3]. Associated hydrocephalus is managed with CSF diversion. Endoscopic interventions can achieve all the necessary objectives, such as tissue diagnosis and CSF diversion. We present our experience with four such patients.

Case Reports

Case 1

A 46-year-old woman presented with chronic, non-specific headache with recent increases in severity. On examination she was alert, oriented, had papilloedema and right-sided pyramidal signs. A CT scan of the brain revealed a predominantly hypodense left thalamic mass with variegated contrast enhancement. There was dilatation of the anterior third and lateral ventricles (Fig. **1**). Through a right frontal burr hole a third ventriculostomy was done, later the bulging thalamic mass was biopsied. A septostomy was done to tackle the potential lateral ventricular dilatation due to the deformed left foramen of Monro. Biopsy revealed a low-grade glioma.

Case 2

A 19-year-old woman presented with symptoms of raised ICP of recent onset. On examination, she was alert, oriented, had papilloedema and bilateral abducens palsy. CT and MR scans of the brain revealed an anterior thalamic mass on the left side. The left lateral ventricle was dilated with the septum deviated to the right. The third ventricle was normal (Fig. **2**). Through a left frontal burr hole, a septostomy was done and later the anterior thalamic mass was biopsied uneventfully. The histopathological examination revealed a low-grade glioma.

Case 3

A 33-year-old man presented with features of abnormal behavior and urinary incontinence of short duration. On examination his GCS was 14/15, he had no focal neurological deficits. A CT scan of his brain revealed a left caudate mass with lateral ventricular

Affiliation
Department of Neurological Sciences, Christian Medical College and Hospital, Vellore, TamilNadu, India

Correspondence
Dr. S. Selvapandian, MCh · Department of Neurological Sciences · Christian Medical College and Hospital · Ida Scudder Road · Vellore–632 004 · TamilNadu · India · Tel.: +91/416/228/43 52 · Fax: +91/416/223/20 35, 223/21 03 · E-mail: sselvapandian@gmail.com

Bibliography
Minim Invas Neurosurg 2006; 49: 194–196 © Georg Thieme Verlag KG · Stuttgart · New York
DOI 10.1055/s-2006-948303
ISSN 0946-7211

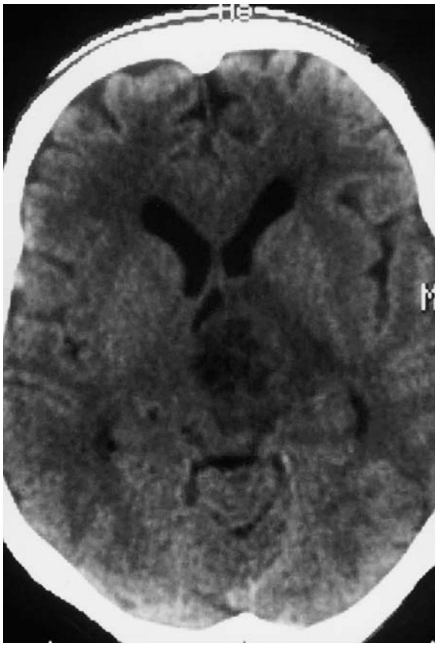

Fig. **1** CT scan of the brain revealing a variegated mass involving the left thalamus. The posterior half of the third ventricle is occluded.

Fig. **2** Contrast-enhanced MRI of the brain revealing an anterior thalamic mass on the left side. The left lateral ventricle is dilated with the septum pellucidum deviated to the right. The third ventricle appears normal.

Fig. **3** Operative photograph showing the left foramen of Monro, the bulging right thalamic mass can be seen. In the depth, the floor of the third ventricle following ventriculostomy.

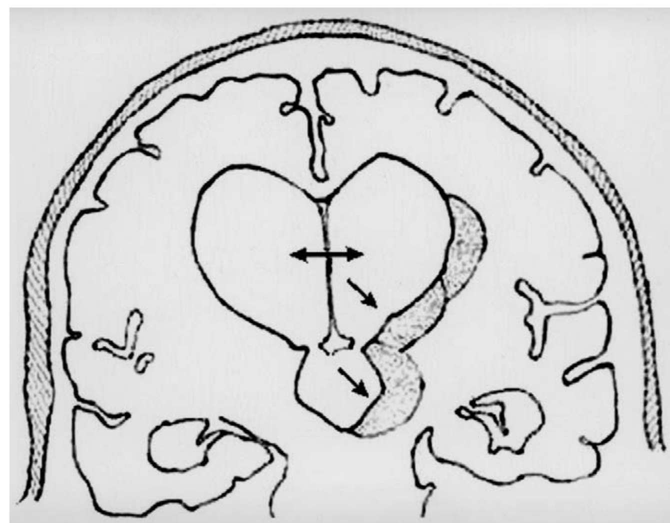

Fig. **4** Coronal section of the brain with arrows indicating the potential sites for biopsy and septostomy.

dilatation. Through a left frontal burr hole approach a third ventriculostomy was done. Later the mass was biopsied followed by a septostomy. The histopathological examination revealed a low-grade glioma of the gemistocytic type.

Case 4

An 11-year-old boy presented with features of raised intracranial pressure. Clinically he had bilateral papilloedema and bilateral lateral rectus paresis. A CT scan of his brain showed an ill-defined mass lesion in the right thalamus with variegated enhancement. The lateral and the anterior third ventricles were dilated. Through a left frontal burr hole a third ventriculostomy, a biopsy of the mass and a septostomy were done (Fig. **3**). Histopathology was reported as an anaplastic astrocytoma.

Discussion

Thalamic gliomas constitute 1–5 % of all intracranial tumors [1]. The incidence is higher in the first two decades of life. Management varies from radiotherapy or chemotherapy with or without histological diagnosis to radical excision. Obstructive hydrocephalus is a common accompanying feature by virtue of the location of these tumors and is usually managed with CSF diversion [4]. Histology determines the type of radiotherapy and the prognosis [1]. Neuroendoscopy offers new modes of achieving the treatment goals, namely histological diagnosis and CSF diversion [5–7]. Stereotaxy was preferred in view of its minimal invasiveness and short procedure. When coupled with CSF diversion this amounts to two independent surgical procedures with their attendant risks. The role of VP shunt and the problems associated with it are well known. Open surgical excision, on the other hand, has been attempted since the early days, and later with technological advances although their role in the final outcome is not yet clear [2, 3].

Third ventriculostomy is a common endoscopic procedure with a high patency rate in obstructive hydrocephalus. The anatomy of the third ventricle is familiar to most endoscopists and, therefore, a biopsy of a mass bulging into it should pose no major hurdle. The neuroendoscope seems to combine the advantages of minimal invasiveness, visualization and importantly of providing real-time guidance to facilitate adjustments if necessary. In our series, the lesions have involved the anterior thalamus, bulged either into the lateral or the third ventricle and hence could be reached with the standard rigid endoscope and the procedure could be tailored according to the need. Third ventriculostomy was done only in cases with obstructive hydrocephalus. The location of these tumors seems to favor foramen of Monro blockage and a septostomy was essential to avoid bilateral shunts (Fig. **4**). The therapeutic flexibility is in our opinion the major advantage of endoscopy. With endoscopy we could achieve all the objectives, that of tissue diagnosis and CSF diversion in a single, short procedure.

References

1 Beks JWF, Bouma OJ, Journee HL. Tumors of the thalamic region. A retrospective study of 27 cases. Acta Neurochir (Wien) 1987; 85: 125–127

2 Kelly PJ, Kall BA, Goerss SJ. Special stereotactic techniques: stereotactic laser resection of deep-seated tumors. In: Heilbrun MP (ed). Concepts in Neurosurgery – Stereotactic Neurosurgery, Vol: 2. Philadephia, Williams & Wilkins, 1988; 239

3 Prakash B. Surgical approach to large thalamic gliomas. Acta Neurochirurgica 1985; 74: 100–104

4 Goel A. Pre-operative shunts in thalamic tumors. Neurol India 2000; 48: 347–350

5 MacArthur DC, Buxton N, Punt J, Vloeberghs, Robertson IJA. The role of neuroendoscopy in the management of brain tumors. Br J Neurosurg 2002; 16: 465–470

6 Gabb MR, Schroeder HWS. Neuroendoscopic approach to intraventricular lesions. Neurosurgery Focus 1999; 6, Article 5

7 Yurtseven T, Ersahin Y, Demirtas E, Mutluer S. Neuroendoscopic biopsy for intraventricular tumors. Minim Invas Neurosurg 2003; 46: 293–299

D. Lindner[1,5]
C. Trantakis[1,5]
C. Renner[1]
S. Arnold[3]
A. Schmitgen[4]
J. Schneider[2]
J. Meixensberger[1,5]

Application of Intraoperative 3D Ultrasound During Navigated Tumor Resection

Abstract

Intraoperative 3D ultrasound (3D-iUS) may enhance the quality of neuronavigation by adding information about brain shift and tumor remnants. The aim of our study was to prove the concept of 3D ultrasound on the basis of technical and human effects. A 3D-ultrasound navigation system consisting of a standard personal computer containing a video grabber card in combination with an optical tracking system (NDI Polaris) and a standard ultrasound device (Siemens Omnia) with a 7.5 MHz probe was used. 3D-iUS datasets were acquired after craniotomy, at different subsequent times of the procedure and overlaid with preoperative MRI. All patients underwent early postoperative 3D MRI including contrast agent within 24 hours after surgery. Acquisition of 3D iUS and the fusion with preoperative MRI was successful in 22/23 patients. The expenditure of time was at least 5 minutes for one intraoperative 3D US dataset. The technique was used three to seven times during surgery. The quality of the ultrasound images was superior in cases of metastasis, meningeoma and angioma over those in malignant glioma. Brain shifting ranged from 2–25 mm depending on localization and kind of tumor. A resection control was possible in 78 %. All six neurosurgeons demonstrated a learning curve. The introduction of 3D ultrasound has increased the value of neuronavigation substantially, making it possible to update several times during surgery and minimize the problem of brain shift. Configuration of both the 3D iUS based on a standard ultrasound system and the MR navigation system is time- and especially cost-effective. Faster navigational datasets and more intuitive image-guided surgery enable novel and user-friendly display techniques.

Key words

Neuronavigation · intraoperative ultrasound · tumor resection · brain shift

Introduction

Intraoperative imaging is beneficial for intraoperative orientation, reducing the extent of craniotomy, aiding the detection of brain shift and for resection control [1–4]. Tumor as well as tumor remnants and normal brain structures can be visualized during a surgical procedure with high sensitivity [5]. Intraoperative 3D-US, iMRI and iCT are established techniques for intraoperative navigation [6–8]. The 3D reconstruction of the iUS information and the transmission into the surgical situation is necessary to identify a target and localize it within the operation field. A combination of preoperative MRI with intraoperative 3D ultrasound (3D-iUS) may enhance the convenience of neuronavigation by adding intraoperative information. Limitations could be the required time for intraoperative data transfer, a possibly lower quality of resliced planes from 3D-ultrasound datasets compared to the conventional 2D mode and the higher costs for a special configurated navigation system [9,10]. In our

Affiliation
[1]Klinik für Neurochirurgie, Universität Leipzig, Leipzig, Germany
[2]Klinik für Diagnostische Radiologie, Universität Leipzig, Leipzig, Germany
[3]Fraunhofer Institut für Angewandte Informationstechnik FIT, St. Augustin, Germany
[4]Localite, Bonn, Germany
[5]Innovations Centrum Computer Assistierte Chirurgie ICCAS, Leipzig, Germany

Correspondence
Dr. med. Dirk Lindner · Department of Neurosurgery · University of Leipzig · Liebigstraße 20 · 04103 Leipzig · Germany · Tel.: + 49/341/971 75 00 · Fax: + 49/341/971 75 09 · E-mail: dlind@medizin.uni-leipzig.de

Bibliography
Minim Invas Neurosurg 2006; 49: 197–202 © Georg Thieme Verlag KG · Stuttgart · New York
DOI 10.1055/s-2006-947997
ISSN 0946-7211

previous paper [11] we demonstrated the development of a new 3D-ultrasound navigation system based on acquired preoperative MRI and iterative intraoperative ultrasound datasets. The application of such a workstation is not only complicated by technical facts. In addition, the intraoperative handling of 3D-iUS and the acceptance by different neurosurgeons both have an impact on the surgical results [3,12]. The aim of our study was to prove the concept of 3D ultrasound with regard to technical effects and human impact [13]. This includes measurement of fusion accuracy, the extent of tumor resection and the suitability for detection and capture of intraoperative brain shift as well as a protocol of operative handling as described by different neurosurgeons.

Patients and Methods

Between May and December 2004, 23 patients were included in the study. Selection criteria were created on the basis of size and location of the cranial tumor. All patients were informed regarding the methodology and agreed to participate in the study. The ethics commission approved our operative protocol.

The lesions exhibited a size from 1–7 cm and were mainly located in the deep-seated supratentoral region of the brain. Locations as well as size are shown in Table **1**.

In our standard protocol under navigational conditions, six different surgeons operated eight metastasis, six glioblastomas, three anaplastic gliomas, three meningeomas, one angioma, one lymphoma and one cyst from the arachnoids. For navigation support, a freehand 3D-ultrasound workstation was used consisting of a standard personal computer (Fujitsu-Siemens CPU Intel 4, 2.8 GHz) containing a video grabber card (nVIDIA GeForce4) in combination with an optical tracking system (NDI Polaris) and a standard ultrasound device (Siemens Omnia) with a standard phased array 7.5 MHz probe [14–16]. No other probe was used in order to compare operative results of different neurosurgeons. Preoperative 3D-MRI-dicom data were acquired with a 1.5 T Siemens scanner and transferred to the navigation workstation (Localite Navigator). MR images with one mm thickness ensured a high level of accuracy. A total of 250 T_1-weighted 3D-MR images per patient with contrast agent were obtained (FOV: 25 cm, matrix: 256 × 256, repetition time: 11.4 msec) for data processing. The area of contrast enhancement (including necrotic tissue) was defined as tumor and determined as volume in a summing of each slice. The registration was performed with skin fiducials. An active pointer and a passive tracker as reference (mounted on a Mayfield clamp) were also used. In addition, the ultrasound probe was tracked with an active tracker. The US phased-array probe was covered with sterile drapes filled with ultrasound gel. The surface of the probe was moistened to prove

Table **1** All kind of tumors displayed for size, brain shift, possibility to be visualized, resection control and intraoperative results in accordance with postoperative MRI. ‘‘yes’’ was defined as exact correlation (right-positive or false-negative) between the last iUS in comparison to postoperative MRI as gold standard for tumor remnants, ‘‘no’’ shows differences between last intraoperative iUS to postoperative MRI with respect to tumor remnants. In four cases a comparison was impossible for reasons of image quality and shift

*Sex**	*Age*	*Kind of tumor*	*Site*	*Shift iUS/MRI (maximal, mm)*	*Resection control/remnant*	*Correlation post-MRI*
1	70	Metastasis	temporal	8.5	good	yes
2	56	Metastasis	frontal	3.5	good	no
1	56	Metastasis	central	7.1	good	no
2	55	Metastasis	central	4.0	good	yes
2	45	Metastasis	central	10.0	good	yes
1	71	Metastasis	temporal	11.0	good	no
1	53	Metastasis	temporal	0.0	good	yes
1	76	Metastasis	frontal	2.0	good	yes
1	54	GBM IV	temporal	15.0	remnant	
1	47	GBM IV	frontal	10.0	remnant	
2	62	GBM IV	temporal	10.0	remnant	
1	48	GBM IV	frontal	2.0	good	no
2	72	GBM IV	frontal	1.0	good, remnant	yes
1	70	GBM IV	frontal	2.0	good	no
2	53	glioma III	temporal	0.0	good	yes
1	19	glioma III	frontal	0.0	good	yes
1	61	glioma III	frontal	0.0	good	yes
1	53	Meningeoma III	central	2.0	remnant	yes
1	69	Meningeoma II	temporal	2.0	good	yes
1	72	Meningeoma I	frontal	0.0	good	yes
2	73	Cyst	frontal	25.0	shift	
2	69	Lymphoma	temporal	2.0	good	yes

*1 = male, 2 = female; age in years.

Table **2** Intraoperative ultrasound performance, definition of ratings (note)

Note 1	Excellent performance, no problem, use of all techniques features
Note 2	Very good performance, visualization and matching with marginal problems
Note 3	Good performance, use of the main US features, interpretation with help possible
Note 4	Acceptable performance, stability problems, but use of 3D-iUS possible and helpful
Note 5	Negative performance, matching and/or stability problems, finish of operation without iUS

for an excellent contact milieu. Rendering images of known orientation in space into a volume could create 3D-iUS data [17–19]. The volume location was previously defined using the ultrasound probe as a pointer, so that the ultrasound imaging could be processed directly in different depths (6–12 cm) [20]. 3D ultrasound datasets were acquired after craniotomy, at different subsequent times of the procedure until the end of the operation and overlaid with preoperative MRI.

All patients underwent early postoperative 3D-MRI including contrast agent within 24 hours after surgery. The data acquisition was carried out in the T_1-weighted 2D spin echo technique and required only a few minutes. In accordance with the preoperative procedure, the postoperative imaging was performed as T_1-weighted scans with and without contrast agent to define tumor remnants. For better identification of tumor remnants, both identical slices were subtracted. Evaluations of complete and incomplete tumor removal were made by the radiologist and neurosurgeon independently and recorded in the protocol [21].

A standard protocol was prepared to describe the additional time using 3D-iUS, the conditional influence of operations and the practicability by the different surgeons. Quality of iUS as well as advantages and disadvantages of different ultrasound adjustments were investigated. Tumor volumes and remnants were analyzed by comparing pre- and postoperative MR images in relation to intraoperative 3D-iUS. Brainshift was measured as highest deviation for anatomic structures between preoperative MR images and iUS datasets. All surgeons gave a range from 1 (very good) to 5 (unsatisfactory) for the intraoperative ultrasound performance (Table **2**).

Results

In all cases except one the acquisition of 3D-iUS and the fusion with preoperative MRI was successful. In one case there was a mismatch of intraoperative 3D-iUS to preoperative T_1-weighted MRI caused by an unintended passive tracker movement during the operation procedure. The expenditure of time was 5 minutes for one 3D-iUS dataset and sets were obtained three to seven times during surgery. In all cases anatomic structures and regions of interest (ROI) could be identified. The quality of the ultrasound images was superior in cases of metastasis, meningeoma and angioma over those in cases of malignant glioma.

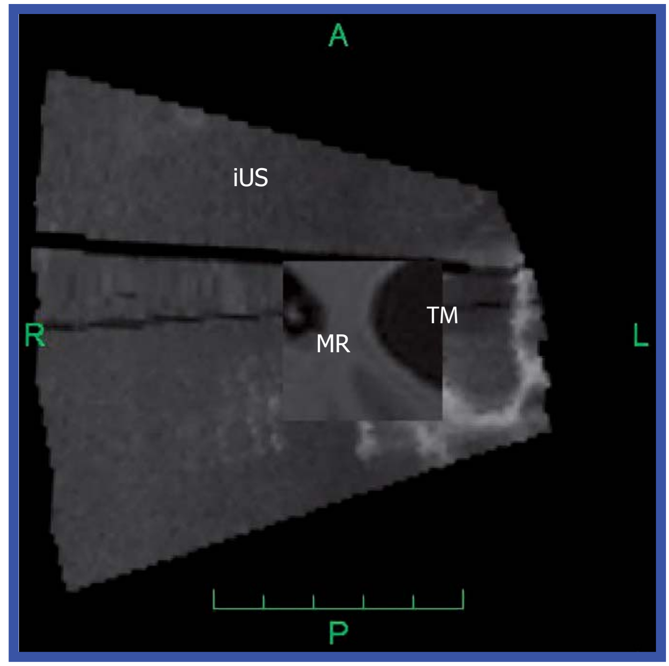

Fig. **1** Extracted slice of 3D-IUS matched with overlaid MRI to detect brain shift and anatomic structures, for example, cystic glioma.

Measurement of shifting was possible in each case. Brain shifting ranged from 2–25 mm with a mean of 5 mm depending on localization and kind of tumor. A rising shift of about 20 mm was detected in a cystic tumor after CSF leakage. Resection control was possible in only 78 % of all tumors. The reason for failed ultrasound visualization of tumor borders in 3 glioblastomas was the blur differentiation between tumor and edema, in the cystic process the shift during resection and the described case with technical problems.

Intraoperative 3D ultrasound discovered tumor remnants in 3 high-grade gliomas and one lymphoma with the consequence of gross total resection. There was no observed permanent neurological impairment after surgery. Finally a high correlation between postoperative MR images and 3D-iUS datasets was demonstrated in 14/22 cases (63.6 %, Table **1**).

Technical factors

The calibration of the US probe in a water-bath model with cross wires inside was done once offline before the operation started and took 2 hours. No special preparation was acquired for intraoperative ultrasound. The navigation scene (with skin fiducials) and the use of preoperative MRI were the same as known from typical neuronavigation. A video cable connects the US probe with the workstation. The first iUS dataset was recorded by a sweep before dura opening. By the movement of the tracked US probe over the operative site a quantity of at least 100 to 500 2D-iUS images created a 3D-iUS dataset. To compare this dataset with the preoperative MRI the new visual appraisal "Magic Lens" (Fig. **1**) was performed. The iUS data were overlaid to the MRI in all planes of the space within a few seconds. This technique allowed a brain shift analysis, differentiation of ROI and tumor, and avoided technical mistakes. For intraoperative orientation, the "Compare panel" feature was offered to compare 2D iUS, 3D-iUS,

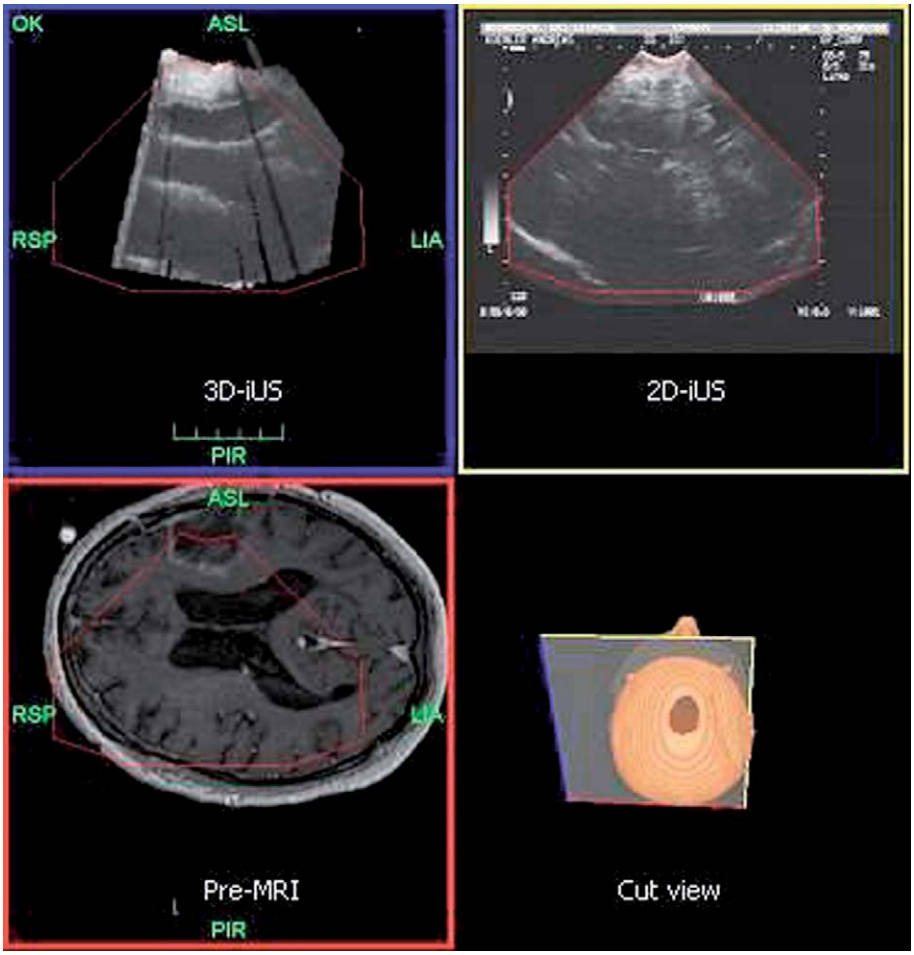

Fig. **2** Extract of 3D-iUS dataset (*left*), 2D-US (*right*) and preoperative MRI (*below*) of the same anatomical position in space comparing different image qualities.
The technique was defined as "Compare panel".

preoperative MRI and an orientated cut view in one plane (Fig. **2**). The "real-time" technique gave a nearly real-time visualization with different tracked devices. Tumor remnants, vessel structures and ROI were colored as well as borders to falx and skull base (Fig. **3**). In the course of the tumor resection the iUS was used up to seven times.

Human factor

All neurosurgeons accepted handling of the system but there was a different learning curve. Four neurosurgeons with only a basic knowledge about ultrasound applied the equipment after a short information in the correct way. But the transformation of ultrasound images in the actual operative situation was not easy and sometimes needed support. The quality rating system, based on experience during the operation procedure, was developed in our department.

The two ultrasound-experienced neurosurgeons improved the intraoperative technique, appraised all possibilities of the ultrasound equipment and assessed it with the note "1".

According to the expectations, the inexperienced neurosurgeons orientated their tumor resection control more on preoperative MR imaging than intraoperative 3D-IUS. They assessed the iUS adjustment with an average note of "3".

Discussion

An ideal navigation system allows the comparison between modified 2D ultrasound as a component of a 3D map with MRI images corresponding to the anatomy in different times [13, 22–25]. We solved the problem of shifting anatomy during operation by navigating with updated 3D-iUS. Even in cases of brain shift the surgeon can get a closer and more confident estimation of the tumor size within a renewed 3D-iUS dataset [17–19, 26, 27].

At least for a group of intracranial echogenic lesions like cysts, abscesses, metastases, meningeomas or solid high-grade gliomas the 3D-US navigation environment seems to be of equivalent usefulness to 3D iMRI datasets. The easy intraoperative repeatability of 3D-iUS offers a considerable benefit with respect to the brain shift problem. The acquisition and presentation of a 3D-iUS dataset requires about five minutes. Compared to a situation without any form of image-based navigational support even the exclusive 3D-iUS dataset alone is a valuable orientation [5, 14, 28]. We compare preoperative MRI and 3D-iUS in the beginning of the resection to detect anatomic homogeneity and inhomogeneity. If the tumor and the border to surrounding tissue could be easily identified, we preferred the use of 3D ultrasound alone. In cases of intracranial lesions that were scarcely visible in iUS images without differentiation of surrounding tissue, the surgeon had only an indirect benefit from the 3D-iUS navigation environment. If the tumor is visible in the MRI images and sur-

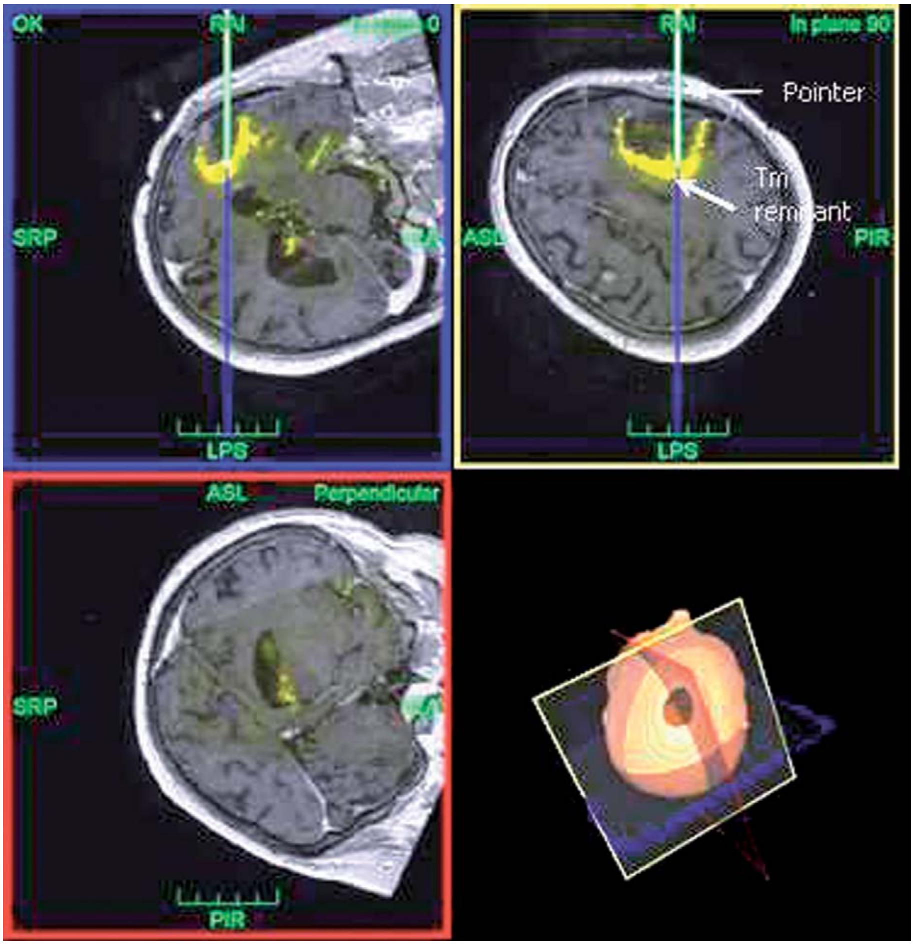

Fig. **3** Intraoperative 3D ultrasound matched with preoperative MRI dataset. Tumor remnants can be clearly identified in several planes (white arrow demonstrates the pointer orientation and direction) with the result of complete resection in this case of left frontolateral meningeoma (WHO III).

rounded by physiological structures that can be identified in both MRI and iUS, the target can be marked and mapped onto the US data set [12, 21, 29]. The Localite navigator worked in a reliable and safe manner. All visualization techniques offered additional information for the neurosurgeon.

The introduction of 3D ultrasound has increased the value of neuronavigation substantially, making it possible to update ultrasound-based navigation several times during surgery and minimize the problem of brain shift. Intraoperative imaging is not only useful for navigation purposes but can, of course, also deliver new information about the surgical process like identification and localization of residual tumor, thus providing enhanced information for the decision of further surgical steps [8, 9, 30].

Accurate fusion of MR images and intraoperatively acquired 3D-iUS was successful in all cases except one. Configuration of both the 3D-iUS based on a standard ultrasound system and the MR navigation system is time- and especially cost-effective. On the other hand the 3D-iUS demonstrated in only 63.6% a high accordance with the gold standard of postoperative MRI. One factor of intraoperative ultrasound is the poor differentiation of tumor remnants, surrounding tissue and edema, especially during progression of the operation procedure. Solutions could be the use of high-end ultrasound devices or the impact of ultrasound contrast agent [31]. In addition, most neurosurgeons are more familiar with MRI and CT than with ultrasound images although, in our study, there was a clear learning curve to interpret ultrasound images.

Tumor resection control was excellent in cases of metastasis, meningeomas and solid gliomas. The image quality of extracted slices in different planes is comparable to 2D images. The high repetition rate of 4 images/sec allows excellent hand-eye coordination. The time delay of about 5 minutes from the acquisition of the iUS data to the calculation of the 3D volume allows for a nearly unlimited updating during the surgical procedure. Novel and user-friendly display techniques will make it possible to perform faster and more intuitive image-guided surgery as compared with conventional neuronavigation systems and real-time 2D ultrasound [29, 32].

However, the unsolved issue of 3D-iUS is the sensitivity and specificity in detecting tumor tissue at the conclusion of the surgery. Further investigation will be needed to explore the scientifically proven value of ultrasound in neuronavigation.

Acknowledgements

The author received an advancement by BMBF and this study is now part of the BMBF project ICCAS in Leipzig. No benefits in any form have been received from a commercial party related directly or indirectly to the subject of the manuscript.

References

1 Bonsanto MM, Staubert A, Wirtz CR, Tronnier V, Kunze S. Initial experience with an ultrasound-integrated single-RACK neuronavigation system. Acta Neurochir (Wien) 2001; 143: 1127–1132
2 Dohrmann GJ, Rubin JM. History of intraoperative ultrasound in neurosurgery. Neurosurg Clin N Am 2001; 12: 155–166
3 Unsgaard G, Ommedal S, Muller T, Gronningsaeter A, Nagelhus Hernes TA. Neuronavigation by intraoperative three-dimensional ultrasound: initial experience during brain tumor resection. Neurosurgery 2002; 50: 804–812
4 Wirtz CR, Tronnier VM, Bonsanto MM, Hassfeld S, Knauth M, Kunze S. [Neuronavigation. Methods and prospects]. Nervenarzt 1998; 69: 1029–1036
5 Woydt M, Horowski A, Krauss J, Krone A, Soerensen N, Roosen K. Three-dimensional intraoperative ultrasound of vascular malformations and supratentorial tumors. J Neuroimaging 2002; 12: 28–34
6 Nabavi A, Gering DT, Kacher DF, Talos IF, Wells WM, Kikinis R, Black PM, Jolesz FA. Surgical navigation in the open MRI. Acta Neurochir 2003; 85 (Suppl): 121–125
7 Nimsky C, Ganslandt O, von Keller B, Romstock J, Fahlbusch R. Intraoperative high-field-strength MR imaging: implementation and experience in 200 patients. Radiology 2004; 233: 67–78
8 Yonekawa Y. Intraoperative imaging in neurosurgery. MRI, CT, ultrasound. Postscript. Acta Neurochir 2003; 85 (Suppl): 143–144
9 Johnson I. Intra-operative ultrasound. J Neurosurg Nurs 1984; 16: 208–210
10 Suhm N, Dams J, van Leyen K, Lorenz A, Bendl R. Limitations for three-dimensional ultrasound imaging through a bore-hole trepanation. Ultrasound Med Biol 1998; 24: 663–671
11 Trantakis C, Meixensberger J, Lindner D, Strauss G, Grunst G, Schmidtgen A, Arnold S. Iterative neuronavigation using 3D ultrasound. A feasibility study. Neurol Res 2002; 24: 666–670
12 Lindseth F, Kaspersen JH, Ommedal S, Lango T, Bang J, Hokland J, Unsgaard G, Hernes TA. Multimodal image fusion in ultrasound-based neuronavigation: improving overview and interpretation by integrating preoperative MRI with intraoperative 3D ultrasound. Comput Aided Surg 2003; 8: 49–69
13 Gronningsaeter A, Kleven A, Ommedal S, Aarseth TE, Lie T, Lindseth F, Lango T, Unsgard G. SonoWand, an ultrasound-based neuronavigation system. Neurosurgery 2000; 47: 1373–1379
14 Gronningsaeter A, Unsgard G, Ommedal S, Angelsen BA. Ultrasound-guided neurosurgery: a feasibility study in the 3–30 MHz frequency range. Br J Neurosurg 1996; 10: 161–168
15 Hata N, Dohi T, Iseki H, Takakura K. Development of a frameless and armless stereotactic neuronavigation system with ultrasonographic registration. Neurosurgery 1997; 41: 608–613
16 Jodicke A, Springer T, Boker DK. Real-time integration of ultrasound into neuronavigation: technical accuracy using a light-emitting-diode-based navigation system. Acta Neurochir (Wien) 2004; 146: 1211–1220
17 Lindseth F, Bang J, Lango T. A robust and automatic method for evaluating accuracy in 3-D ultrasound-based navigation. Ultrasound Med Biol 2003; 29: 1439–1452
18 Prager RW, Rohling RN, Gee AH, Berman L. Rapid calibration for 3-D freehand ultrasound. Ultrasound Med Biol 1998; 24: 855–869
19 Roche A, Pennec X, Malandain G, Ayache N. Rigid registration of 3-D ultrasound with MR images: a new approach combining intensity and gradient information. IEEE Trans Med Imaging 2001; 20: 1038–1049
20 Schlaier JR, Warnat J, Dorenbeck U, Proescholdt M, Schebesch KM, Brawanski A. Image fusion of MR images and real-time ultrasonography: evaluation of fusion accuracy combining two commercial instruments, a neuronavigation system and a ultrasound system. Acta Neurochir (Wien) 2004; 146: 271–276
21 Renner C, Lindner D, Schneider JP, Meixensberger J. Evaluation of intra-operative ultrasound imaging in brain tumor resection: a prospective study. Neurol Res 2005; 27: 351–357
22 Comeau RM, Sadikot AF, Fenster A, Peters TM. Intraoperative ultrasound for guidance and tissue shift correction in image-guided neurosurgery. Med Phys 2000; 27: 787–800
23 Hernes TA, Ommedal S, Lie T, Lindseth F, Lango T, Unsgaard G. Stereoscopic navigation-controlled display of preoperative MRI and intraoperative 3D ultrasound in planning and guidance of neurosurgery: new technology for minimally invasive image-guided surgery approaches. Minim Invas Neurosurg 2003; 46: 129–137
24 Lindseth F, Lango T, Bang J, Nagelhus Hernes TA. Accuracy evaluation of a 3D ultrasound-based neuronavigation system. Comput Aided Surg 2002; 7: 197–222
25 Reinacher PC, van Velthoven V. Intraoperative ultrasound imaging: practical applicability as a real-time navigation system. Acta Neurochir 2003; 85 (Suppl): 89–93
26 Jodicke A, Deinsberger W, Erbe H, Kriete A, Boker DK. Intraoperative three-dimensional ultrasonography: an approach to register brain shift using multidimensional image processing. Minim Invas Neurosurg 1998; 41: 13–19
27 Trantakis C, Tittgemeyer M, Schneider JP, Lindner D, Winkler D, Strauss G, Meixensberger J. Investigation of time-dependency of intracranial brain shift and its relation to the extent of tumor removal using intra-operative MRI. Neurol Res 2003; 25: 9–12
28 van Velthoven V. Intraoperative ultrasound imaging: comparison of pathomorphological findings in US versus CT, MRI and intraoperative findings. Acta Neurochir 2003; 85 (Suppl): 95–99
29 Sure U, Benes L, Bozinov O, Woydt M, Tirakotai W, Bertalanffy H. Intraoperative landmarking of vascular anatomy by integration of duplex and Doppler ultrasonography in image-guided surgery. Technical note. Surg Neurol 2005; 63: 133–141
30 Letteboer MM, Willems PW, Viergever MA, Niessen WJ. Brain shift estimation in image-guided neurosurgery using 3-D ultrasound. IEEE Trans Biomed Eng 2005; 52: 268–276
31 Kanno H, Ozawa Y, Sakata K, Sato H, Tanabe Y, Shimizu N, Yamamoto I. Intraoperative power Doppler ultrasonography with a contrast-enhancing agent for intracranial tumors. J Neurosurg 2005; 102: 295–301
32 Coenen VA, Krings T, Weidemann J, Hans FJ, Reinacher P, Gilsbach JM, Rohde V. Sequential visualization of brain and fiber tract deformation during intracranial surgery with three-dimensional ultrasound: an approach to evaluate the effect of brain shift. Neurosurgery 2005; 56: 133–141

T. Nishizaki[1]
K. Saito[2]
Y. Jimi[2]
N. Harada[3]
K. Kajiwara[1]
S. Nomura[1]
H. Ishihara[1]
K. Yoshikawa[1]
H. Yoneda[1]
M. Suzuki[1]
I. C. Gibbs[4]

The Role of Cyberknife Radiosurgery/Radiotherapy for Brain Metastases of Multiple or Large-Size Tumors

Abstract

Objective: Focused, highly targeted radiosurgery and fractionated radiotherapy using the Cyberknife are useful treatments for multiple or large metastases. Here we present our results of Cyberknife® radiosurgery for 71 patients with 148 metastatic brain lesions. **Methods:** There were 32 women and 39 men with a median age of 63 (range: 30–88) years. Radiographic follow-up was available for 60 patients with 104 lesions. The mean and median initial volumes of the tumor per lesion were 6.6 and 2.9 cm^3 (range: 0.1–53.2 cm^3), respectively, at the time of the initial Cyberknife treatment. Forty patients (56%) had a single lesion, and 31 (44%) had multiple lesions (range: 2–7) at initial treatment. The number of fractions ranged from 1 to 3, and forty (27%) of 148 lesions were treated by a fractionated course of Cyberknife therapy. The mean marginal dose was 20.2 Gy (range 7.8–30.1 Gy, median: 20.7 Gy). **Results:** At 44 weeks of median follow-up, there were no permanent symptoms resulting from radiation necrosis. Overall 6-month and 1-year survival rates were 74% and 47%, respectively, and the median survival time was 56 weeks. The Karnofsky performance score and extracranial metastasis were significant prognostic factors at 6 months and 1 year, respectively, in both univariate and multivariate analyses. Age or multiple metastases did not influence prognosis at 6 months and 1 year. Local control was achieved in 83% (86 lesions). After additional radiosurgical or surgical salvage, no patient died as a result of intracranial disease. Twenty-five patients developed 92 new metastases (range 1–13) outside of the treated lesions with 22.4 weeks of median follow-up. Among them, 21 patients (84 lesions) were treated by salvage Cyberknife. **Conclusion:** Despite the inclusion of an unfavorable group of patients with large tumors, our results for survival and tumor control rates are comparable to those of published series. The Cyberknife provides the advantage of allowing for fractionated treatment to multiple or large-size tumors.

Key words

Metastatic brain tumor · Cyberknife · radiosurgery · radiotherapy

Introduction

Stereotactic radiosurgery is widely used in the treatment of brain metastases, and has achieved better local control and may impact survival compared with whole-brain radiation therapy (WBRT) [1–4]. Stereotactic radiosurgery of intracranial targets has been possible because of rigid target fixation with a skull frame. More recently, with the advent of image guidance, the Cyberknife (Accuray, Sunnyvale, CA, USA), has been used to deliver precision radiosurgery. The Cyberknife, developed in 1997 [5–7], is a modification of LINAC-based radiosurgery in which a compact linear accelerator is mounted on a highly maneuverable robotic manipulator. The Cyberknife eliminates the need for skeletal fixation or rigid immobilization of the patient by its use of real-time image guidance. Gamma-knife units have several limitations, including rigid target fixation and limited de-

Affiliation
[1]Departments of Neurosurgery, Yamaguchi University School of Medicine, Yamaguchi, Japan
[2]Department of Neurosurgery, Kounan Saint Hill Hospital, Yamaguchi, Japan
[3]Department of Hygiene, Yamaguchi University School of Medicine, Yamaguchi, Japan
[4]Department of Radiation Oncology, Stanford Medical Center, Stanford, CA, USA

Correspondence
Takafumi Nishizaki, M.D. · Department of Neurosurgery · Ube Industrial Central Hospital · 750 Nishikiwa · Ube · Yamaguchi 755-0151 · Japan · Tel.: + 81/836/51 92 21 · Fax: + 81/836/51 92 52 · E-mail: nishiza@jeans.ocn.ne.jp

Bibliography
Minim Invas Neurosurg 2006; 49: 203–209 © Georg Thieme Verlag KG · Stuttgart · New York
DOI 10.1055/s-2006-947998
ISSN 0946-7211

grees of treatment freedom, which could be major drawbacks when treating patients with multiple, large, or non-spherical tumors. Such patients could benefit from the use of homogeneous irradiation and the delivery of fractionated Cyberknife therapy. To our knowledge, no previous reports have quantified the use of the Cyberknife in the treatment of metastatic brain tumors. Here we describe initial results of Cyberknife radiosurgery/radiotherapy in patients with brain metastases treated at our institution. In this study, we also investigate relevant factors affecting patient survival and local tumor control.

Materials and Methods

Patient population

Seventy-one patients with metastatic brain tumors (148 lesions) were treated with Cyberknife radiosurgery at Kounan Saint Hill Hospital between 1997 to 2001. Patients with clinical follow-up for more than 3 months were included in this study. Patient age ranged from 30 to 88 years, with a median of 63 years. Thirty-two patients (45 %) were female and 39 (55 %) were male. The median and mean volumes of the tumors were 3.0 and 6.6 cm^3 (range: 0.1–53.2 cm^3), respectively, at the time of the initial Cyberknife surgery. The median volume of the main tumors per patient was 7.4 cm^3. Forty (56 %) patients had a single lesion, and 31 (44 %) had multiple lesions (mean number: 2.1; range: 2–13) at initial Cyberknife treatment. Primary tumor sites included carcinomas of the lung (43 %), breast (29 %), intestine (8 %), stomach (3 %), kidney (4 %), and others (13 %). The median score on the Karnofsky performance scale (KPS) at the time of the initial Cyberknife treatment was 80 % (range: 20–100 %). Eleven patients were treated by Cyberknife for recurrent tumors after WBRT had been administered (median dose: 27.6 Gy), and four had received gamma radiosurgery in other institutions prior to Cyberknife treatment. Forty-three percent of the patients had uncontrolled primary lesions, and 42 % had extracranial metastases before Cyberknife treatment. Patients with cystic tumors were excluded from this study.

Treatment parameters

Stereotactic radiosurgery was performed using the Cyberknife. The marginal dose was defined as that delivered at an isodose surface surrounding 90 % of the entire tumor volume. In cases with fractionated irradiation, the marginal dose representing the dose equivalent to that delivered as a single dose was calculated based on the linear-quadratic model based on an α/β ratio of 2 Gy and assuming equivalent late effects [8]. The mean marginal dose was 20.2 Gy (range: 7.8–30.1 Gy; median: 20.7 Gy).

Fractionated Cyberknife radiotherapy was performed in tumors located in eloquent areas of the brain, or for large tumors, defined as greater than 2.99 cm^3. The mean number of fractions was 1.4 (range: 1–3). Single-dose radiosurgery was performed on 108 lesions with a median tumor volume of 4.3 cm^3. Two sessions of fractionated radiotherapy were performed on 28 lesions with a median tumor volume of 7.4 cm^3. Three sessions of fractionated radiotherapy were performed on 12 lesions with a median tumor volume of 20.0 cm^3.

Survival rates and local tumor control

Survival rates were investigated at 6 and 12 months after the initial Cyberknife treatment. Prognostic factors affecting patient survival were also determined by univariate and then multivariate analyses. Parameters with p values less than or equal to 0.40 were included in the multivariate analysis, which used the Cox proportional hazard model with the backward stepwise method [9]. A p value of ≤ 0.05 was regarded as statistically significant.

Local tumor control was evaluated in 104 lesions obtained from 60 patients in whom radiological follow-up longer than 100 days were available. The average tumor volume per lesion was 3.0 cm^3 (range 0.12–53.2 cm^3) at the time of the initial Cyberknife treatment. Local recurrence of treated metastases was defined as an increase of greater than 25 % in the contrast of images obtained by magnetic resonance imaging (MRI), or where neurological deterioration occurred. Time to local failure was assessed for each lesion, and was measured from the date of initial Cyberknife radiosurgery. Because only 18 tumors recurred locally during the follow-up periods after Cyberknife treatment, the times to local failure were analyzed using the Kaplan-Meier method [10], by arbitrarily dividing categorized variables into two groups by changing the cutoff values. The log-rank test was used to evaluate the effects of patient characteristics and treatment factors on these outcomes [11]. The variables that independently contributed to local failure were detected statistically as described in the previous paragraph.

Results

No permanent symptoms resulting from radiation necrosis during the follow-up periods after the Cyberknife treatment were observed.

Survival time

Overall 6-month and 1-year survival rates were 74 % and 47 %, respectively. The median survival time was 56 weeks after the initial Cyberknife treatment. There were 40 deaths. Causes of death were verified in 35 of 40 cases, consisting of 3 (9 %) progressive brain metastases, 13 (37 %) progressive primary cancers, 15 (43 %) extracranial metastases, and 4 (11 %) other diseases such as infection or gastric bleeding.

Prognostic factors affecting 6-month and 1-year survival rates are shown in Tables **1** and **2**, respectively. The possible prognostic factors for survival were tumor volume, number of lesions per patient, KPS score, age, sex, marginal dose, number of fractions, control of primary tumor, extracranial metastases, adjuvant WBRT, doubling time, primary lesions (lung or breast cancers vs. others), and previous operations. The KPS score was a significant prognostic factor at 6 months in both univariate ($p < 0.01$) and multivariate analyses ($p < 0.05$). Kaplan-Meier analysis revealed significant differences between patients with KPS scores of 70 or higher, and those with scores less than 70 (Fig. **1**). A lack of control of the primary tumor and extracranial metastases were associated with unfavorable prognosis at 6 months in the multivariate analysis, but their significance was borderline ($p = 0.0899$ and 0.089, respectively). Extracranial metastases were significantly associated with shorter survival rates at 1 year

Table **1** Analysis of prognostic factors for 6-month survival

	Univariate	*Multivariate*
tumor volume	0.0315	0.6620
no. of lesions	0.1985	0.9907
KPS score	< 0.0001	0.0223
age	0.3369	0.7269
sex	0.0950	0.1884
marginal dose	0.4004	NI
no. of fractions	0.0421	0.1576
control of primary tumor	0.2957	0.0899
other distant metastases	0.0173	0.0809
adjuvant WBRT	0.1310	0.9003
doubling time	0.0263	0.9206
lung cancer	0.719	NI
breast cancer	0.5411	NI
previous operation	0.6930	NI

NI = not included; WBRT = whole-brain radiation therapy

Table **2** Analysis of prognostic factors for 1-year survival

	Univariate	*Multivariate*
tumor volume	0.0686	0.6729
no. of lesions	0.8354	NI
KPS score	0.0491	0.4982
age	0.8501	NI
sex	0.1138	0.2466
marginal dose	0.8931	NI
no. of fractions	0.4947	NI
control of primary tumor	0.3787	0.3299
other distant metastases	0.0258	0.0500
adjuvant WBRT	0.0265	0.3875
doubling time	0.1552	0.9784
lung	0.4056	NI
breast	0.6715	NI
previous operation	0.0766	NI

after Cyberknife treatment in both univariate ($p < 0.05$) and multivariate ($p = 0.05$) analyses. The Kaplan-Meier analysis also demonstrated a significantly worse survival rate in patients with extracranial metastasis than in those without it (Fig. **2**). Age or multiple metastases were not associated with patient prognosis at 6 months and 1 year in both univariate and multivariate analyses.

When 32 patients with multiple metastasis were analyzed, the 6-month and 1-year survival rates were 73 % (22 of 30 cases) and 43 % (12 of 28 cases), respectively. The median survival time of patients with multiple metastases was 51 weeks. The Kaplan-Meier analysis revealed no difference in survival rates between patients with single and multiple metastases (Fig. **3**).

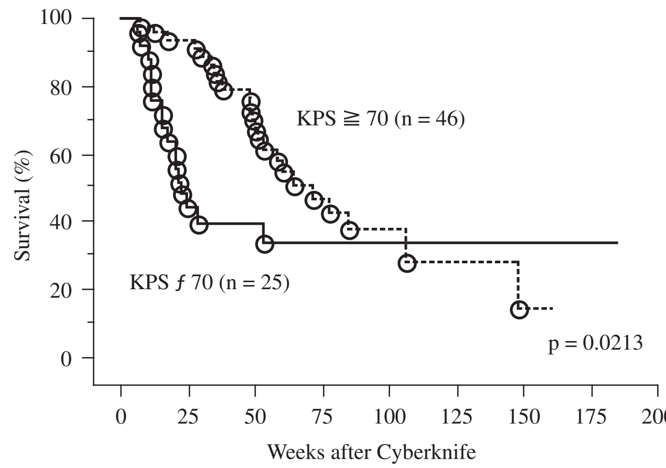

Fig. **1** The Kaplan-Meier model with log-rank test applied to each categorization demonstrated significantly longer survival rates in patients with a higher KPS score (≥ 70) ($p < 0.05$).

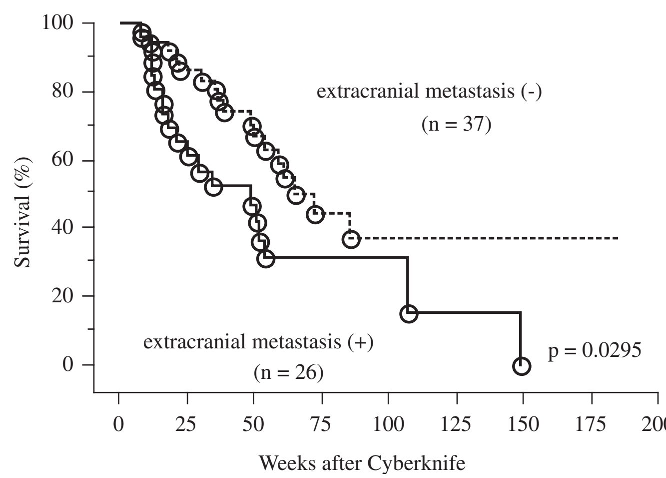

Fig. **2** The Kaplan-Meier model with log-rank test applied to each categorization demonstrated significantly shorter survival rates in patients with extracranial metastasis ($p < 0.05$).

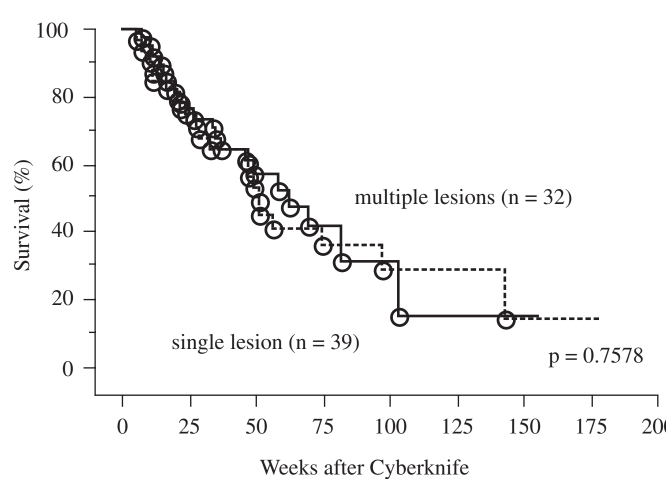

Fig. **3** The Kaplan-Meier model with log-rank test applied to each categorization demonstrated no significant difference in survival rates between patients with single and multiple metastases.

Table **3** Analysis of local tumor control (104 lesions)

	Univariate	*Multivariate*
tumor volume (< 2.99 vs > 2.99 cm³)	0.0157	0.4327
marginal dose (< 21.9 vs > 21.9 Gy)	0.0281	0.1727
adjuvant WBRT	0.0701	0.3318
lung cancer vs. others	0.4072	NI
breast cancer vs. others	0.4417	NI
infratentorial location	0.0203	0.2287
recurrent tumor	0.1178	0.5458
eloquent tumor	0.0629	0.5766

Local tumor control

Actuarial local control rates were 88 % and 63 % at 6 months and 1 year, respectively. The median time to local failure was 25 weeks, with a range of 13–94 weeks. The possible prognostic factors for local tumor control were tumor volume, marginal dose, adjuvant WBRT, primary lesions (lung or breast cancers vs. others), location of the tumor (infratentorial), recurrent tumor, and eloquent tumor location such as motor and speech areas, or brainstem. The results are shown in Table **3**. A large tumor volume (greater than 2.99 cm^3), infratentorial location, and a marginal dose of radiation (21.9 Gy or less) were also associated with poor tumor control ($p < 0.05$) in the Kaplan-Meier analysis (Table **3**, Figs. **4**–**6**). However, multivariate analysis by Cox proportional hazards regression modeling showed no statistical significance of these factors. In the univariate analysis, adjuvant WBRT before Cyberknife treatment and tumor in a non-eloquent brain area were associated with favorable tumor control, but their significances were borderline ($p = 0.0701$ and 0.0629, respectively). Multiplicity did not affect local tumor control in either univariate or multivariate analyses.

Eighteen of 104 tumors (in 18 patients) showed failure of local control during the follow-up period (Table **4**). The average marginal dose for the 18 tumors was 19.5 Gy (range: 11.6–24.7 Gy, median: 19.9 Gy). The median and mean volumes of the 18 progressive tumors were 9.1 and 4.3 cm^3 (range: 0.2–38.4 cm^3), respectively, at the time of the initial Cyberknife treatment. Twelve patients received additional radiosurgery (Cyberknife for ten tumors and gamma knife for two tumors) at the time of recurrence. Ten of eighteen recurrent lesions remained locally controlled after a second course of radiosurgery. Two lesions eventually required surgical treatment after the second Cyberknife treatment. Three of 18 patients underwent surgical treatment at the first recurrence to relieve symptomatic mass effect at the site of local failure. Two of them received Cyberknife treatment immediately after the surgery for the residual tumor, while one case was proven to be radiation necrosis by histological examination. Three patients who did not undergo either additional radiosurgery or surgical treatment died of progressive brain metastasis.

Four of 14 patients who received Cyberknife treatment died of extracranial metastases other than brain metastasis. Eleven patients were still alive after a median follow-up period of 61

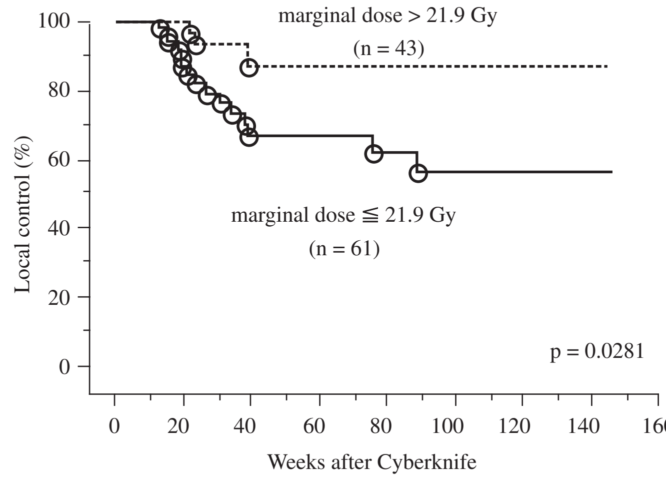

Fig. **4** The Kaplan-Meier model with log-rank test applied to each categorization demonstrated significantly longer tumor control rates in patients a marginal dose of greater than 21.9 Gy ($p < 0.05$).

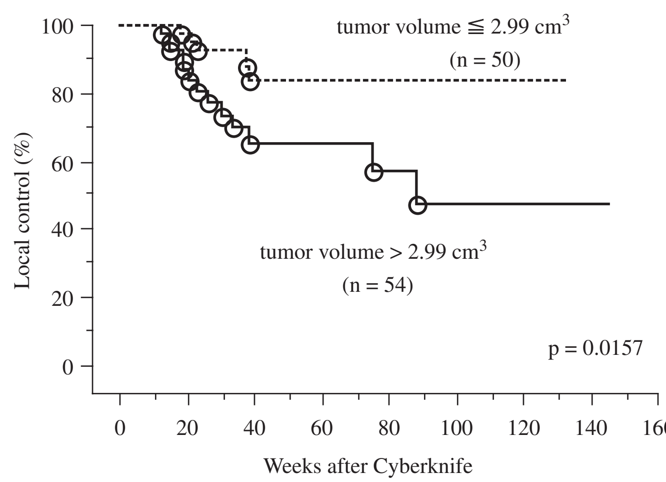

Fig. **5** The Kaplan-Meier model with log-rank test applied to each categorization demonstrated significantly longer tumor control rates in patients with a tumor volume of 2.99 cm^3 or less ($p < 0.05$).

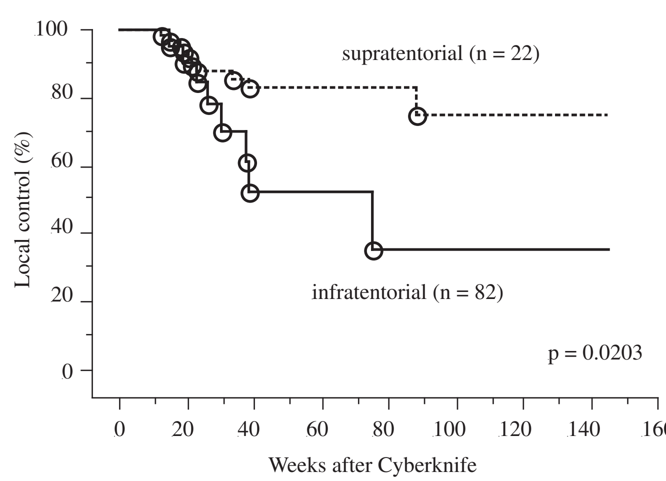

Fig. **6** The Kaplan-Meier model with log-rank test applied to each categorization demonstrated significantly longer tumor control rates in patients with supratentorial tumors ($p < 0.05$).

Table **4** Lesions with local control failure

Location	*Volume (cm³)*	*Dose*	*Second treat.*	*Third treat.*	*Outcome (weeks after initial CK)*
1) L motor	3.2	20.4	CK	no rec.	A (159)
2) L premotor	4.3	18.8	CK	no rec.	A (21)
3) R putamen	3.8	21.4	CK	no rec.	A (61)
4) cerebe.	1.4	24.3	CK	no rec.	A (62)
5) cerebe.	38.4	16.1	γK	no rec.	A (41)
6) R occipital	26.2	16.1	γK	no rec.	A (44)
7) L parietal	5.5	18.0	CK	no rec.	D (ex. met.)
8) L cerebe	23.5	16.1	CK	no rec.	D (ex. met.)
9) medulla	3.0	11.6	CK	no rec.	D (ex. met.)
10) L parietal	0.9	21.7	CK	no rec.	D (ex. met.)
11) R cerebe.	14.8	19.6	CK	surg. (tumor)	A (82)
12) L cerebe.	12.8	20.0	CK	surg. (tumor)	A (87)
13) R cerebe.	2.1	19.8	surg. (tumor)	CK	A (73)
14) L parietal	4.3	21.8	surg. (tumor)	CK	A (34)
15) R frontal	0.2	24.7	surg. (nec.)	no rec.	A (43)
16) L parietal	0.8	22.0	no treat.	–	D (brain met.)
17) R C-P angle	7.0	16.9	no treat.	–	D (brain met.)
18) L occipital	3.4	18.0	no treat.	–	D (brain met.)

Abbreviations: treat. = treatment; surg. = surgery; R = right; L = left; motor = motor area; A = alive; D = dead; CK = Cyberknife; γK = gamma knife; ex. = extracranial; met. = metastasis; nec. = necrosis; cerebe. = cerebellum; C-P angle = intraaxial tumor near cerebellar peduncle

weeks (range 21–159 weeks) from the date of the initial Cyberknife treatment.

Twenty-five patients developed 92 new metastases (range 1–13) outside of the treated lesions within 22.4 weeks of median follow-up. Among them, 21 patients (84 lesions) were treated by salvage Cyberknife. The median and mean volume of the treated lesions were 1.4 and 3.0 cm^3 (range: 0.1–21.7 cm^3), respectively, at the time of the Cyberknife treatment. Because the size of new lesions was smaller than that at the time of initial treatment, fractionated radiotherapy were performed only for eight lesions. After additional Cyberknife treatment, no patient died as a result of intracranial disease of new metastases.

Discussion

There is much literature indicating that tumor volume is a statistically significant factor associated with patient survival in studies of gamma-knife treatment [3,12,13], although the results are still controversial [4]. Focused, highly targeted irradiation and the delivery of fractionated Cyberknife therapy can be effective treatment for large metastatic tumors.

Indeed, the tumors in the present study were larger (median: 7.4 cm^3) than in recent series involving the gamma knife (range of median: 2.1–3.9 cm^3) [1,3,12] (Table **5**). Despite the large size of lesions included in this analysis, only three (4 %) of 71 patients died of brain metastasis, and the 6-month and 1-year survival rates were similar to those of previous reports. In the prognostic factor analysis, an association of tumor volume with shorter survival was observed only at 6 months after Cyberknife treatment, solely in univariate analysis.

The correlation of smaller tumor volume with better tumor control has been reported using the gamma knife [1,3], through a few reports indicate that dose and tumor size are not significant [4]. Six-month and 1-year actuarial local tumor control rates in our series were similar to those in previous studies: i.e., 82 % at 6 months [3], and 48 %–85 % at 1 year [1,2,3,14]. In the factor analysis, we found that tumor volume affected local tumor control significantly in the univariate analyses but not in the multivariate analysis. A higher dose of radiation delivered to the tumor was significantly associated with improved local tumor control [14]. Based on dose-volume effects and in an effort to avoid radiation injury, radiation dose was reduced to large tumors (cases 5, 6, and 8 in Table **4**). Furthermore, dose was reduced for tumors located in eloquent areas even if the tumor was small (cases 9 and 17 in Table **4**). This clinical practice resulted in reduced local control of such treated lesions, requiring a repeat course of Cyberknife treatment. This observation, together with the absence of permanently symptomatic radionecrosis, suggests that more aggressive irradiation may be acceptable in the treatment of larger tumors by using the fractionated method in order to improve local control. A recent report stated that surgical excision of the tumor before radiosurgery provides better tumor control [15]. Indeed, in the present study a single Cyberknife treatment could fail to control 3 of 104 tumors (cases 13, 14, and 15 in Table **4**). However, our results suggest that even large tumors can be treated by fractionated Cyberknife radiosurgery, Table **5** Previous reports concerning survival times and clinical features

Report	*Median volume (cm³)*	*Median KPS*	*Multiple lesions*	*Median survival (months)*
Alexander, 1995	3.0	(> 80)	31 %	9.4
Auchter, 1996	–	–	0 %	13
Breneman, 1997	< 4.0 cm	90 (> 60)	57 %	10
Shiau, 1997	1.3	90 (50–100)	46 %	11
Shirato, 1997	> 2 cm: 36 %	60 (30–90)	0 %	9
Pirzkall, 1998	–	80 (50–100)	26 %	5.5
Kim, 2000	2.1	90 (50–100)	15 %	11
present study	7.2	80 (20–100)	45 %	13

and subsequent treatment either by radiosurgery or surgical procedure can be satisfactorily reserved as salvage management of recurrent tumors.

Fractionated Cyberknife therapy is also effective on multiple tumors: such cases represented 44 % of cases in this study (Table **5**). Some reports have suggested that the number of lesions does not influence patient survival [13,16]. Kim et al., however, reported that patients with a single lesion survived longer than those with multiple lesions only in univariate analysis [3]. Also, Alexander suggested that the presence of three or more brain metastases is significantly associated with decreased survival in univariate analysis [1]. In that study, the median survival period of patients with four brain metastases was lower (at 3 months) than those with two or three metastases (at 9 and 11 months, respectively), although the difference was not significant [17]. Our results using the Cyberknife did not demonstrate any statistical difference between single and multiple lesions in both univariate and multivariate analyses. In a recent report involving only multiple brain metastases, the 1-year survival and median survival rates were 26 % and 6 months, respectively [13]. In our study, tumor multiplicity did not influence patient survival either at 6 months or at 1 year, and the median survival rate was 12 months. Furthermore, in the present study, most patients with new metastases that developed during the follow-up could be treated by salvage Cyberknife when there were no other contraindications. Our results support the hypothesis that the Cyberknife is useful for the treatment of multiple metastatic lesions from the viewpoint of patient survival and local tumor control.

Although this study did not exclude any cases with low pre-KPS scores, the median KPS was 80 % (range: 20–100 %). In many series studies involving radiosurgery, patients with lower pre-KPS scores were excluded from the analyses (Table **5**). Many reports have claimed that the KPS score was a statistically significant prognostic factor [3], patients with KPS scores of 70 or higher exhibiting higher survival rates [12,13,18,19]. In the present cases, the KPS score significantly affected patient survival at 6 months. This phenomenon is probably because the KPS score is influenced by factors other than the patient's neurological deterioration. Previous reports concluded that both a controlled primary cancer and the absence of extracranial metastases were associated with longer survival [18]. Our results are concordant with these reports: adjuvant WBRT combined with radiosurgery influenced patient survival and local tumor control in our study. Although there have been many reports similar to ours [3,15,19], some authors have claimed that prophylactic WBRT is mandatory in the treatment of brain metastases [4,12,17,20–23]. Although further study is required, our results suggest that Cyberknife radiosurgery can be used as the sole treatment for brain metastases. Whether there is an association between patient age and survival rates is still controversial. Reports have stated that patients aged 60 years or more [1] or those aged 50 years or more [19] had shorter survival rates, while others demonstrated no age significance [4,12]. While our series included many elderly patients (as shown in Table **5**), there was no significant difference between their results and those of younger subjects.

Conclusions

Despite the inclusion of an unfavorable group of patients with large tumors, our results for survival and tumor control rates are comparable to those of published series. The Cyberknife provides the advantage of allowing for fractionated treatment to larger tumors. Further investigation is required to explore the optimal dose fractionation scheme for such large tumors.

References

1 Alexander E, Moriarty TM, Davis RB, Wen PY, Fine HA, Black PM, Kooy HM, Loeffler JS. Stereotactic radiosurgery for the definitive, noninvasive treatment of brain metastases. J Natl Cancer Inst 1995; 87: 34–40

2 Breneman JC, Warnick RE, Albright RE, Kukiatinant N, Shaw J, Armin D, Tew J. Stereotactic radiosurgery for the treatment of brain metastases. Results of a single institution series. Cancer 1997; 79: 551–557

3 Kim DG, Chung HT, Gwak HS, Paek SH, Jung HW, Han DH. Gamma knife radiosurgery for brain metastases: prognostic factors for survival and local control. J Neurosurg 2000; 93 (Suppl 3): 23–29

4 Flickinger JC, Kondziolka D, Lunsford LD, Coffey RJ, Goodman ML, Shaw EG, Hudgins WR, Weiner R, Harsh GR, Sneed PK. A multi-institutional experience with stereotactic radiosurgery for solitary brain metastasis. Int J Radiat Oncol Biol Phys 1994; 28: 797–802

5 Adler JR, Cox RS. Preliminary clinical experience with the CyberKnife: image-guided stereotactic radiosurgery In: Kondziolka D (ed.) Radiosurgery. Basel, Karger, 1996; 316–326

6 Adler JR. The Cyberknife: a frameless robotic system for radiosurgery. Stereot Funct Neurosurg 1997; 69: 124–128

[7] Chang SD, Murphy M, Geis P, Martin DP, Hancock SL, Doty JR, Adler JR Jr. Clinical experience with image-guided robotic radiosurgery (the CyberKnife) in the treatment of brain and spinal cord tumors. Neurol Med Chirur 1998; 38: 780–783
[8] Fowler JF. The linear-quadratic formula and progress in fractionated radiotherapy. Brit J Radiol 1989; 62: 679–694
[9] Cox DR. Regression models and life tables. J R Stat Soc Series B 1972; 34: 187–202
[10] Kaplan EL, Meier P. Nonparametric estimation from incomplete observations. J Am Stat Assoc 1958; 53: 457–481
[11] Peto R, Peto J. Asymptotically efficient rank invariant test procedures. J R Stat Soc Series A 1972; 135 (Part II): 185–207
[12] Sneed PK, Lamborn KR, Forstner JM, McDermott MW, Chang S, Park E, Gutin PH, Phillips TL, Wara WM, Larson DA. Radiosurgery for brain metastases: is whole brain radiotherapy necessary? Int J Radiat Oncol Biol Phys 1999; 43: 458–549
[13] Schoeggl A, Kitz K, Ertl A, Reddy M, Bavinzski G, Schneider B. Prognostic factor analysis for multiple brain metastases after gamma knife radiosurgery: results in 97 patients. J Neurooncol 1999; 42: 169–175
[14] Shiau CY, Sneed PK, Shu HK, Lamborn KR, McDermott MW, Chang S, Nowak P, Petti PL, Smith V, Verhey LJ, Ho M, Park E, Wara WM, Gutin PH, Larson DA. Radiosurgery for brain metastases: relationship of dose and pattern of enhancement to local control. Int J Radiat Oncol Biol Phys 1997; 37: 375–383
[15] Serizawa T, Iuchi T, Ono J, Saeki N, Osato K, Odaki M, Ushikubo O, Hirai S, Sato M, Matsuda S. Gamma knife treatment for multiple metastatic brain tumors compared with whole-brain radiation therapy. J Neurosurg 2000; 93 (Suppl 3): 32–36
[16] Suzuki S, Omagari J, Nishio S, Nishiye E, Fukui M. Gamma knife radiosurgery for simultaneous multiple metastatic brain tumors. J Neurosurg 2000; 93 (Suppl 3): 30–31
[17] Kondziolka D, Patel A, Lunsford LD, Kassam A, Flickinger JC. Stereotactic radiosurgery plus whole brain radiotherapy versus radiotherapy alone for patients with multiple brain metastases. Int J Radiat Oncol Biol Phys 1999; 45: 427–434
[18] Auchter RM, Lamond JP, Alexander E, Buatti JM, Chappell R, Friedman WA, Kinsella TJ, Levin AB, Noyes WR, Schultz CJ, Loeffler JS, Mehta MP. A multiinstitutional outcome and prognostic factor analysis of radiosurgery for resectable single brain metastasis. Int J Radiat Oncol Biol Phys 1996; 35: 27–35
[19] Pirzkall A, Debus J, Lohr F, Fuss M, Rhein B, Engenhart-Cabillic R, Wannenmacher M. Radiosurgery alone or in combination with whole-brain radiotherapy for brain metastases. J Clin Oncol 1998; 16: 3563–3569
[20] Buatti JM, Friedman WA, Bova FJ, Mendenhall WM. Treatment selection factors for stereotactic radiosurgery of intracranial metastases. Int J Radiat Oncol Biol Phys 1995; 32: 1161–1166
[21] Cho KH, Hall WA, Gerbi BJ, Higgins PD, Bohen M, Clark HB. Patient selection criteria for the treatment of brain metastases with stereotactic radiosurgery. J Neurooncol 1998; 40: 73–86
[22] Coffey RJ, Flickinger JC, Bissonette DJ, Lunsford LD. Radiosurgery for solitary brain metastases using the cobalt-60 gamma unit: methods and results in 24 patients. Int J Radiat Oncol Biol Phys 1991; 20: 1287–1295
[23] Davey P, O'Brien PF, Schwartz ML, Cooper PW. A phase I/II study of salvage radiosurgery in the treatment of recurrent brain metastases. Brit J Neurosurg 1994; 8: 717–723

Original Article

Application of Neuronavigation System to Brain Tumor Surgery with Clinical Experience of 420 Cases

T.-Y. Jung[1]
S. Jung[1]
I.-Y. Kim[1]
S.-J. Park[1]
S.-S. Kang[1]
S.-H. Kim[1]
S.-C. Lim[2]

Abstract

A new era of neurosurgery has recently been unveiled with the advent of image-guided surgery. The use of neuronavigation is beginning to have a significant impact on a variety of intracranial procedures. Herein, we report our clinical experience using a neuronavigation system with different surgical applications and techniques for a variety of brain tumors. We used the BrainLab VectorVision® neuronavigation system, which is a frameless and image-guided system. We operated on 420 cases having various types of brain tumor with the help of this system. The mean target localizing accuracy and mean volume were 1.15 mm and 30.8 mL (0.2–216.4 mL), respectively. We utilized this system to effectively make bone flaps, to detect critically located, deep-seated, subcortical, skull-base and skull bone tumors, and to operate on intraparenchymal lesions with grossly unclear margins, such as gliomas. We also performed tumor biopsy using the combination of a conventional stereotactic biopsy instrument and an endoscope. The application of the neuronavigation system not only revealed benefits for operative planning, appreciation of anatomy, lesion location and the safety of surgery, but also greatly enhanced surgical confidence.

Key words

Brain tumor · neuronavigation · surgery

Introduction

Deep-seated or small brain lesions are particularly problematic for neurosurgeons. In order to meet this challenge, stereotactic neurosurgery has been developed to make the precise spatial information provided by the CT or MR images available during the actual operative procedure, and several neurosurgical navigational systems have recently been designed [1–7].

These image-guided surgical systems provide the surgeon with almost real-time localization, orientation and guidance, typically using preoperative imaging. Therefore, they have benefits for the appreciation of anatomy and operative planning and reduce surgical morbidity. Neuronavigator systems have been widely used for the treatment of brain tumors, as well as for other operations such as endoscopic procedures, catheter placement into cerebral cysts, puncture of very small ventricles, drainage of hematomas or abscesses and for biopsies.

Herein, we report our clinical experience with 420 patients using a neuronavigation system with different surgical applications and techniques for a variety of brain tumors.

Materials and Methods

From March 2000 through October 2003, 420 patients with various pathological conditions of the brain underwent surgical treatment in conjunction with the BrainLab VectorVision® neuronavigation system.

Affiliation
[1]Department of Neurosurgery, Chonnam National University Research Institute of Medical Sciences, Chonnam National University Hwasun Hospital & Medical School, Gwangju, Republic of Korea
[2]Department of Otorhinolaryngology, Chonnam National University Research Institute of Medical Sciences, Chonnam National University Hwasun Hospital & Medical School, Gwangju, Republic of Korea

Correspondence
Shin Jung, M.D., Ph.D. · Department of Neurosurgery · Chonnam National University Hwasun Hospital · 160 Ilsim-ri · Hwasun-eup · Hwasun-gun · Jeollanam-do 519-809 · Republic of Korea · Tel.: + 82/61/37 97 66 6 · Fax: + 82/61/37 97 67 3 · E-mail: sjung@chonnam.ac.kr

Bibliography
Minim Invas Neurosurg 2006; 49: 210–215 © Georg Thieme Verlag KG · Stuttgart · New York
DOI 10.1055/s-2006-948305
ISSN 0946-7211

The basic instrumentation of this system consisted of two infrared cameras, a touch screen monitor and other accessory neuronavigation tools. Preoperatively, six fiducials were glued onto the head of the patient, and CT or MRI scanning was performed. To avoid the dislocation of the skin markers, the patients underwent the imaging procedures in the morning on the day of surgery, just before being moved to the operating room. The data were quickly transferred to the computer in the operating room and the images were displayed on the computer screen. Reconstruction was performed in both the triplanar and three-dimensional formats. All of the patient data were transferred to the workstation computer by means of a zip diskette. After the patient's head was positioned with a Mayfield or Sugita headrest, the reference star was fixed on the surgical head frame, and the monitor and infrared cameras were moved to the appropriate location. Then, marker registration was performed with the pointer under non-sterile conditions. After registration, the operator planned the optimal surgical approach on the computer screen with the three-dimensional images. This procedure was used for a variety of different procedures, viz., craniotomy and tumor removal, endoscopic surgery, biopsy and ventriculostomy.

All of the patients were operated on using the above methods and the registration procedure permitted an accuracy of less than 2.0 mm. We analyzed the mean volume and accuracy, the different pathologies and the methods of operation. We also introduced the surgical application of neuronavigation system to brain tumor surgery.

Results

Patients, registration accuracy, volume and location of tumor

From March 2000 to October 2003, we operated on 420 patients with brain tumors with the help of the neuronavigation system. 229 patients (54.5 %) were females and 191 patients (45.5 %) were males. The male to female ratio was 1:1.2 and the patients' ages ranged from 1.4 to 80 years (mean: 51.4 years).

For the preoperative registration process, CT scans were performed for 326 patients (77.6 %) and MRI scans for 94 patients (22.4 %). The CT images with or without contrast medium had 1.5 to 2.5 mm slices. All of the MRI images used either contrast medium or T_2-weighted images. The mean reference accuracy, given as a computer-calculated value, was 1.15 mm. The lesions ranged from 0.2 to 216.4 mL in volume (mean: 30.8 mL).

The locations of the tumors were the cerebrum in 323 patients (76.9 %), the skull-base in 52 (12.4 %), the ventricles in 18 (4.3 %), the cerebellum in 15 (3.6 %), the brain stem in 5 (1.2 %), and the skull bone in 1 (0.2 %) (Table **1**).

Pathological diagnosis and surgical methods of operation

Pathologically, meningioma was present in 128 patients (30.4 %), glioma in 100 patients (23.8 %), metastasis in 79 patients (18.8 %), with the remaining 113 patients suffering from various other tumors, such as schwannoma, pituitary adenoma, arachnoid cyst, chordoma and so on.

Table **1** Locations of mass

Location	*Number of patients (n = 420)*
Cerebrum	323 (76.9 %)
Skull base	52 (12.4 %)
Ventricle	18 (4.3 %)
Cerebellum	15 (3.6 %)
Tentorium	6 (1.4 %)
Brain stem	5 (1.2 %)
Skull bone	1 (0.2 %)

Table **2** Surgical methods of operation

Surgical methods	*Number of patients (n = 420)*
Microscopic operation	381 (90.7 %)
Endoscopic procedure	12 (2.9 %)
Biopsy	26 (6.2 %)
Catheterization	1 (0.2 %)

For 381 of the 420 patients (90.7 %), the neuronavigation system was used for craniotomy and microsurgical treatment under general anesthesia. Of the remaining 39 patients, 26 underwent tissue biopsy, 12 underwent endoscopic surgery and 1 patient underwent insertion of a catheter on the isolated ventricle due to the presence of a tumor (Table **2**).

Application 1: making the bone flap

When we made the bone flaps, we were able to avoid the dangerous areas. The neuronavigation system allowed us to know the location of the frontal sinus and to safely perform the frontal craniotomy avoiding the sinus (Fig. **1A**). In those cases where the retrosigmoid approach was used, we were able to identify the location of the sigmoid and transverse sinus on the enhanced images and the mastoid air cells on the pre-enhanced CT images. We were able to properly perform the occipital craniotomy and avoid tearing the sinus and diminishing the exposure of the air cells. Especially in the cases of vestibular schwannoma, the small craniotomy hampers the removal of the tumor and the drilling of the posterior wall of the internal acoustic canal; however, by using this system, we were able to determine the proper size of the craniotomy (Fig. **1B**).

Application 2: tumor localization

Critically located tumors (motor and language cortex)

Magnetic resonance images in one patient revealed a single metastatic tumor on the left precentral gyrus. When the tumor was located in the motor area subcortically, we were able to exactly localize the tumor under neuronavigational guidance. We were then able to decide the proper entry point and remove the tumor safely after performing motor strip mapping by cortical stimulation (Fig. **2**).

Deep-seated small tumors

In cases of deep-seated and small tumors, the system was very helpful in determining the appropriate trajectory and finding the

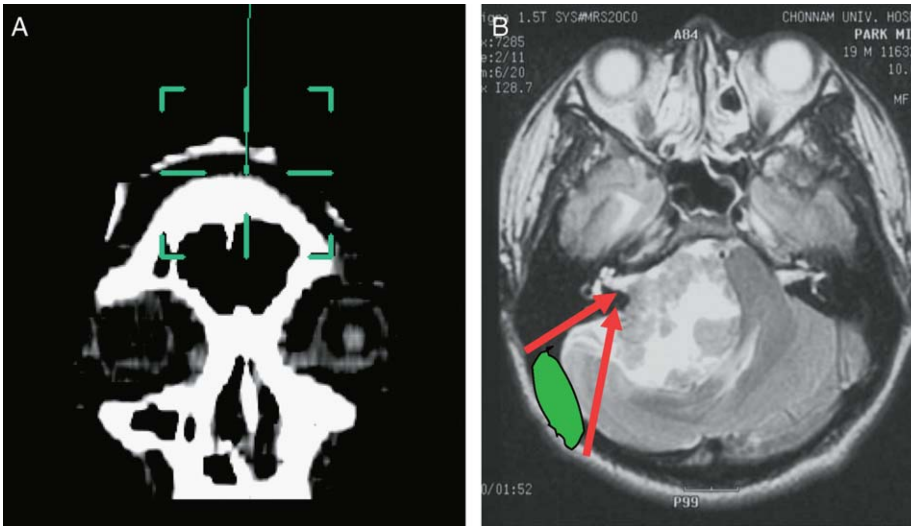

Fig. **1** Making the bone flaps. **A** Avoiding the frontal sinus. **B** Determining the proper size of the craniotomy in the case of vestibular schwannoma (green area: the size of the craniotomy, red arrow: the distance from the bone to the internal acoustic canal).

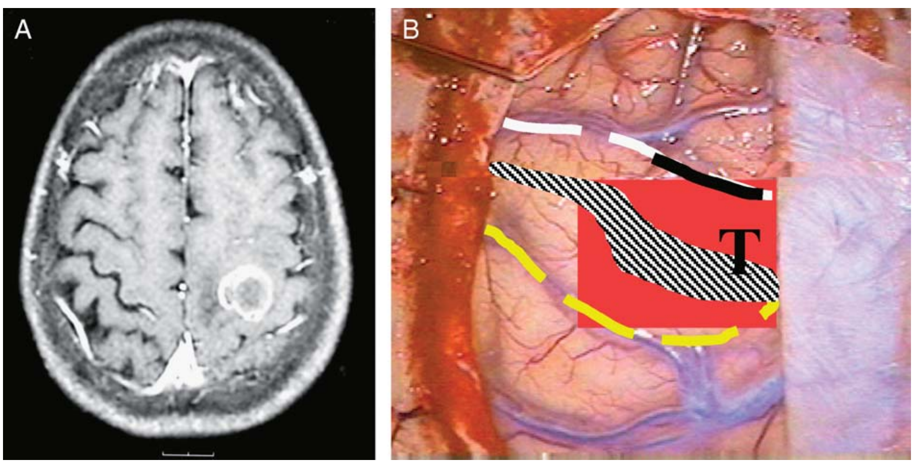

Fig. **2** Critically located tumors. **A** Single metastatic tumor on the left precentral gyrus. **B** Determining the proper entry point and removing the tumor (T = tumor, white dotted line = precentral gyrus, yellow dotted line = postcentral gyrus, striped area = motor strip mapping, black line = cortical incision).

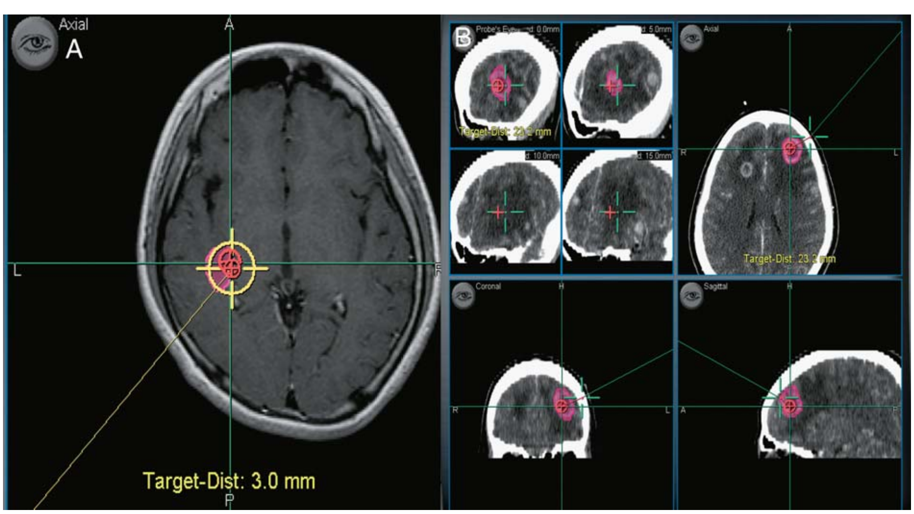

Fig. **3** Deep-seated small tumors and subcortical tumors. **A** Localizing the deep-seated small tumors on the vertical and shortest trajectory. **B** Exactly targeting subcortical tumors.

tumor under navigational guidance. In one patient, a 1 cm enhancing mass located in the left deep temporal lobe was visualized on the MR images. Using the three-dimensional images displayed on the computer screen, we localized the mass on the vertical and shortest surgical trajectory and performed the operation using the posterior middle temporal gyrus approach (Fig. **3A**).

Subcortical tumors

A 1.5 cm enhancing mass that was located in the left subcortical frontal lobe in one patient was visualized on the MR images. In the case of this small subcortical tumor, we exactly targeted the mass on the vertical surgical trajectory (Fig. **3B**). We performed a small craniotomy and easily removed the mass.

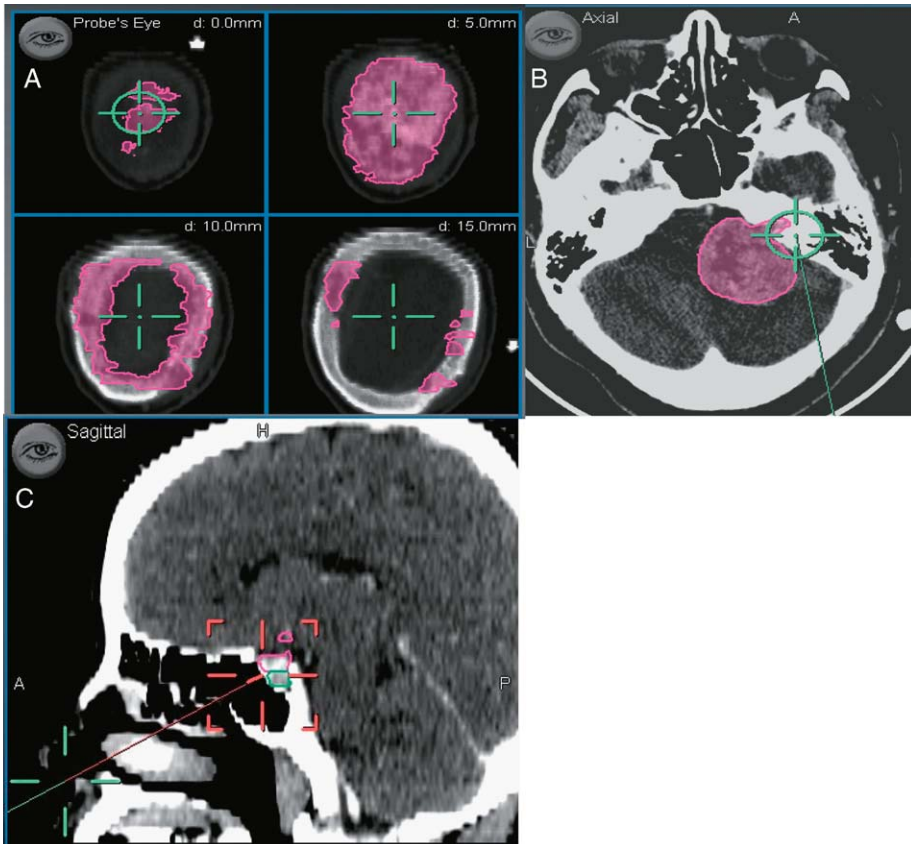

Fig. **4** Bone tumors and skull-base tumors. **A** Targeting multiple masses of the invaded bone structures. **B** Safe internal debulking and unroofing of the internal acoustic canal. **C** Localizing the sphenoid bone and the pituitary mass without the aid of the C-arm.

Bone tumors and skull-base tumors

Image-guided surgery was also utilized for some of the skull-base or skull bone tumor surgeries. The bone structure was rendered immovable. After the head was positioned with the surgical head frame, the skull bone tumor was delineated and removed. In cases of chordoma and metastatic bone tumor, we were able to easily map out the single or multiple masses of the invaded bone structures (Fig. **4A**).

In cases of vestibular schwannoma surgery, we were able to safely perform internal debulking and unroofing of the internal acoustic canal (Fig. **4B**). In cases of pituitary adenoma, we were easily able to localize the sphenoid bone and the pituitary mass without the aid of the C-arm (Fig. **4C**).

Tumors with indistinct margins, especially glioma

In one such case, the MRI scan revealed a 4 cm ring-enhanced right parietotemporal lobe mass with surrounding edema. To minimize the brain shift and local tissue deformation, excessive mannitolization and hyperventilation were avoided and we performed the MRI scanning in the morning just before the surgery. We localized the mass on the vertical surgical trajectory, performed early dissection of the tumor margin using CUSA and removed the mass in an en bloc fashion (Figs. **5A** and **B**).

In one patient, the MRI scan revealed a 6 cm sized ring-enhanced mass in the right frontotemporal lobe with substantial surrounding edema. After inserting multiple catheters to act as markers for the boundaries of the mass, the tumor was removed. In general, we attempted to remove tumors with poor margins in an en bloc fashion and, if this was not possible, we removed the boundaries first and then the central portion later (Figs. **5C** and **D**).

Application 3: biopsy

Brain tumor biopsy

We performed tumor biopsy under navigational guidance using a conventional stereotactic biopsy instrument. Numerous surgical biopsy procedures were performed with this navigation system, with the adaptors being simply screwed onto the surgical instruments.

Endoscopic biopsy and 3rd ventriculostomy

We utilized the neuronavigation system to perform endoscopic biopsy and third ventriculostomy as one of the initial treatment options in patients with a pineal tumor accompanying hydrocephalus. With this system, we defined the optimal combination of trajectories and entry-points for third ventriculostomy and tumor biopsy. We used a rigid endoscope and made use of 2 different trajectories through 2 different burr holes, one for pineal biopsy and the other for 3rd ventriculostomy.

Discussion

Conventional stereotactic frame systems have recently been modified to accept CT or MRI images. Horsley and Clark first reported stereotactic operations in animals in 1908 [8]. Almost 40 years later, Spiegel et al. introduced the stereotactic method into clinical use [9]. Stereotactic head frames compatible with CT or MR imaging systems are widely used for tumor biopsy or for

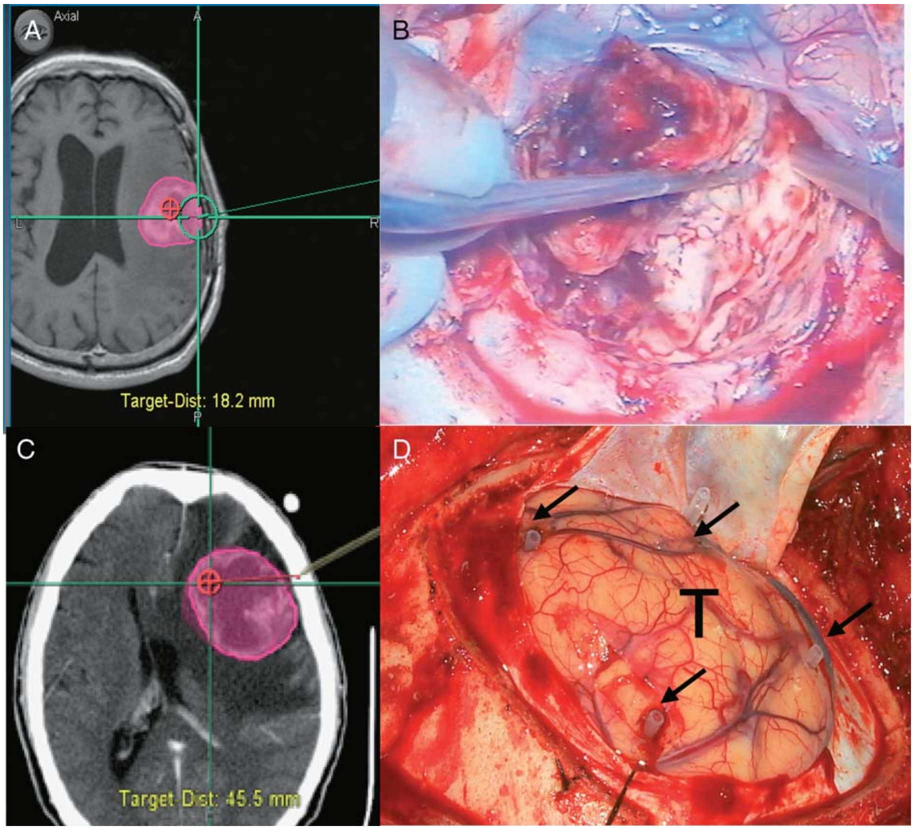

Fig. **5** Tumors with indistinct margins. **A**, **B** Early dissection of tumor margin and removal of the tumor in an en bloc fashion. **C**, **D** Insertion of multiple catheters on the boundaries to act as markers (short arrow = catheter, T = tumor).

aspiration of intracranial hematoma. The target localization with these head frames is very accurate, but their application to standard open surgery can impede the operative process. The route of surgical approach seems somewhat limited. Moreover, the operator cannot obtain the anatomical information intraoperatively.

In 1986, Roberts et al. reported the development of a frameless, computer-based system for the integration and display of CT image data obtained with the operating microscope [5]. Because of the ultrasonic pulses used by this technique, ultrasonic noise and drafts in the operating room may interfere with the technique. Watanabe et al. described the multi-joint arm-guided navigational system [10,11]. Several other authors have reported their developments and experiences with arm-based navigation systems. In this system, one end of the multi-joint arm is fixed to the skull clamp or the surgical table, and the free end of the arm is used as a pointing device, which is introduced into the surgical field with the assistance of the preoperative CT images. However, the long articulated arm can cause considerable inconvenience in the operative field.

To solve the above problems, various armless image-guided systems have been proposed, using magnetic, sonic and optical digitalization. However, most of these frameless and armless navigational systems have recently switched to using the passive reflection of infrared flashes. These infrared systems are highly accurate, insensitive to the room temperature and light, and use a relatively simple infrared emitter [12]. The BrainLab VectorVision® neuronavigation system has infrared light-emitting diodes (LEDs) that are positioned around the cameras for the purpose of detecting the positions of objects.

The most important factor in neuronavigation systems is accuracy, which is determined by the technical accuracy, the registration accuracy and the target-localizing accuracy resulting from positioning, mannitol application and cerebral spinal fluid drainage. The digitizer accuracy of the Brainlab system, tested on a phantom, was less than 0.5 mm, which was similar to that of other systems, and the registration accuracy was 1.4 mm (with a standard deviation of 0.5 mm) [6]. In our department, most of the registration accuracies were less than 2 mm, but 13 of 420 patients had a registration accuracy of more than 2 mm. Those factors affecting the accuracy include changes during scanning, location change of the fiducial markers, head position on the operating table and movement of the scalp with respect to the pin fixations on the headrest frame. Therefore, for biopsies of small lesions and surgical treatment of small, deeply located thalamic lesions, where a precision of 1 to 2 mm is required, Gumprecht et al. preferred the frame-based stereotactic approach [13]. Galloway suggested that the registration accuracy is related to the CT or MRI slice thickness [14]: the smaller the slice thickness, the higher is the accuracy. In our department, CT or MRI images were scanned with 1.5 to 2.5 mm slices. If the registration accuracy was more than 2 mm, we performed re-registration. This procedure restored the initial registration of the patient, which was kept in the computer memory. Using three-dimensional images on the computer screen, the operator identified those fiducial markers whose positions had changed and re-registered them to their initial location before they were moved. In our experience, six fiducials should be glued to the head of the patient in such a way as to maximize the occupied space, in order to improve the registration accuracy.

Many surgical procedures can be performed with this navigation system. Recently, neuronavigator systems have been used for operations other than brain tumor surgery. Once the adaptors are screwed onto the surgical instruments (bipolar forceps, suction tubes, endoscopes, and catheters), endoscopic procedures, catheter placement into cerebral cysts, puncture of very small ventricles and biopsies can be performed. In our department, this technique was used for a variety of surgical methods, including tissue biopsy in 26 patients, for endoscopic surgery in 12 patients and for ventriculostomy in 1 patient. After craniotomy or partial removal of large intraparenchymal tumors, brain shifting renders the navigation system relatively useless. Updating of the anatomic features during surgery, by using ultrasonography, intraoperative CT or MRI scanning can help overcome this difficulty [15]. To minimize the brain shift, we avoided the use of mannitol, hyperventilation, and diuretics. Whenever possible, we tried to remove the boundaries of the tumor first and then the central portion later in an en bloc fashion, especially for glioma with indistinct margins, after inserting multiple catheters on the boundaries as markers. We also did not attempt ventricular puncture and cyst drainage during the early stages of the operations.

The navigation system is very useful for planning the surgical approach. The skin incisions and craniotomies were smaller when using this system than without it. Using virtual planning of the trajectory, we never performed an exploration with negative results.

References

1. Lunsford LD. Magnetic resonance imaging stereotactic thalamotomy: report of a case with comparison to computed tomography. Neurosurgery 1988; 23: 363–367
2. Leksell L, Leksell D, Schwebel J. Stereotaxis and nuclear magnetic resonance. J Neurol Neurosurg Psychiatry 1985; 48: 14–18
3. Barnett GH, Kormos DW, Steiner PC, Weisenberger J. Use of a frameless, armless sterotactic wand for brain tumor localization with two-dimensional and three-dimensional neuroimaging. Neurosurgery 1993; 33: 674–678
4. Guthrie BL, Adler JR Jr. Frameless stereotaxy: computer interactive neurosurgery. Perspect Neurol Surg 1991; 2: 1–22
5. Roberts DW, Strohbein JW, Hatch JF, Murray W, Kettenberger H. A frameless stereotactic integration of computerized tomographic imaging and the operative microscope. J Neurosurg 1986; 65: 545–549
6. McInerney J, Roberts DW. Frameless sterotaxy of the brain. Mt Sinai J Med 2000; 67: 300–301
7. Schulder M, Sernas TJ, Carmel PW. Cranial surgery and navigation with a compact intraoperative MRI system. Acta Neurochir Suppl 2003; 85: 79–86
8. Horsley V, Clarke RH. The structure and the function of the cerebellum examined by a new method. Brain 1908; 31: 45–124
9. Spiegel EA, Wycis HT, Marks M, Lee AJ. Stereotaxic apparatus for operations on the human brain. Science 1947; 106: 349–350
10. Watanabe E, Watanabe T, Manaka S, Mayanagi Y, Takakura K. Three-dimensional digitizer (Neuronavigator): new equipment for computed tomographic-guided stereotaxic surgery. Surg Neurol 1987; 27: 545–547
11. Watanabe E, Mayanagi Y, Kosugi Y, Manaka S, Takakura K. Open surgery assisted by the Neuronavigator, a stereotactic, articulated, sensitive arm. Neurosurgery 1991; 28: 792–800
12. Bucholz RD, Smith KR. A comparison of sonic digitizers versus light emitting diode-based localization. In: Maciunas RJ (editor). Image-guided Committee. Neurosurgery. AANS publications, 1994; 179–200
13. Gumprecht HK, Widenka DC, Lumenta CB. Brain vector vision neuronavigation system: technology and clinical experience in 131 cases. Neurosurgery 1999; 44: 97–105
14. Galloway RL, Maciunas RJ. An articulated localizing arm for neurosurgical use. In: Maciunas RJ (editor). Interactive Image-Guided Neurosurgery. Park Ridge, American Associated of Neurosurgical Surgeon, 1993; 159–168
15. Giorgi C, Casolino DS, Eisenberg MS, Eisenberg HM. Intraoperative image fusion in microneurosurgery: ultrasound and MRI/CT data superimposed to optical images. Comp Aid Surg Abstracts from CIS 1997; 97: 7–35

Endoscopic Carpal Tunnel Release in the Elderly

M. Nagaoka
S. Nagao
H. Matsuzaki

Abstract

The present study is aimed to clarify the postoperative outcome of endoscopic carpal tunnel release in elderly patients with carpal tunnel syndrome. Endoscopic carpal tunnel release was performed on 37 hands of 27 patients (2 men, 25 women) who were aged 70 years or older and clinically and electrophysiologically diagnosed with carpal tunnel syndrome. Mean age at the time of surgery was 74.5 years (range: 70–85 years). Mean postoperative follow-up was 35.5 months (range: 12–114 months). Pain was present preoperatively in 20 hands, but quickly resolved postoperatively in all cases. Numbness completely disappeared in 13 of 37 hands (35.1 %), but some degree of numbness remained in the remaining cases. Preoperative severity of thenar muscle atrophy was none in 4 hands, mild in 7 hands, moderate in 12 hands and severe in 14 hands. Postoperative severity of thenar muscle atrophy at final follow-up was none in 13 hands, mild in 16 hands, moderate in 2 hands and severe in 6 hands, confirming that thenar muscle atrophy improves even in elderly patients. However, moderate or severe thenar muscle atrophy remained in 8 hands (21.6 %). Endoscopic carpal tunnel release should be considered in the elderly, even though clinical symptoms may not improve substantially in advanced cases.

Key words

Carpal tunnel syndrome · entrapment neuropathy · endoscopic carpal tunnel release · elderly patients

Introduction

Carpal tunnel syndrome (CTS) is commonly found in middle-aged women [1–3], but it can also affect elderly individuals. Clinical manifestations of CTS in the elderly are often severe according to previous reports [4,5]. Recently, the surgical outcome in elderly patients has been the focus of many studies [6–12]. However, no studies have investigated the outcome of endoscopic carpal tunnel release (ECTR) in elderly patients. The present study was conducted to ascertain whether the same satisfactory results of open carpal tunnel release (OCTR) can be obtained through ECTR in patients aged 70 years or older with CTS.

Patients and Methods

Subjects comprised 27 patients (37 hands; 2 men, 25 women) with CTS who were aged 70 years or older and underwent ECTR between 1992 and 2000. In all cases, preoperative diagnosis of carpal tunnel syndrome was confirmed by electrophysiological testing. At the time of surgery, mean age was 74.5 years (range: 70–85 years). CTS was unilateral in 17 cases (right hand, n = 10; left hand, n = 7) and bilateral in 10 cases. While patients with diabetes (n = 5) or rheumatoid arthritis (n = 1) were included, patients undergoing dialysis were excluded. In addition, patients who wished to improve thumb opposition early were excluded from the present series, and instead underwent surgery to reconstruct thumb opposition. Mean postoperative follow-up was 35.5 months (range: 12–114 months).

Affiliation
Orthopaedic Department, Surugadai Nihon University Hospital, Tokyo, Japan

Disclaimer
No benefits in any form have been or will be received from any commercial party related directly or indirectly to the subject of this article.

Correspondence
Masahiro Nagaoka, M.D. · Orthopaedic Department · Surugadai Nihon University Hospital · 1-8-13 Kanda Surugadai · Chiyoda-ku · Tokyo 101-8309 · Japan · Tel.: + 81/3/3293/17 11 · Fax: + 81/3/3292 03 07 · E-mail: mnagaoka@mub.biglobe.ne.jp

Bibliography
Minim Invas Neurosurg 2006; 49: 216–219 © Georg Thieme Verlag KG · Stuttgart · New York
DOI 10.1055/s-2006-947999
ISSN 0946-7211

Two-portal ECTR was performed according to the methods described by Chow [13]. In the 10 bilateral cases, staged ECTR was performed on 7 patients (14 hands), and simultaneous ECTR was performed on 3 patients (6 hands). Either local anaesthesia or axillary block was induced, and ECTR was performed by the senior author in all cases.

Preoperative numbness was classified as intermittent or persistent with respect to the presence or absence of pain [14]. Postoperative severity of numbness was classified as: 0) completely disappeared; 1) mild numbness remaining only at the fingertips; 2) no pain, but some remaining numbness; and 3) no improvement or exacerbation. A Semmes-Weinstein monofilament test was conducted to assess sensory function, and severity of thenar muscle atrophy was classified as severe, moderate, mild or none. Mild atrophy comprised slight flattening of the abductor pollicis brevis muscle in the resting position, evident only when the contour was compared to the unaffected hand. Moderate atrophy involved a more visibly apparent flattening of the thenar eminence, evident without comparison to the unaffected hand. Severe atrophy was considered present when the anterior border of the first metacarpal bone beneath the abductor pollicis brevis was palpably evident. Strength of the abductor pollicis brevis was graded from 0 to 5, according to the criteria of the American Orthopaedic Association [15] and pre- and postoperative changes were assessed. Changes in key pinch and pulp pinch strength were assessed pre- and postoperatively in 35 and 26 hands, respectively.

As an electrophysiological test, distal latency of the abductor pollicis brevis and sensory nerve conduction velocities between the wrist and middle finger were measured preoperatively in all cases. Patient consent for measurement was not obtained for 6 hands postoperatively, so the above 2 parameters were measured pre- and postoperatively in 31 hands.

Results

No major complications associated with ECTR were identified.

Preoperatively, intermittent numbness was seen in two hands, with persistent numbness in the remaining 35 hands. The two hands with intermittent preoperative numbness displayed complete resolution of symptoms. Among the 35 hands that exhibited persistent numbness preoperatively, the severity of numbness improved to 3 in 0 hands, 2 in 13 hands, 1 in 11 hands, and 0 in 11 hands.

Preoperative pain was present in 20 hands, but resolved rapidly in all cases after endoscopic release, and no patients complained of pain on final observation. Among the 20 hands with preoperative pain, postoperative severity of numbness was 3 in 0 hands, 2 in 11 hands and 1 in 7 hands.

Marking as assessed by Semmes-Weinstein monofilament tests was the same before and after surgery in only 3 hands. In the other 34 hands, marking improved by more than one grade (Fig. **1**). Preoperative severity of muscle atrophy was none in 4 hands, mild in 7 hands, moderate in 12 hands and severe in 14 hands. Postoperative severity of muscle atrophy was none in 13 hands, mild in 16 hands, moderate in 2 hands and severe in 6 hands. Regarding changes before and after surgery for each level of severity, among the 7 hands with mild atrophy, severity of atrophy changed to none in 5 hands and remained mild in 2 hands; among the 12 hands with moderate atrophy, severity of atrophy changed to none in 4 hands and mild in 8 hands; among the 14 hands with severe atrophy, severity of atrophy changed to mild in 6 hands and moderate in 2 hands, but remained severe in 6 hands (Table **1**).

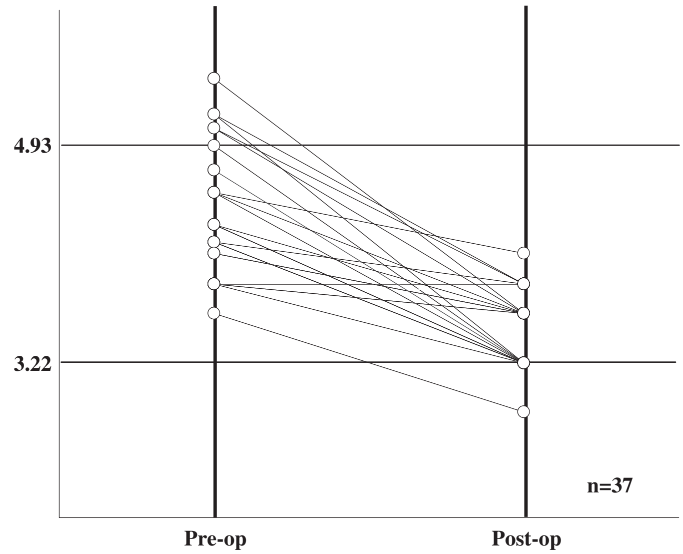

Fig. **1** Changes in Semmes-Weinstein monofilament marking.

Table **1** Changes in severity of thenar muscle atrophy (no. of hands)

Pre op \ Post op	*None*	*Mild*	*Moderate*	*Severe*
None	4	0	0	0
Mild	5	2	0	0
Moderate	4	8	0	0
Severe	0	6	2	6

Preoperative strength of the abductor pollicis brevis was 5 in 3 hands, 4 in 13 hands, 3 in 36 hands, 2 in 0 hands and 0 or 1 in 8 hands, while postoperative strength of the abductor pollicis brevis was 5 in 15 hands, 4 in 14 hands, 3 in 20 hands, 2 in 0 hands and 0 or 1 in 4 hands.

Mean key pinch was 3.6 ± 1.4 kg preoperatively, compared to 4.5 ± 1.4 kg postoperatively. Mean pulp pinch was 2.4 ± 1.1 kg preoperatively, compared to 3.2 ± 1.1 kg postoperatively (Fig. **2**).

Regarding electrophysiological findings, all 37 hands underwent preoperative testing, and compound muscle action potentials (CMAPs) could not be evoked from the abductor pollicis brevis in 14 hands (37.8 %). Mean distal latency for hands with CMAP was 8.1 ± 3.0 ms. Similarly, sensory nerve conduction velocities

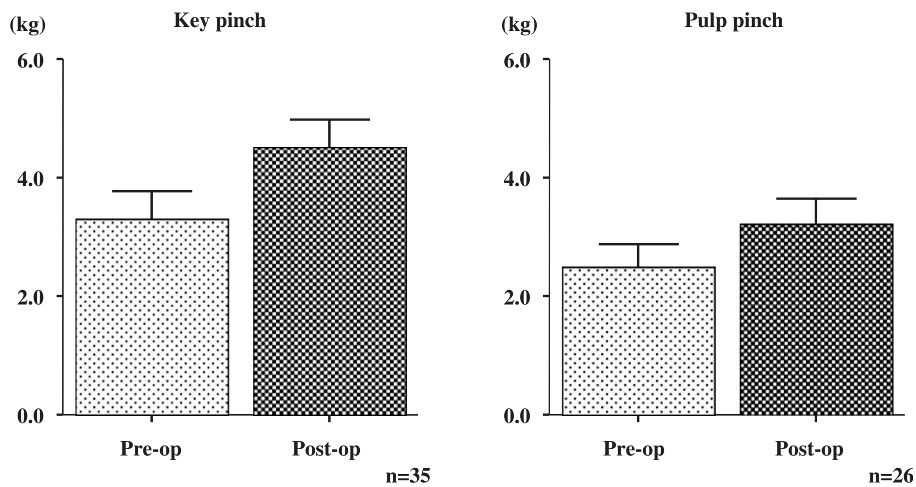

Fig. **2** Changes in key and pulp pinch strength.

between the wrist and middle finger could not be evoked in 29 hands (78.4 %).

In the 31 hands in which electrophysiological testing was performed before and after surgery, CMAPs could not be evoked from the abductor pollicis brevis in 11 hands (35.5 %) preoperatively and 4 hands (12.9 %) postoperatively. In the 7 hands in which CMAPs were evoked postoperatively, mean distal latency was 4.7 ± 0.9 ms. Among hands in which distal latency of the abductor pollicis brevis could be measured preoperatively, values improved from a preoperative mean of 8.0 ± 2.9 ms to a postoperative mean of 4.1 ± 0.6 ms.

Even in the presence of moderate or severe thenar muscle atrophy (n = 26), thumb opposition was not impaired in 4 hands. Thumb opposition was impaired preoperatively in 22 hands, but improved in 17 hands. In one hand, the trapeziometacarpal joint was severely arthritic, and while thenar muscle atrophy improved, opposition was not possible. Slight thumb opposition was possible starting at a mean of 5.1 months postoperatively (range: 2–15 months). At the time of final follow-up, impairment of thumb opposition had not improved in 4 hands. These patients were given the option of secondary tendon transfer, but none wanted to undergo additional surgery.

Discussion

Carpal tunnel syndrome is uncommon in elderly patients [1, 3]. Phalen's study contained only 37 patients who were aged 70 years or older out of 384 total patients (9.6 %) [3], and the study by Stevens et al. contained only 85 out of a total of 1016 (8.4 %) [16]. Among studies on CTS in the elderly, Seror examined 100 hands of 57 CTS patients aged 70 years or older, and reported that electrophysiological severity of CTS was more severe, while duration of symptoms prior to diagnosis was shorter when compared to middle-aged patients (50- to 60-year-olds) [5]. However, no mention was made of surgical outcome.

Recently, the surgical outcome of elderly patients has been the focus of many studies [6–12]. Porter et al. compared outcomes for carpal tunnel release among different age groups, and reported differences in the degree of improvement in symptom severity scores between patients above and below the age of 60 years, with age representing a clear factor affecting outcomes after carpal tunnel release [8]. According to studies conducted by Leit et al., carpal tunnel release is unlikely to result in total elimination of symptoms or complete restoration of function when performed in elderly patients with advanced disease [9]. However, they reported favourable patient satisfaction, and thus concluded that surgery is indicated for elderly patients with advanced disease. Comparable findings were reported in studies by Mondelli et al., Weber et al., and Townshend et al. [10–12].

These previous studies investigated the open method [6–12]. The present study was conducted because no studies have yet examined the outcomes of ECTR among elderly patients. In the present study, thenar muscle atrophy was moderate or severe preoperatively in 26 hands (70.3 %). In addition, CMAP could not be evoked from the abductor pollicis brevis by electrophysiological testing in 37.8 % of cases. CTS was thus severe in many cases, supporting the findings of previous reports on open carpal tunnel release.

Pain represented the biggest concern for patients, and was resolved in all cases. While patients were generally satisfied and numbness completely disappeared in 13 of the 37 hands (35.1 %), some degree of numbness persisted in the remaining cases. Furthermore, moderate or severe thenar muscle atrophy remained in 8 of the 37 hands (21.6 %). In our previous study, which was not age specific, moderate or severe thenar muscle atrophy remained in 8 of 68 patients (11.9 %) [17]. Therapeutic outcomes were thus poorer for elderly patients.

Thorough preoperative consultation is necessary to determine whether to reconstruct thumb opposition in patients with impaired thumb opposition. Even when elderly patients complain of impaired thumb opposition, some do not wish to undergo surgery to reconstruct thumb opposition, as this surgery is more invasive than the endoscopic release. Furthermore, in elderly patients, the frequency of arthritis of the trapeziometacarpal joint is high. There have been many studies concerning the coexistence of CTS and arthritis of the trapeziometacarpal joint, which has a negative effect on the outcome of opponensplasty [18, 19].

We believe that the results of our study compared favourably to the results of previous studies involving OCTR. We encountered similar rates of improvement and a similar likelihood of advances cases to show little or no improvement. The advantage of ECTR is that it offers the patient an earlier return to the activities of daily life.

References

1 Hybbinette CH, Mannerfelt L. The carpal tunnel syndrome. A retrospective study of 400 operated patients. Acta Orthop Scand 1975; 46: 610–620

2 Padua L, Padua R, Aprile, Tonali P. Italian multicentre study of carpal tunnel syndrome. Differences in the clinical and neurophysiological features between male and female patients. J Hand Surg [Br] 1999; 24: 579–582

3 Phalen GS. The carpal-tunnel syndrome. Clinical evaluation of 598 hands. Clin Orthop Relat Res 1972; 83: 29–40

4 Bodofsky EB, Campellone JV, Wu KD, Greenberg WM. Age and the severity of carpal tunnel syndrome. Electromyogr Clin Neurophysiol 2004; 44: 195–199

5 Seror P. Carpal tunnel syndrome in the elderly. "Beware of severe cases". Ann Chir Main Memb Super 1991; 10: 217–225

6 Todnem K, Lundemo G. Median nerve recovery in carpal tunnel syndrome. Muscle Nerve 2000; 23: 1555–1560

7 Tomaino MM, Weiser RW. Carpal tunnel release for advanced disease in patients 70 years and older: does outcome from the patient's perspective justify surgery? J Hand Surg [Br] 2001; 26: 481–483

8 Porter P, Venkateswaran B, Stephenson H, Wray CC. The influence of age on outcome after operation for the carpal tunnel syndrome. A prospective study. J Bone Joint Surg [Br] 2002; 84: 688–691

9 Leit ME, Weiser RW, Tomaino MM. Patient-reported outcome after carpal tunnel release for advanced disease: a prospective and longitudinal assessment in patients older than age 70. J Hand Surg [Am] 2004; 29: 379–383

10 Mondelli M, Padua L, Reale F. Carpal tunnel syndrome in elderly patients: results of surgical decompression. J Peripher Nerv Syst 2004; 9: 168–176

11 Townshend DN, Taylor PK, Gwynne-Jones DP. The outcome of carpal tunnel decompression in elderly patients. J Hand Surg [Am] 2005; 30: 500–505

12 Weber RA, Rude MJ. Clinical outcomes of carpal tunnel release in patients 65 and older. J Hand Surg [Am] 2005; 30: 75–80

13 Chow JC. Endoscopic release of the carpal ligament for carpal tunnel syndrome: 22-month clinical result. Arthroscopy 1990; 6: 288–296

14 Rosen B, Lundborg G, Abrahamsson SO, Hagberg L, Rosen I. Sensory function after median nerve decompression in carpal tunnel syndrome. Preoperative vs postoperative findings. J Hand Surg [Br] 1997; 22: 602–606

15 American Orthopaedic Association. Manual of Orthopaedic Surgery. Chicago: American Orthopaedic Association, 1979; 27–31

16 Stevens JC, Sun S, Beard CM, O'Fallon WM, Kurland LT. Carpal tunnel syndrome in Rochester, Minnesota, 1961 to 1980. Neurology 1988; 38: 134–138

17 Nagaoka M, Nagao S, Matsuzaki H. Endoscopic release for carpal tunnel syndrome accompanied by thenar muscle atrophy. Arthroscopy 2004; 20: 848–850

18 Florack TM, Miller RJ, Pellegrini VD, Burton RI, Dunn MG. The prevalence of carpal tunnel syndrome in patients with basal joint arthritis of the thumb. J Hand Surg [Am] 1992; 17: 624–630

19 Melone CP Jr., Beavers B, Isani A. The basal joint pain syndrome. Clin Orthop Relat Res 1987; 220: 58–67

Morphological Study of the Spinal Canal Content for Subarachnoid Endoscopy

M. Zaaroor[1]
G. Kósa[2]
A. Peri-Eran[3]
I. Maharil[4]
M. Shoham[2]
D. Goldsher[3]

Abstract

Study Design and Objective: This study was designed to examine the morphology of the spinal dural sac and contents, using magnetic resonance imaging in order to define the inner geometrical dimensions that confine the manoeuvre of an endoscope inserted in the lumbar region and along the thoracic and cervical spine. **Background:** The morphology of the spine has been studied since the development of myelography. However, most studies have measured the diameters of the spinal cord only, not the size of the subarachnoid space. In addition, the few studies available on the subarachnoid space have focused on the cervical spine, leaving a near-complete dearth of data on the subarachnoid space dimensions along the thoracic spine. **Methods**: Based on MRI images of the spine from 42 patients, the dimensions of the spinal cord, dural sac, and subarachnoid space were measured at mid-vertebral and inter-vertebral disc levels. **Results:** It was found that at each selected transverse level, the subarachnoid space tends to be symmetrical on the right and left sides of the cord, and measures 2.5 mm on average. However, the posterior and anterior segments, measured on the mid-sagittal plane, are generally asymmetrical and vary widely in size, ranging from 1 to 5 mm. These measurements match those found in previous studies, where these are available. The coefficient of variance for the dimensions of the subarachnoid space is as high as 42.4 %, while that for the dimensions of the spinal cord is 10–15 %. **Conclusions:** The findings presented here expand our knowledge of the spinal canal's morphology, and show that an endoscope designed to travel within the subarachnoid space must be smaller than 2.5 mm in diameter.

Key words

Subarachnoid space · spinal canal · morphology · MRI · endoscopy

Introduction

Endoscopic treatment of various anatomical areas is an expanding field in modern medicine. Endoscopic visualization of the spinal canal contents is still limited, partly because of the technical problems inherent in developing a miniature device that fits into and is safely steered inside the delicate and hazardous area of the spinal canal and the subarachnoid space. Meeting these challenges requires a clear understanding of the spinal canal morphology, and accurate measurement of its different compartments.

The aim of this investigation is to detail the dimensions of the subarachnoid space as prerequisite for an ongoing project of developing a steerable endoscope for the spinal canal under the EU's MINOSC project.

Affiliation
[1]Department of Neurosurgery, Rambam Medical Center, Haifa, Israel
[2]Medical Robotics Laboratory, Department of Mechanical Engineering, Technion–Israel Institute of Technology, Haifa, Israel
[3]Department of Radiology, Rambam Medical Center, Haifa, Israel
[4]Department of Orthopedic Surgery, Carmel Medical Center, Haifa, Israel

Correspondence
Prof. Moshe Shoham · Medical Robotics Laboratory · Department of Mechanical Engineering · Technion – Israel Institute of Technology · Technion City · Haifa 32000 · Israel · Tel.: + 972/4/829 32 64 · Fax: + 972/4/829 57 11 · E-mail: shoham@technion.ac.il

Bibliography
Minim Invas Neurosurg 2006; 49: 220–226 © Georg Thieme Verlag KG · Stuttgart · New York
DOI 10.1055/s-2006-948000
ISSN 0946-7211

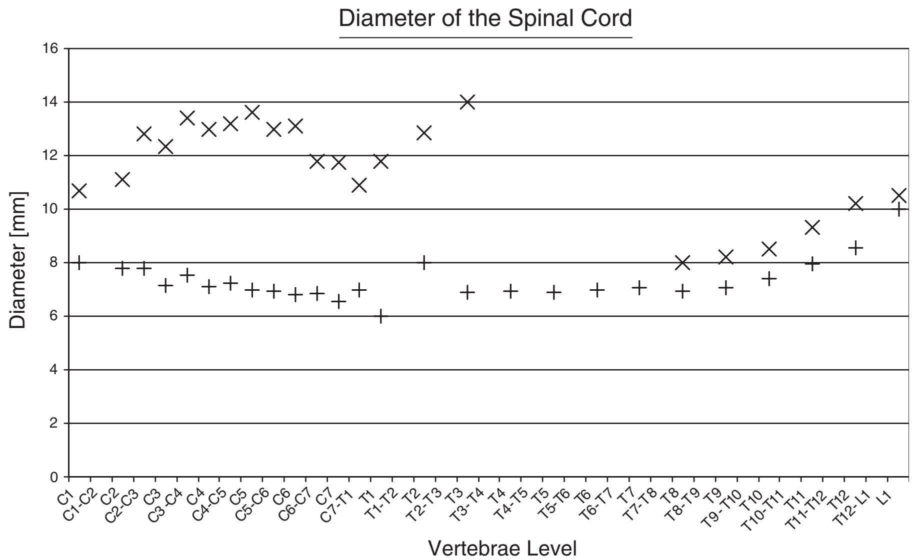

Fig. **1** Transverse (triangle sign and regular error bar) and sagittal (circle sign and bold error bar) diameter of dural sac.

There have been several studies on the dimensions of the dural sac, the subarachnoid space, and the spinal cord. These studies have either been carried out on cadavers, or have used radiological methods such as myelography, CT myelography, and MRI [1–10].

The sagittal and transverse diameters of the spinal cord were studied by pneumo-myelography as early as the 1960s [1]. In those studies, the cord was measured from the level of the second cervical vertebra to the first lumbar vertebral body. Thijssen et al. [2] used CT myelography to measure the sagittal and transverse diameters of the spinal cord. Yu et al. [3] recorded the sagittal and transverse diameters between the vertebrae in the cervical spine (from C2/C3 to C7/T1), also using CT myelography. Yone et al. [4], using MRI, measured the sagittal diameter of the cervical cord at the level of the vertebral body and at the level of the inter-vertebral disc. Fujiwara et al. [5] measured the cross section area and the sagittal and transverse diameters of the cervical spinal cord by comparing cadaver specimens and CT myelography images.

Yirout [6] measured the sagittal diameter of the spinal cord, from C1 to D12, using pneumo-myelography. Yirout also defined the dimensions of the posterior and anterior subarachnoid spaces at the cervical spine. Using CT myelography, Innou et al. [7] measured the sagittal diameter and cross-section area of the spinal cord, the dural sac, and the spinal canal of the cervical spine, and also attempted to determine to what degree these were truly circular in shape. Stanley et al. [8] and Okada et al. [9] measured the same areas using MRI. Muhle et al. [10] conducted an extensive study of the cervical spine, and used MRI to measure the sagittal diameter and the anterior and posterior subarachnoid space. These measurements were made at different angles of neck flexion and extension. Fig. **7** summarizes the published results on the size of the subarachnoid space. The transverse diameter and the anterior and posterior sagittal diameters are the most common measurements used to characterize the subarachnoid space.

Fig. **1** summarizes the published results, illustrating the average (mean) diameter of the spinal cord and its standard deviation for the sagittal (plus) and transverse diameters (cross). The measurements found in previous studies were averaged arithmetically, without taking into consideration differences in group size or the different methodologies (CT, MRI, myelography). As shown in Fig. **1**, even when all previous studies are combined, the data on the spinal cord remain incomplete. For example, to the best of our knowledge, there are no data available on the spinal cord dimensions in the transverse diameter between the T4 and T7 vertebral levels.

There is also a vast information on the morphology of the bony spinal canal. These data permit a rough estimate for the size of the subarachnoid space in which the endoscope is planned to move, but such an estimate would by no means be accurate.

Only a few studies have measured the size of the subarachnoid space [6, 7, 10], and these focused primarily on the cervical spine. Fig. **2** summarizes the published results on the size of the subarachnoid space. The transverse diameter and the anterior and posterior sagittal diameters are the most common measurements used to characterize the subarachnoid space.

The present study complements the current data on the morphology of the spinal contents, and in particular, the spinal subarachnoid space, by analyzing MRI images taken from normal examinations. These data are essential for designing intradural instruments such as spinal endoscope and intradural robotic instruments, as well as for understanding the normal spinal anatomy.

Materials and Methods

Patients

Normal MRI images of 42 patients, 28 males and 14 females, were studied. Overall, 19 studies of the cervical spine and 23 studies of thoracic spine were performed. The patients ranged in age from 16 to 80 years, with an average age of 38.1 years. The

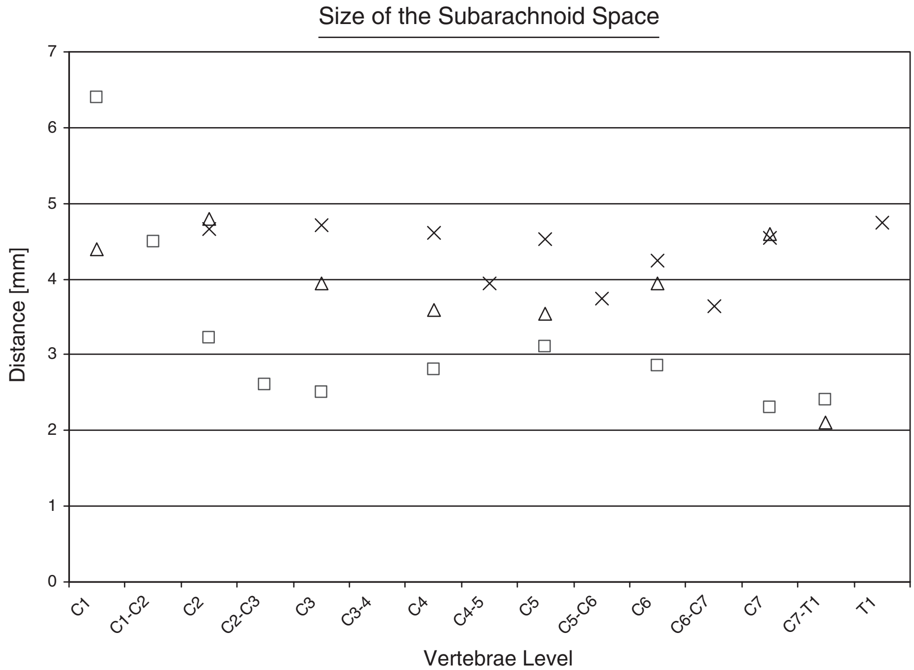

Fig. **2** Transverse (cross), sagittal posterior (square) and sagittal anterior (triangle) dimensions of the subarachnoid space – previously published results.

average height of the patients was 167 cm with a standard deviation of 10 cm. Only normal vertebral and intervertebral disks were included, degenerative cases were omitted.

Measurement method

The geometrical dimensions of the dural sac and the subarachnoid space, from the first cervical vertebra (C1) to the 2nd lumbar vertebra (L2), were measured.

Measured dimensions are marked on a cross-section of a vertebra as illustrated in Fig. **3**. The morphology of the spinal cord was characterized by measurements of the transverse (SCt) and sagittal diameters (SCs). The subarachnoid space was evaluated by measuring the distance between the dura mater and the spinal cord on its left (SAStl), right (SAStr), anterior (SASsa) and posterior (SASsp) aspects. In addition, the sagittal (DSs) and transverse (DSt) diameters of the dural sac were measured. For each segment, the dimensions were obtained at the mid-height of the vertebra, and/or at the level of the adjacent disc (for example, at the mid-height of the 2nd cervical vertebra C2 and the adjacent intervertebral disc – C2/C3).

The number of measurements performed at each level is shown in Table **1**. As this Table illustrates, most findings are based on 15–25 measurements performed at a given level.

Instrumentation

MRI imaging, using a 0.5 T Elscint system that produces standard T_1- (SE) and T_2- (FSE) weighted images, was performed on the axial and sagittal planes for each patient. The dimensions of the spinal cord and the subarachnoid space were measured on the transverse (axial) images, at the mid-sagittal and mid-coronal virtual lines through both the mid-vertebral body height (designated as C3, for example), and the intervertebral disc levels (designated as C3/C4 for example). All measurements were performed using PACS stations (Agfa) and were based mainly

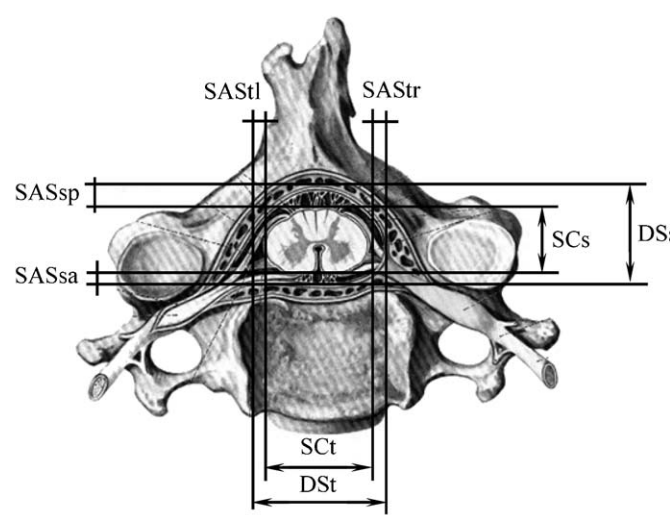

Fig. **3** Cross-section of a vertebra with illustration of the different measurements taken in this study: DSs = sagittal diameter of the dural sac, DSt = transverse diameter of the dural sac, SCs = sagittal diameter of the spinal cord, SCt = transverse diameter of the spinal cord, SASsp = the distance between the arachnoid and the pia on the posterior side of the sagittal diameter, SASsa = the distance between the arachnoid and the pia on the anterior side of the sagittal diameter, SAStl = the distance between the arachnoid and the pia on the left side of the transverse diameter, SAStr = the distance between the arachnoid and the pia on the right side of the transverse diameter.

on the T_2-weighted images, which better delineate the borders of both the spinal cord and the dural sac.

Results

Fig. **4** presents the average diameters and standard deviations obtained for the spinal cord in our study. The transverse (circle sign and bold error bar) and sagittal diameters (triangle sign and regular error bar) are measured from C1 to L1 at every vertebral and intervertebral level. A normal distribution test shows that

Table **1** Number of measurements at each level

Level	*DTt*	*DTs*	*SAStr*	*SASsa*	*SASsp*	*SCt*	*SCs*
C1			1	17	17		19
C1-C2	1	19	3	1	2	1	19
C2	3	18	6	18	18	3	19
C2-C3	6	3	8	4	6	6	19
C3	8	19	16	18	18	8	19
C3-C4	16	5	16	6	16	16	19
C4	16	19	19	18	19	16	19
C4-C5	19	6	16	7	19	19	19
C5	16	19	17	19	19	16	19
C5-C6	18	5	17	4	17	18	19
C6	17	19	19	18	19	17	19
C6-C7	19	7	19	7	19	19	19
C7	19	19	18	19	19	19	19
C7-T1	18	8	15	9	18	18	19
T1	15	19	3	18	19	15	19
T1-T2	3	1	14	1	3	3	17
T2		20	6	17	17	13	18
T2-T3	14		18		14		16
T3	6	23	9	21	20	5	21
T3-T4	18		20		18	18	21
T4	9	22	13	22	22	8	22
T4-T5	20		19		20	20	21
T5	13	22	13	22	22	13	22
T5-T6	19		19		19	19	21
T6	13	22	15	22	22	13	22
T6-T7	19		22		19	19	21
T7	15	23	10	23	23	15	23
T7-T8	22		21		22	22	23
T8	10	23	9	23	23	10	23
T8-T9	21		20		21	20	22
T9	9	23	7	23	23	9	23
T9-T10	20		17		20	20	23
T10	7	23	5	23	23	7	23
T10-T11	17		12		17	17	22
T11	5	22	1	21	21	5	22
T11-T12	12		4		12	12	18
T12	1	18		17	17	1	20
T12-L1	4				4	4	5
L1		3					1

the 25th and 75th percentiles of the measured data fit the normal statistical distribution, with some outlier measurements (none were omitted).

The cervical and thoracic intumescences are well seen in this Figure. The sagittal diameter decreases monotonically from the cervical to the lumbar spine. The coefficient of variance for the sagittal diameter of the spinal cord is 15.7 %, and for the transverse diameter, 11.2 %. A coefficient of 4–10 % is considered normal for biological studies [11].

The dimensions of the subarachnoid space are shown in Figs. **5**, **6**. Fig. **5** presents the posterior and anterior dimensions of the subarachnoid space. This figure shows that the posterior sagittal subarachnoid space (triangle sign and regular error bar) is larger than the anterior part (plus sign and bold error bar) in the

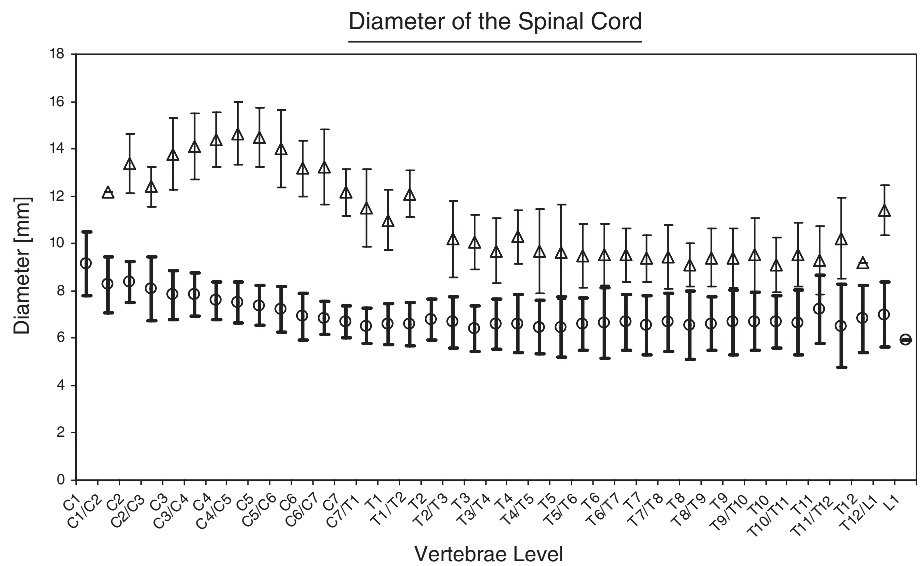

Fig. **4** The sagittal (triangle sign and regular error bar) and transverse (circle sign and bold error bar) diameters of the spinal cord.

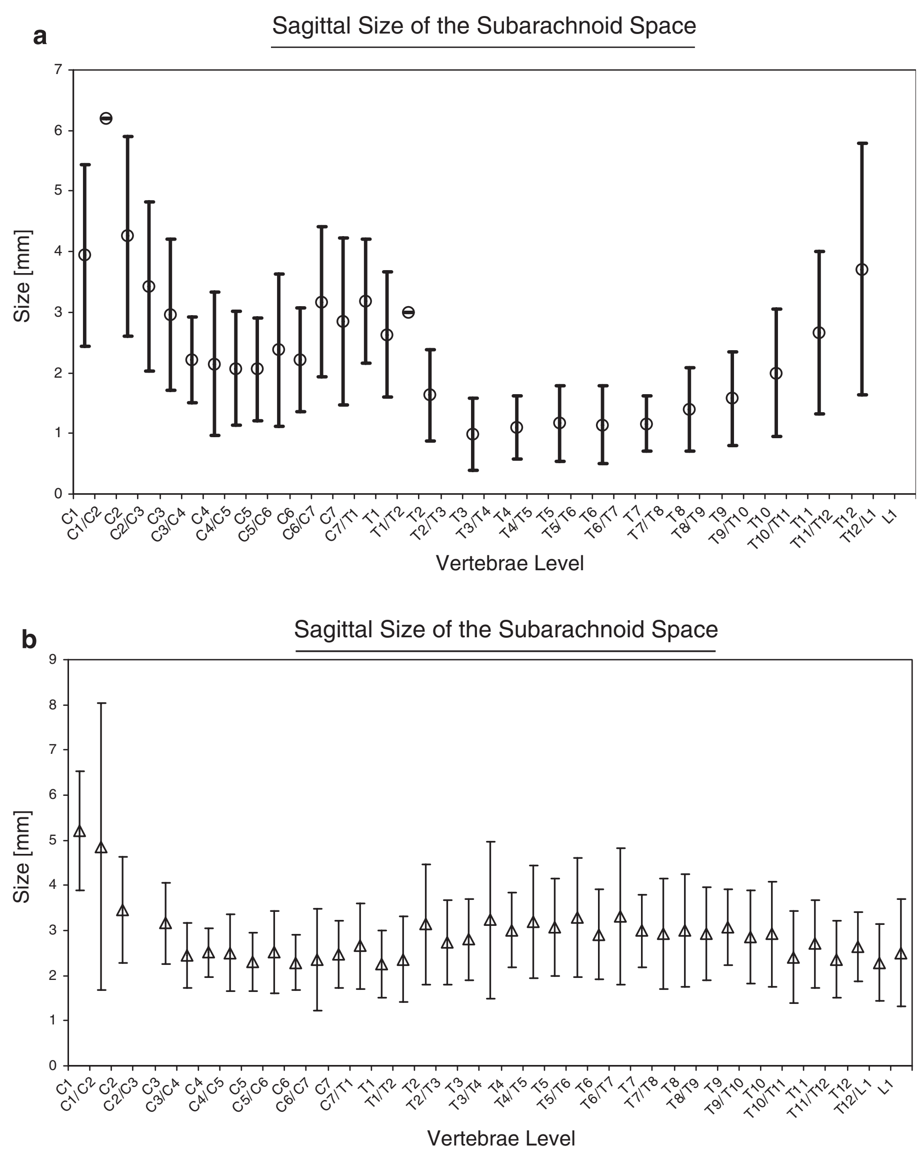

Fig. **5** **a** The sagittal posterior (triangle sign and regular error bar) dimension of the subarachnoid space. **b** The sagittal anterior (circle sign and bold error bar) dimension of the subarachnoid space.

thoracic region, but that the spaces are about equal in the cervical region. The average coefficient of variance is 42.4 % in the anterior region and 36.2 % in the posterior region.

Fig. **6** shows the left and right transverse dimensions of the subarachnoid space. The left (triangle sign and regular error bar) and right dimensions (plus sign and bold error bar) of the

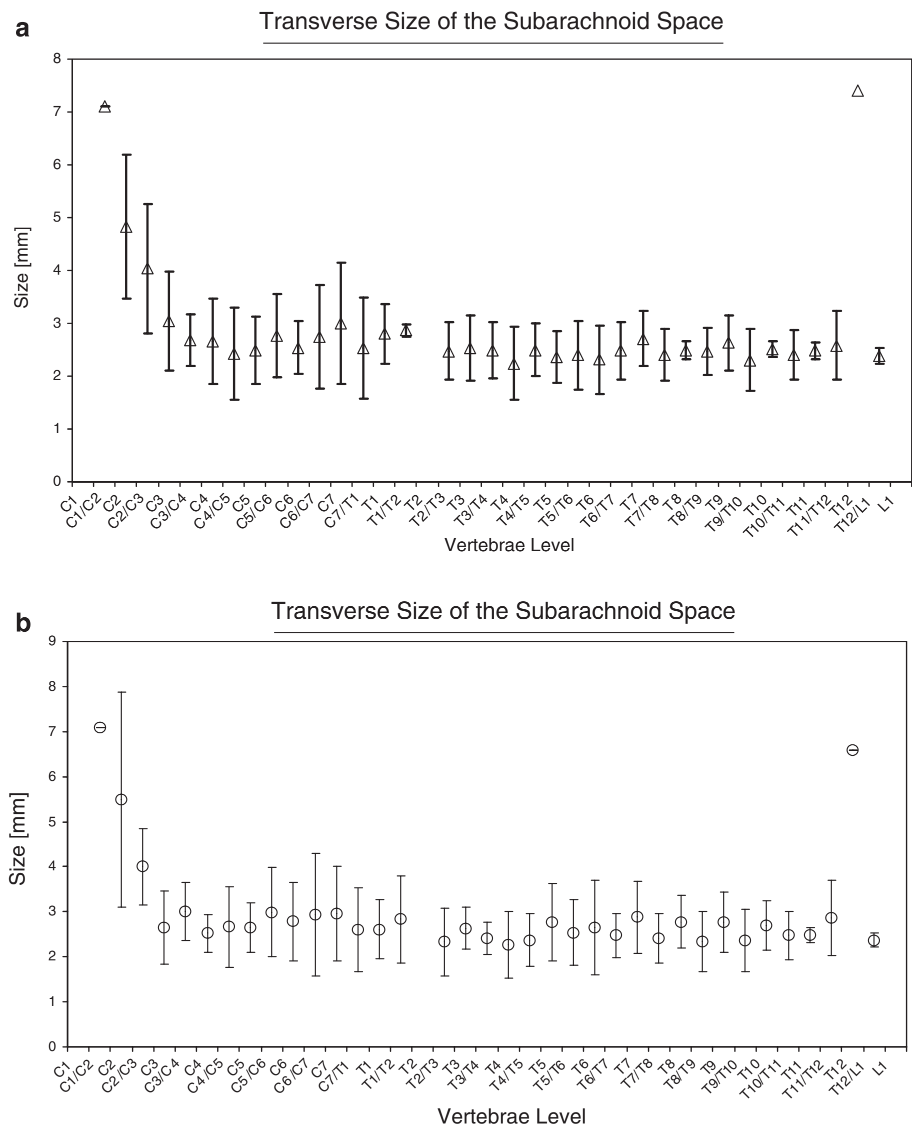

Fig. **6** **a** The transverse left size of the subarachnoid space. **b** The transverse right size of the subarachnoid space.

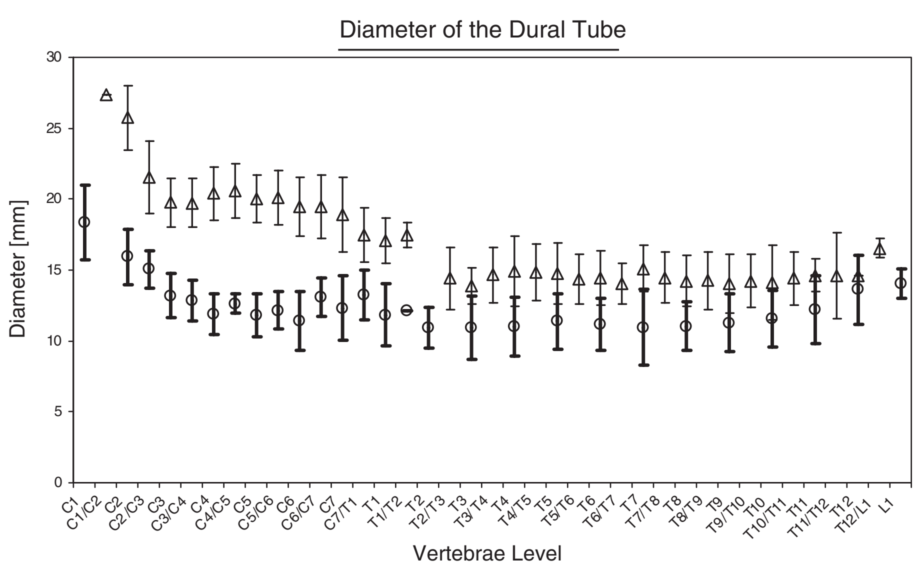

Fig. **7** Transverse (triangle sign and regular error bar) and sagittal (circle sign and bold error bar) diameter of dural sac.

subarachnoid space are similar in size. The coefficient of variance for the transverse subarachnoid space is 21.4 % on the left side and 25.2 % on the right.

To determine the accuracy of the measurements of the spinal cord and subarachnoid space, the dimensions of the dural sac as a whole were measured. Fig. **7** illustrates the transverse (triangle sign and regular error bar) and sagittal (plus sign and bold error bar) diameters of the dural sac. As can be seen, the difference between the sagittal and transverse diameters is smaller in the thoracic region than in the cervical region. The average coefficient of variance for dural sac measurements is 14.2% in the sagittal diameter and 11% in the transverse diameter. The bulge noted in the cervical spinal cord can be observed also in the dural sac.

Shapiro [1] suggested that one could evaluate the dimensions of the spinal cord by finding the ratio between the transverse diameter of the spinal cord and that of the dural sac. We found that this ratio ranges from 0.44 to 0.72, with a mean value of 0.66. The ratio between the sagittal diameters ranges from 0.44 to 0.64, with a mean value of 0.56.

A low correlation was found between the measurements and the height of the patients (average correlation value of 0.32) and the age of the patients (average correlation value of 0.45). No significant differences were noted in the cord or in the dural sac measurements taken at mid-vertebral and adjacent inter-vertebral disks levels.

Conclusions

The current study was prompted by the need to define the dimensions of an endoscope for subarachnoid visualization and treatment. A survey of the literature revealed that the available morphological data on the spine are not complete, and that additional measurements were needed.

We carefully analyzed MRI images of 42 patients, and found that the axial dimensions of the spinal cord and the cervical subarachnoid space match those in the published literature. No earlier study measured in detail the size of the subarachnoid space in the thoracic region, which we found to be 2.5 mm in the laterolateral dimension from both sides of the spinal cord, 3 mm posterior to, and 1 mm anterior to the spinal cord.

The coefficients of variance of the dural sac measurements are similar to those of the spinal cord (14.2% in the sagittal diameter and 11% in the transverse diameter). Even though the variance in size of the subarachnoid space is similar to that of the spinal cord and the dural sac, the coefficients of variance for the subarachnoid space are considerably larger (about 40% in the sagittal view and 22% in the transverse view) since its size is only about quarter of that of the cord.

From design considerations, to design a steerable subarachnoid endoscope or autonomous robotic system, it is possible to advance along the transverse side through the thoracic and cervical spine, with a device diameter of no more than 2.5 mm.

Acknowledgements

This work has been carried out in the framework of the "Quality of Life and Management of Living Resources" European Programme, under the MINOSC Project (Micro Neuroendoscopy of the Spinal Cord). The authors gratefully acknowledge the European Commission for funding this research with contract n. QLG5-CT-2001-02150.

References

1 Shapiro R. Myelography. Chicago: Year Book Medical Publisher, 1975
2 Thijssen HOM, Keyser A, Horstink MWM, Meijer E. Morphology of the cervical spinal cord on computed myelography. Neuroradiology 1979; 18: 57–62
3 Yu YL, du Boulay GH, Stevens JM, Kendall BE. Morphology and measurements of the cervical spinal cord in computer-assisted myelography. Neuroradiology 1985; 27: 399–402
4 Yone K, Sakou T, Yanase M, Ijiri K. Preoperative and postoperative magnetic resonance image evaluation of the spinal cord in cervical myelopathy. Spine 1992; 17: 388–392
5 Fujiwara K, Yonenobu K, Hiroshima K, Ebara S, Yamashita K, Ono K. Morphometry of the cervical spinal cord and its relation to pathology in cases with compression myelopathy. Spine 1988; 13: 1212–1216
6 Yirout Y. Pneumomyelographia. Prague, Gosudarstvennoe Izdatelstvo Medicinskoj Literatury, 1964
7 Inoue H, Ohmori K, Takatsu T, Teramoto T, Ishida Y, Suzuki K. Morphological analysis of the cervical spinal canal, dural sac and spinal cord in normal individuals using CT myelography. Neuroradiology 1996; 38: 148–151
8 Stanley YM, Schabel SI, Frey GD, Hungerford GD. Quantitative analysis of the cervical spinal canal by computed tomography. Neuroradiology 1986; 28: 139–143
9 Okada Y, Ikata T, Katoh S, Yamda H. Morphologic analysis of the cervical spinal cord, dural sac and spinal canal by magnetic resonance imaging in normal adults and patients with cervical spondylotic myelopathy. Spine 1994; 19: 2331–2335
10 Muhle C, Wiskirchen J, Weinert D, et al. Biomechanical aspects of the subanachnoid space and cervical cord in healthy individuals examined with kinematic magnetic resonance imaging. Spine 1998; 23: 556–567
11 Simpson G, Roe A, Lewontine RC. Quantitative Zoology. New York, Harcourt Brace & Co, 1960

S. Carilli[1]
T. Oktenoglu[2]
A. F. Ozer[2]

Open-Window Laparotomy During a Transperitoneal Approach to the Lower Lumbar Vertebrae: New Method for Reducing Complications

Abstract

There are numerous approaches for exploring the lower lumbar vertebrae, and the anterior transperitoneal route is one of the most popular. Like all surgical techniques, this approach has advantages and disadvantages. It provides direct access to the target tissue through a small incision, exposes the anterior portion of the vertebrae well, and permits good visualization of the major vessels, thus reducing risk of vascular injury and life-threatening hemorrhage. However, compared to the extraperitoneal route, the transperitoneal approach carries higher risks for peritoneal complications. This article describes a new practical method for creating an extraperitoneal passageway or "window" during transperitoneal approaches to the lower lumbar vertebrae. Isolation of the peritoneal cavity and its contents with this technique can reduce peri- and postoperative abdominal complications.

Key words

Anterior lumbar interbody fusion · vertebra surgery · surgical technique

Introduction

Carpener first described anterior lumbar interbody fusion in 1932, and Mayer modified the technique to a minimally invasive surgery in 1997 [1, 2]. Various techniques for lumbar anterior interbody fusion and the recent advancement of disk prostheses has expanded the possibilities for surgical intervention in the lumbar spine. Various approaches to the lumbar vertebral bodies and intervertebral disks have been described, including posterior, anterior and lateral approaches via extraperitoneal and transperitoneal routes. Despite its associated difficulties and risks, we prefer to use the anterior transperitoneal approach for appropriate cases.

Here we present a new method in which an extraperitoneal passageway or "window" is created during the anterior transperitoneal approach to the lower lumbar vertebrae. This technique is an excellent way to prevent peri- and postoperative intra-abdominal complications.

Patients and Methods

Surgical technique

The operation is performed with the patient in the supine position. The lesion level is identified using a C-arm fluoroscope and is marked on the skin. Then a 4–cm midline skin incision is made over the lesion site, and the layers of the abdominal wall are incised to expose the anterior parietal peritoneum. This layer is then incised in craniocaudal direction. The small intestines are shifted to the right upper portion of the abdomen and the sigmoid colon is shifted left. We use Tobold retractors to keep the intestinal segments in the desired position, and thus allow access to the posterior parietal peritoneum lying superficial to the retroperitoneal tissues. Clamps are applied to elevate the posterior peritoneum over the surgical site, and then scissors are used to make a 6- to 8 cm-long opening in the craniocaudal

Affiliation
[1]General Surgery Department, V.K.F. American Hospital, Istanbul, Turkey
[2]Neurosurgery Department, V.K.F. American Hospital, Istanbul, Turkey

Correspondence
Senol Carilli, M.D. · General Surgery Department · V.K.F. American Hospital · Guzelbahce sk. No. 20 · Nısantası – 34365 · Istanbul · Turkey · Tel.: + 90/212/311/20 00 · Fax: + 90/212/311/23 44 · E-mail: carillis@yahoo.com

Bibliography
Minim Invas Neurosurg 2006; 49: 227–229 © Georg Thieme Verlag KG · Stuttgart · New York
DOI 10.1055/s-2006-948304
ISSN 0946-7211

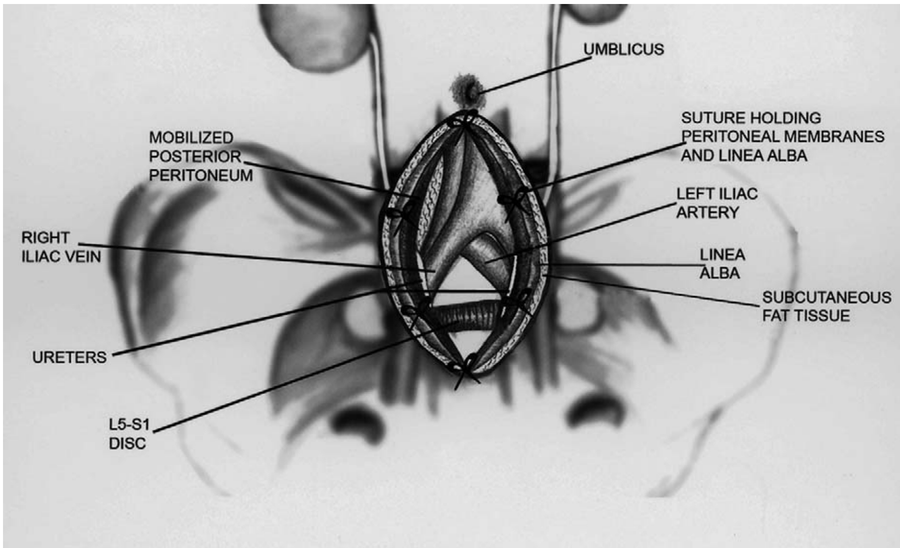

Fig. **1** Anterior view of the operative area. Layers are sutured to form the "window."

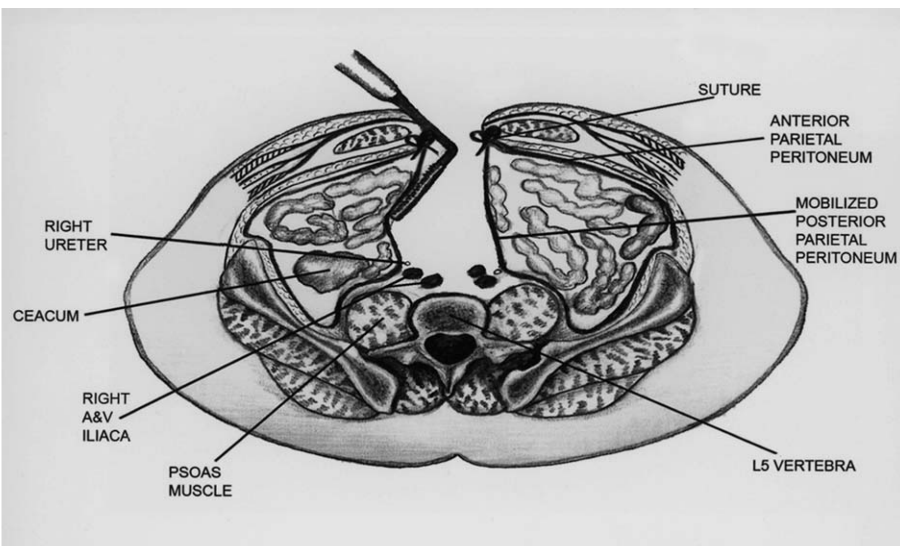

Fig. **2** Cross-sectional view of the surgical plane. Posterior parietal peritoneum has been mobilized and sewn. Iliac vessels and ureters have not yet been retracted.

direction centered over the lesion. Upon entering the retroperitoneal space, the clamps are kept in place to continue elevating the incised posterior parietal peritoneum, and blunt dissection is performed to free the membrane from underlying fat for 2 to 3 cm in all directions. Then each free edge of posterior peritoneum is sutured to the combined layers of anterior parietal peritoneum and linea alba on the corresponding side using interrupted 00 monofilament sutures spaced 1 cm apart (Figs. **1** and **2**). The cranial limit and cranial portions of the anterior and posterior peritoneal membranes should be secured first because this is the zone where the risk of accidental bowel injury is greatest. Once suturing is complete, two retractors of any type can be applied to achieve adequate exposure in the retroperitoneal area to mobilize and to retract the iliac vessels laterally and up by vascular tapes, care should be taken for the injury of small branches. The ureters are located lateral to the surgical field and fall more laterally while hanging the vessels. Subsequently the anterior aspect of the disks or vertebrae is ready for access.

After the spinal intervention is completed, the sutures joining the anterior and posterior peritoneal layers on each side of the opening are cut; Tobold retractors are reapplied to keep the viscera in place; and clamps are applied to elevate the margins of the posterior peritoneum. The edges of posterior peritoneum are apposed and sutured in a continuous pattern with 000 absorbable material. Then the edges of the anterior peritoneum plus linea alba are closed as a single layer with a continuous pattern of 0 polydioxanone suture material. Finally, the skin is closed with intradermal continuous 0000 polyglactin suture.

Discussion

With the advancements that have been made in surgical technology, many conventional operations can now be performed endoscopically or through smaller incisions. Such procedures are associated with less pain, less scarring, quicker recovery, and also reduce health care costs.

For any type of surgery, proper incision location and size, and adequate exposure are essential for a safe and successful operation. Transperitoneal access to the L4-S1 region of the spine offers several advantages over the extraperitoneal approach: more direct access to the target tissue through a smaller incision; better exposure of the anterior portion of each vertebra; and better visualization of the major vessels, which is important for preventing vascular injury and life-threatening hemorrhage. However, when the transperitoneal approach is used, risks of injury to intra-abdominal organs, spillage of resected disk material and bone fragments into the peritoneal cavity, blood leakage from the surgical site into the peritoneal cavity, and dehydration of mesothelial surfaces are inevitable. Also, it has been shown that lesions in the peritoneal cavity caused by abrasion, ischemia, desiccation, infection, thermal injury, and foreign bodies can result in adhesion formation [3].

Small bowel obstruction due to postoperative adhesions is a common problem in general surgical practice, and any laparotomy is associated with a lifelong risk of this complication. Abdominal adhesions can cause recurrent or chronic gastrointestinal complaints and pain, and they are the most common cause of intestinal obstruction. Five to 17 % of patients who have had a previous abdominal operation develop adhesive small bowel obstruction [4, 5]. Studies have identified intestinal obstruction as the most life-threatening condition related to peritoneal adhesions, with mortality rates ranging from 5 to 15 %. As well, reports indicate that postoperative adhesions are responsible for approximately 30 % of all cases of female infertility [4–7].

Our new open-window technique provides transperitoneal access to the lumbar vertebrae through a 4-cm skin incision. This method prevents spillage of surgical debris or blood leakage into the peritoneal cavity, protects against desiccation or thermal injury, and reduces abrasion of intraperitoneal organs. All these features help minimize mesothelial cell injury, and thus reduce adhesion formation after surgery.

References

1. Carpener N. Spondylolisthesis. Br J Surg 1932; 19: 374–386
2. Mayer HM. A new microsurgical technique for minimally invasive anterior lumbar interbody fusion. Spine 1997; 22: 691–699
3. Muller SA, Treutner KH, Tietze H, Anurow M, Titkova S, Palidova M, Oettinger AP, Schumpelick V. Efficacy of adhesion prevention and impact on wound healing of intraperitoneal phospholipids. J Surg Res 2001; 96: 68–74
4. Beck DE, Opelka FG, Bailey HR, Rauh SM, Pashos CL. Incidence of small bowel obstruction and adhesiolysis after open colorectal and general surgery. Dis Colon Rectum 1999; 42: 241–248
5. Scovill WA. Small bowel obstruction. In: Cameron JL (ed). Current Surgical Therapy. 5th edition, Mosby-Yearbook, Inc. St. Louis, Missouri, 1995; 100–104
6. Treutner KH, Bertam P, Lvser S, Winkeltau G, Schumpelick V. Prevention and treatment of peritoneal adhesions – A questionnaire survey on 1,200 hospitals in Germany. Chirurg 1995; 66: 398–403
7. Wilson MS, Ellis H, Menzies D, Moran BJ, Parker MC, Thompson JN. A review of the management of small bowel obstruction. Ann R Coll Surg Engl 1999; 81: 320–328

Trigeminal Neuroma with Extracranial Extension: The 31st Case

A. M. Kafadar
T. Tanriverdi
B. Canbaz
C. Kuday

Original Article

Abstract

Neuromas arising from the distal branches of the trigeminal nerve with extracranial extension are unusual. Here, we present the clinical features, disgnosis and treatment of 28-year-old woman with trigeminal neuroma with extension to the infratemporal fossa.

Key words

Extracranial extension · intracranial extension · trigeminal neuroma

Introduction

Trigeminal neuromas (TN) are uncommon and benign lesions that can be cured by complete surgical resection. The incidence accounts for less than 1 % of all intracranial tumors and for 0.8 to 8 % of all intracranial neuromas [1]. The trigeminal nerve root, the gasserian ganglion, and one of the three divisions may be the origin of such lesions, indicating that TNs may grow into distinct compartments including the cerebellopontine angle, cavernous sinus/Meckel's cave, and extracranial spaces (orbit, infratemporal fossa, and pterygopalatine fossa). Neuromas arising from the distal branches of the trigeminal nerve with extracranial extension (Jefferson's type D tumors) are extremely rare, with 30 cases having been recognized in the English literature since 1955 [1–18]. Table **1** summarizes the literature describing cases with TNs involving infratemporal fossa.

Here, we describe the 31st case with a large TN arising probably from the mandibular division of the trigeminal nerve and extending down into the infratemporal fossa and up into the middle temporal fossa through the enlarged foramen ovale. The neurosurgeon should consider TNs in the differential diagnosis of unusual tumors, because total surgical resection is curative.

Case Report

A 28-year-old woman was admitted to our clinic with a 4-year history of right visual disturbances. The patient did not report facial pain and there were no cutaneous stigmata of neurofibromatosis. The physical examination revealed no abnormality. The eye examination disclosed a significant loss of vision in the right eye. We found right facial hypesthesia in the neurological examination.

Magnetic resonance imaging (MRI) of the patient showed a large solid tumor arising from the greater wing of the sphenoid bone and extending into the infratemporal fossa through the enlarged foramen ovale. The temporal lobe, the right cavernous sinus, and the optic chiasm were pushed aside by intracranial extension. There was also the right lateral ventricle effacement and subfalcian shift to the left because of the mass effect. The tumor was hypointense on T_1-weighted imaging with intense enhancement after gadolinium injection and heterogeneously hypointense on T_2-weighted imaging (Figs. **1a–c**). Cerebral angiograms revealed medial displacement of the anterior cerebral, middle cerebral, posterior cerebral and basilar arteries.

Affiliation
Department of Neurosurgery, Cerrahpasa Medical Faculty, Istanbul University, Istanbul, Turkey

Correspondence
Taner Tanriverdi, M.D. · P.K: 4 · Cerrahpasa · 34301 Istanbul · Turkey · Tel./Fax: +90/212/414/34 27 · E-mail: tanerato2000@yahoo.com

Bibliography
Minim Invas Neurosurg 2006; 49: 230–233 © Georg Thieme Verlag KG · Stuttgart · New York
DOI 10.1055/s-2006-947995
ISSN 0946-7211

Table **1** Summary of cases of trigeminal neuromas with infratemporal extension

No.	Series (Ref. No.)	Age/ Sex	Duration of Symptoms	Initial Symptoms	Trigeminal Symptoms	Approach
1	Fleury and Furtado, 1955 [2]	51/F	3 years	Facial hypesthesia, cheek mass, double vision	Hypesthesia	TM
2	Lin et al., 1974 [3]	54/M	No data	Cheek mass	No	ST-ED-TM
3	Arena and Hilal, 1976 [4]	16/F	1 year	Left visual disturbance	No	TZ
4	Yamada et al., 1980 [5]	36/F	3 year	Left blindness, vertigo	No	FT
5	Bitoh et al., 1983 [6]	38/F	1 month	Visual disturbance, facial paresthesia	No	ST-ID-TMax
6	Fushimi et al., 1987 [7]	60/F	15 years	Facial paresthesia	Hypesthesia	Biopsy
7	Nager, 1984 [8]	25/M	3 years	Hearing loss, ear pain	No	ST-ED
8	Iwai et al., 1988 [9]	7/F	1 year	Nasal obstruction, exophthalmos	No	OZ-IT
9	McCormick et al., 1988 [10]	49/M	3 months	Facial pain, hearing loss	Pain	ST-ID
10	Lunardi et al., 1989 [11]	55/F	3 months	Facial hypesthesia, double vision	Hypesthesia	ST
11	Pollack et al., 1989 [1]	41/F	3 months	Nasal obstruction	Hypesthesia	FT-IT
12	Pollack et al., 1989 [1]	58/F	1 year	Hearing loss	Hypesthesia	FT-IT
13	Yasui et al., 1989 [12]	46/F	3 years	Facial hypesthesia, double vision	Pain, hypesthesia	FT-SO
14	Beauvillain et al., 1991 [13]	28/F	2 years	Visual disturbance, exophthalmos	No	ST-ID-TMax
15	Visot et al., 1992 [14]	42/F	18 months	Facial pain	Pain	ST
16	Visot et al., 1992 [14]	42/F	18 months	Facial pain, double vision	Pain	ST
17	Visot et al., 1992 [14]	23/F	18 months	Headache	No	IT-ED
18	Visot et al., 1992 [14]	31/F	18 months	Facial pain	Pain	IT-ED
19	Visot et al., 1992 [14]	34/F	18 months	Facial pain	Pain	ST-TZ
20	Samii et al., 1995 [15]	50/F	1 year	Facial paresthesia	No	FT-ED
21	Paquis et al., 1998 [16]	36/M	5 years	Facial pain, hypesthesia	Hypesthesia	ST-ED-TMax
22	Paquis et al., 1998 [16]	60/M	2 years	Facial pain, hypesthesia	Pain, hypesthesia	ST-ED-TMax
23	Paquis et al., 1998 [16]	63/F	3 months	Double vision	No	ST-ED-TMax
24	Yoshida and Kawase, 1999 [17]	9/F	7 years	Photophobia, exophthalmos	Pain	ST
25	Yoshida and Kawase, 1999 [17]	58/F	2 months	Facial pain, hypesthesia	Pain, hypesthesia	ST
26	Yoshida and Kawase, 1999 [17]	61/F	3 yr.	Facial pain	Pain	Zygomatic IT
27	Yoshida and Kawase, 1999 [17]	25/F	9 days	Hypesthesia	Pain	Zygomatic IT-Ant. TP
28	Yoshida and Kawase, 1999 [17]	36/F	4 months	Facial hypesthesia	Hypesthesia	Zygomatic IT-Ant. TP
29	Yoshida and Kawase, 1999 [17]	36/F	6 months	Hearing disturbance, tinnitus	No	Zygomatic IT
30	Akhaddar et al., 2000 [18]	35/F	4 months	Otitis media, facial paresthesia	Hypesthesia	ST-ID-ED
31	Kafadar et al., 2006 (present case)	28/F	4 years	Visual disturbances	Hypesthesia	FT

TM = temporomandibular; ST = subtemporal; ED = extradural; TZ = transzygomatic; FT = frontotemporal; ID = intradural; Tmax = transmaxillary; OZ = orbitozygomatic; IT: infratemporal; SO = suboccipital; Ant. TP = anterior transpetrosal.

The patient underwent a surgical intervention in which a right fronto-temporal craniotomy was performed (Fig. **2**). Total resection was achieved and a histological examination of the surgical specimen revealed a schwannoma.

The postoperative period of the patient was uneventful and she was discharged home on the 7th postoperative day. Twenty months later the patient had no visual disturbances but did have right facial hypesthesia. Postoperative MRI 20 months after the surgery revealed no recurrence or residue lesion (Figs. **3a**–**c**).

Discussion

Neuromas arising from the distal branches of the trigeminal nerve with extension to the extracranial compartments are unusual and only 30 cases have been recognized in the literature [1–18]. All of the tumors are histologically benign and slow-growing, indicating that the diagnosis usually occurs late as it was in our case. All patients with TNs extending to the extracranial compartments showed no findings related to neurofibromatosis.

As expected, the majority of the patients showed the subjective complaints of trigeminal dysfunction, frequently localized to the second or third division of the trigeminal nerve. The clinical presentation of our patient was unique because there was only a complaint of right visual disturbances in spite of the huge size of the tumor. This was due to compression of the optic chiasm aside by the lesion. The patient regained his vision to normal in the postoperative period. We found that the most commonly affected cranial nerve is the 6th nerve followed by the 2nd and

Fig. 1 Preoperative T_1-weighted axial (**a**), coronal (**b**) and sagittal (**c**) MR images after gadolinium injection demonstrating a large lesion arising from the sphenoid wing extending to the infratemporal fossa. Note the compression of the mesencephalon and the fourth ventricle and displacement of the Sylvian fissure.

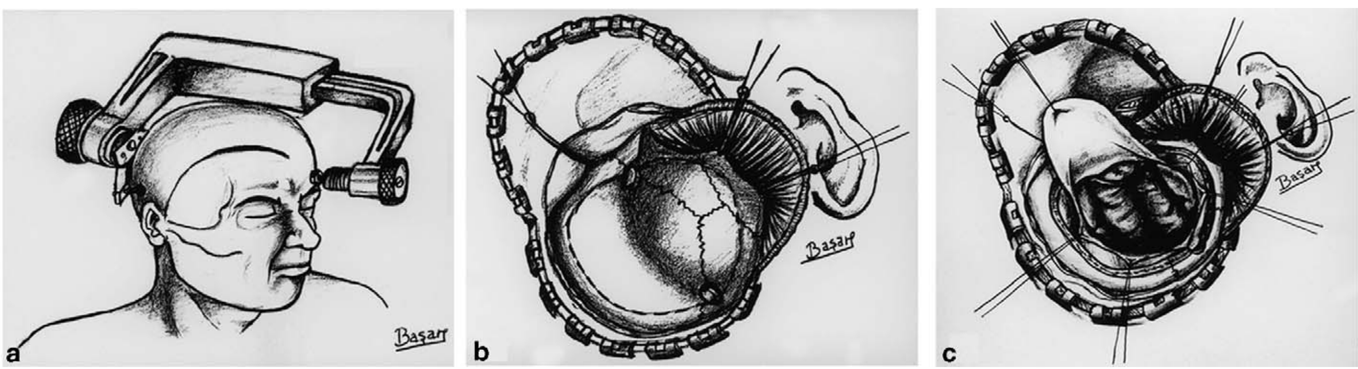

Fig. 2 The scheme depicting the fronto-temporal approach performed in our case. The head is in a fixed position and a fronto-temporal skin incision is made extending from the midline to the zygoma and curving to stay approximately 1 cm behind the hairline (**a**). The scalp and temporalis fascia are reflected anteriorly and postero-inferiorly, respectively, and two burr holes are placed (**b**). After the dura incision and reflection anteriorly, the superior part of the lesion is seen (asterisk) (**c**).

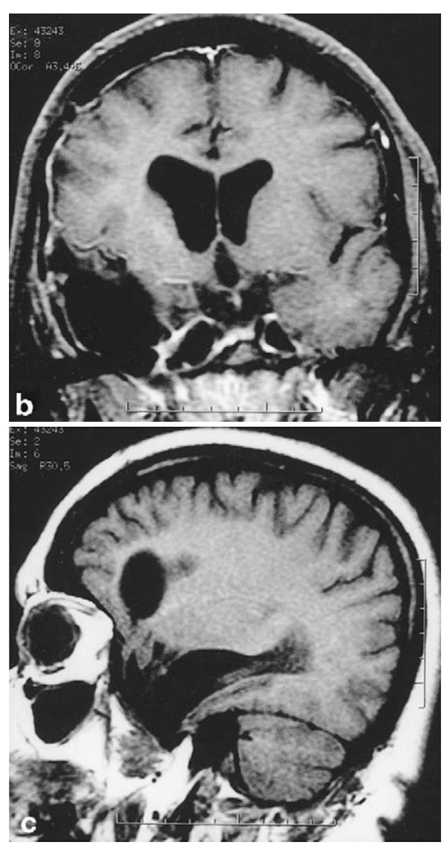

Fig. 3 Postoperative T_1-weighted axial (**a**), coronal (**b**) and sagittal (**c**) MR images after contrast injection showing no residual tumor 20 months after surgery.

8th nerves in 30 patients with TNs extending to the extracranial compartments at the time of admission.

The literature with the limited number of the patients including ours shows us that the diagnosis of TNs does not depend solely on the clinical presentation. Therefore, radiological studies are of vital importance for the preoperative diagnosis. Significant advances in neuroimaging, particularly MRI, have made significant contributions towards achieving preoperative diagnosis and complete surgical tumor removal with minimal morbidity. Digital subtraction angiography should be performed in cases of large tumors, as in this case, to demonstrate the tumor's relationship to and displacement of vascular structures before the surgical intervention.

Surgical intervention is the treatment of choice but the choice of surgical approach is the main difficulty. TNs with extracranial extension can be removed by various surgical approaches [1, 15, 17, 18], however; it has been underlined that cranial base approaches provide better exposure as compared to conventional approaches [15, 19, 20]. In our patient, total tumor removal was achieved by a fronto-temporal craniotomy due mainly to its well-circumscribed nature, which enabled us to dissect the lesion easily from the surrounding structures.

In conclusion, TNs with infratemporal fossa extension are an uncommon entity that may also be removed totally by a fronto-temporal craniotomy in cases of well-circumscribed large lesions.

Acknowledgements

The authors thank Basar Abuzayed, M.D., for his excellent drawing of the scheme of our approach.

References

1. Pollack IF, Sekhar LN, Jannetta PJ, Janecka IP. Neurilemomas of the trigeminal nerve. J Neurosurg 1989; 70: 737–745
2. Fleury P, Furtado R. Deux cas de neurinomes de la fosse pterygomaxillaire. Ann Otolaryngol Chir Cervicofac 1955; 72: 920–925
3. Lin SR, Lin ZS, Tatoian JA. Trigeminal neurinoma with extracranial extension. Neuroradiology 1974; 8: 183–185
4. Arena S, Hilal EY. Neurilemomas of the infratemporal space: Report of a case and review of the literature. Arch Otolaryngol 1976; 102: 180–184
5. Yamada H, Sakai N, Ando T, Nishimura Y, Kishimoto Y, Shimokawa K. [Trigeminal neurinoma with massive extracranial extension, report of a case.]. No Shinkei Geka 1980; 8: 469–473
6. Bitoh S, Hasegawa H, Ohtsuki H, Obashi J, Furukawa Y, Sakurai M. Schwannoma of the skull base with intracranial extension. Surg Neurol 1983; 20: 143–146
7. Fushimi S, Miura S, Suda Y, Fujii S, Kowada M. A case of trigeminal neurinoma with marked extracranial extension. No Shinkei Geka 1987; 15: 1117–1122
8. Nager GT. Neurinomas of the trigeminal nerve. Am J Otolaryngol 1984; 5: 301–333
9. Iwai Y, Hakuba A, Noguchi K, Nishimura S. A gigantic neurilemoma originating in the pterygopalatine fossa: Case report. Surg Neurol 1988; 30: 452–456
10. McCormick PC, Bello JA, Post KD. Trigeminal schwannoma: Surgical series of 14 cases with review of the literature. J Neurosurg 1988; 69: 850–860
11. Lunardi P, Missori P, Gagliardi FM, Fraioli B. Trigeminal schwannoma with infratemporal extension: Case report. J Neurosurg Sci 1989; 33: 292–295
12. Yasui T, Hakuba A, Kim SH, Nishimura S. Trigeminal neurinomas: Operative approaches in eight cases. J Neurosurg 1989; 71: 506–511
13. Beauvillain C, Calais C, Launay MC, Bordure P, Zanaret M, Legent F. Nervous tumors of the infratemporal fossa. Ann Otolaryngol Cervicofac 1991; 108: 107–111
14. Visot A, Derome P, De Leon J. Sphenocavernous and infratemporal trigeminal neuromas: surgical series of 15 cases. Skull Base Surg 1992; 3: 142–149
15. Samii M, Migliori MM, Tatagiba M, Babu R. Surgical treatment of trigeminal schwannomas. J Neurosurg 1995; 82: 711–718
16. Paquis P, Castillo L, Lonjon M, Santini J, Grellier P. Extracranial trigeminal schwannomas with middle temporal fossa development. Neurochirurgie 1998; 44: 38–45
17. Yoshida K, Kawase T. Trigeminal neurinomas extending into multiple fossae: Surgical methods and review of the literature. J Neurosurg 1999; 91: 202–211
18. Akhaddar A, el-Mostarchid B, Zrara I, Boucetta M. Intracranial trigeminal neuroma involving the infratemporal fossa: case report and review of the literature. Neurosurgery 2002; 50: 633–638
19. Goel A, Nadkarni T. Basal lateral subtemporal approache for trigeminal neurinomas: Report of an experience with 18 cases. Acta Neurochir (Wien) 1999; 141: 711–719
20. Taha JM, Tew JM Jr, van Loveren HR, Keller JT, el-Kalliny M. Comparison of conventional, and skull base surgical approaches for the excision trigeminal neurinomas. J Neurosurg 1995; 82: 719–725

Original Article

"Triple Cross" of the Hypoglossal Nerve and its Microsurgical Impact to Entrapment Disorders

G. Bademci[1]
F. Batay[2]
M. G. Yaşargil[3]

Abstract

Objective: Cadaveric dissections were performed to review the intracranial and extracranial course of the hypoglossal nerve. The neurological significance of a newly defined "triple cross" of the hypoglossal nerve is discussed. **Materials and Methods:** 10 cadaveric heads (left and right; 20 sides) were dissected using microsurgical techniques. **Results:** In the cisternal segment of hypoglossal nerve, the diameter of the rostral trunk amounted to 155–680 µm (mean 435 µm), and the caudal trunk to 210–820 µm (mean 482 µm). The roots formed three trunks in 20 % of the hypoglossal nerves and two trunks in the rest. As a first cross, the anterior medullary segment of the vertebral artery crossed the hypoglossal nerve roots in 14 of 20 sides (70 %). As a rare variation, the vertebral artery extended medial to the nerve (25 %) or between its roots (5 %). The second cross was found between the descendens hypoglossus and the occipital artery (75 %), sternocleidomastoid artery and vein complex (15 %) and external carotid artery (10 %). The third cross was shown in the submandibular triangle between the lingual hypoglossus and its drainage vein; vena committans nervus hypoglossus. **Conclusion:** Throughout its way, the hypoglossal nerve passes over vascular structures in three crossing points which may serve as a probable cause of hypoglossal nerve entrapment disorders.

Key words

Hypoglossal nerve · triple cross · cross-compression · entrapment disorders · microsurgical anatomy

Introduction

The hypoglossal nerve (HN), also known as cranial nerve XII, supplies motor fibers to the tongue. The HN is also functional in respiration and swallowing. The HN may be involved in various pathological entities from the cisternal segment to the end of the extracranial portions. This anatomic study aims to disclose the course of the HN and point out three important crosses between the HN and the neighbouring vascular structures to help the management of rare cross-compression syndromes of HN.

Materials and Methods

The intracranial and extracranial parts of the HN were studied on 10 formalin-fixed adult cadaver heads (20 sides). The specimens were obtained after routine autopsy procedures had been performed and had been embalmed in 10 % formaldehyde solution. The internal carotid arteries (ICA), the vertebral arteries (VA) and the internal jugular veins (IJV) were dissected, cannulated and irrigated with saline solution to remove any residual blood clots in the lumens. The vascular structures were perfused with colored latex in 8 specimens, and with colored silicon in the remaining 2 specimens in order to facilitate their definition. Cadaveric heads were examined under 3 to 40 × magnification using the Opmi-Zeiss surgical microscope. Measurements were made with 8 inch/200 mm electronic digital calipers (Marathon, Richmond Hill, Ontario, Canada). The whole length of the HN was exposed intracranially and extracranially under the surgical microscope and all stages of the dissections were measured and photographed.

Affiliation
[1]Department of Neurosurgery, University of Kirikkale, Kirikkale, Turkey
[2]Division of Neurosurgery, Bayindir Hospital Neurological Sciences Center, Ankara, Turkey
[3]Department of Neurosurgery, University of Arkansas Medical Sciences, Little Rock, Arkansas, USA

Correspondence
Gulsah Bademci, M.D. · Buketkent Mh. · Iller Sitesi · 9.Blok No:9 · 06530 Cayyolu · Ankara · Turkey · Tel.: + 90/312/24 15 82 0 · Fax: + 90/318/22 52 81 9 · E-mail: bademci70@yahoo.com

Bibliography
Minim Invas Neurosurg 2006; 49: 234–237 © Georg Thieme Verlag KG · Stuttgart · New York
DOI 10.1055/s-2006-948299
ISSN 0946-7211

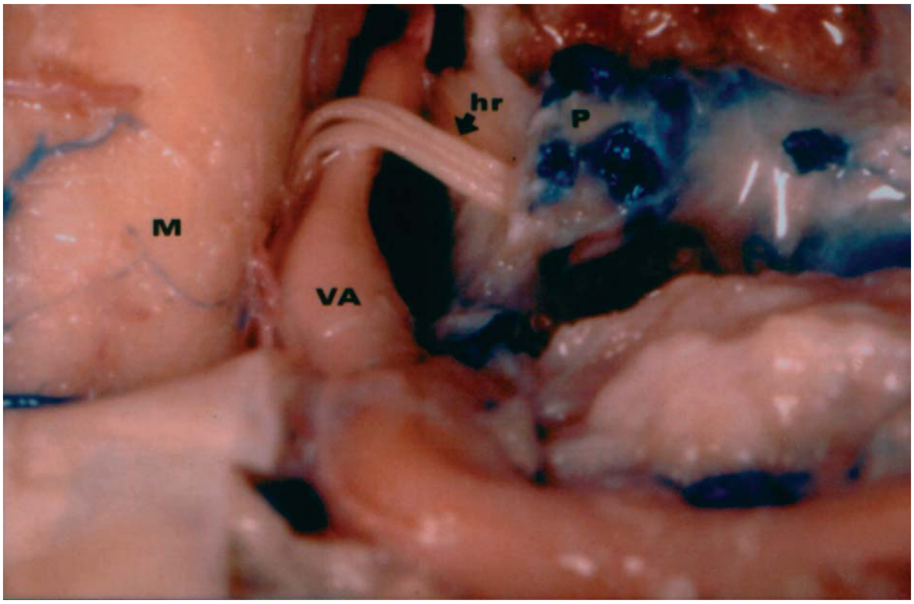

Fig. **1** The right-side cadaveric dissection demonstrates the exit of the right hypoglossal nerve rootlets from the medulla and the relationship between the hypoglossal nerve and the vertebral artery. The occipital condyle was removed. M = medulla; VA = vertebral artery; hr = hypoglossal rootlets; P = the venous plexus of the canalis hypoglossus; thin arrow = crossing point).

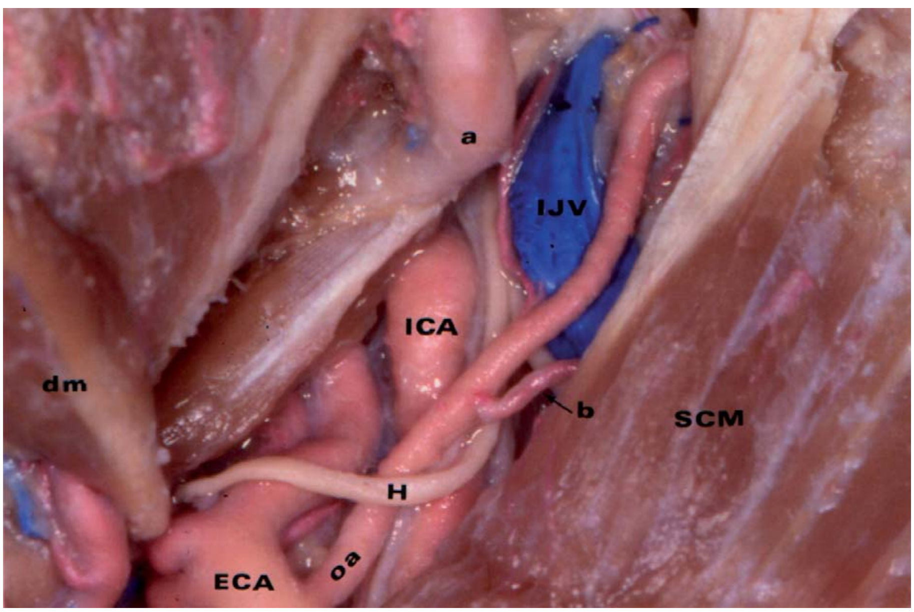

Fig. **2** The left-side cadaveric dissection demonstrates the cross between the hypoglossal nerve and the occipital artery. SCM = sternocleidomastoid muscle; b = sternocleidomastoid artery; ICA = internal carotid artery; ECA = external carotid artery; IJV = internal jugular vein; oa = occipital artery; H = hypoglossal nerve; a = angulus mandibulae; DM = digastric muscle; thin arrow = crossing point.

Results

The HN can be divided into intracranial and the extracranial parts. The intracranial part comprises the cisternal and the intracanalicular portions [1]. The extracranial part may be divided into the descendens, transverse and lingual parts. The rootlets of the HN leave the medulla through the preolivary sulcus, that is, from the level of the pyramidal decussation to the pontomedullary sulcus. The rootlets and roots converge to form trunks. It was noted that the roots form two trunks, the rostral and caudal, in 80 % of the cadaveric sides and three trunks in the remaining sides. The diameter of rostral trunk was measured as 155–680 µm (mean: 435 µm). The caudal trunk ranged in diameter from 210 to 820 µm (mean: 482 µm).

The first cross was exposed in the cisternal segment of the HN (Fig. **1**). The anterior medullary segment of the VA crossed the HN roots in 14 sides (70 %). As a rare variation, the VA extended medial to the nerve (25 %) or between its roots (5 %).

The HN had its second cross between the descendens hypoglossus and the carotid arteries (Fig. **2**). After descending along the posterolateral surface of the ICA, the nerve turns abruptly, curves medially, hooking under the artery to the sternocleidomastoid muscle close to its origin from the occipital artery. Then the transverse hypoglossus starts. Although the HN is located posterior to the ICA as it exits the hypoglossal canal, this nerve passes anterior to the ICA 14.5–25.2 mm (mean: 19.24 mm) above the carotid bifurcation. The descendens hypoglossus crossed the occipital artery (OA) in the majority of sides (75 %), the sternocleidomastoid artery and vein complex (SCMA-V) in 15 % of sides and the external carotid artery in 10 % of 20 sides. The OA arose from the posterior surface of the ECA 6–9 mm (mean: 7 mm) above the carotid bifurcation. The SCMA-V complex runs 17.1–21.5 mm (mean: 18.47 mm) away from the carotid bifurcation creating a sling over the HN. In all cadavers the crossing point between the HN and OA was 7.1–9.4 mm (mean: 8.27 mm) superior to the emergence of the OA from the ECA. In 33 % of the sides, a low-lying hypoglossal loop was determined.

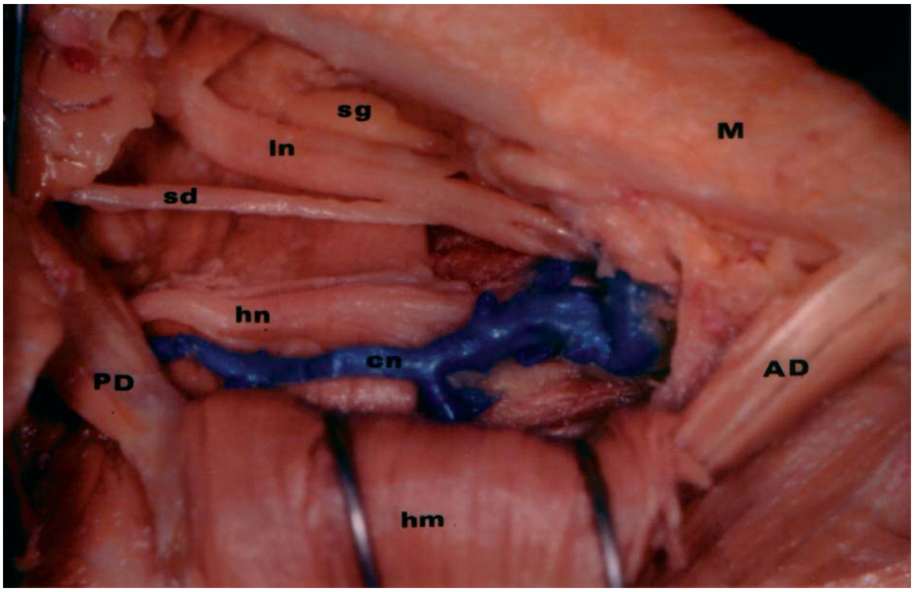

Fig. **3** The right-side cadaveric dissection shows the anatomical structures in the right submandibular region. M = right ramus mandibula; AD = anterior belly of the digastric muscle; PD = posterior belly of the digastric muscle; hm = mylohyoid muscle; cn = vena committans nervi hypoglossi; hn = hypoglossal nerve; sd = submandibular duct; ln = lingual nerve; sg = submandibular ganglion; thin arrow = crossing point.

The third cross is placed in the submandibular triangle between the lingual hypoglossus and its drainage vein, the vena committans nervus hypoglossus (VCNH) (Fig. **3**). The veins reveal the most variable anatomy in the neck. As a very tiny structure, the VCNH could not have been detected in 95 % of the sides. In only one side, the VCNH was seen draining into the facial vein. In the majority of the sides, drainage of the nerve was achieved by the lingual and the superior thyroidal veins. The anterior and posterior facial veins commonly unite close to the angle of the mandible to form the common facial vein which empties into the IJV near the greater cornu of the hyoid bone. The VCNH and HN coursed together in the beginning of the lingual part. When the lingual part revealed a fascicular pattern (1–7 fascicles, mean: 5), the VCNH can be found just superior to the HN forming a narrow-angled cross.

Discussion

The HN provides purely motor innervation to the tongue. Complete hypoglossal paralysis is manifested by impaired protrusion of the tongue ipsilateral to the nerve injury so that the tongue deviates to the side of the lesion. Partial injury to the HN may cause paresis of the tongue, leading to articulation and mastication disturbances. Severe or bilateral trauma to the nerve can affect the protrusion motion of the tongue, causing it to fall back towards the pharynx resulting possibly in airway obstruction [2].

Recognizing the entire course of the HN not only minimizes the risk of injury during surgery but also the identification of constant landmarks become critical. Defining the triple cross of the HN is extremely important in rare cases with vascular cross-compression syndromes. Advances in neuroradiology provide enormous knowledge about the pathologies due to neurovascular contact of the VA and HN [3–5]. In daily practice, the HN can be easily distinguished on magnetic resonance images not only to assess the course of the nerve, but also to display its relationships to adjacent vessels. Yousry et al. identified neurovascular contact in the cisternal segment of the HN in 61 % of root bundles in MR images [6]. Similarly, the posterior inferior cerebellar artery (PICA) may extend ventral and/or dorsal to the nerve roots or lie between these roots [7]. In all these instances the VA or PICA may compress, displace, distort and/or stretch the roots of the HN. This cross is significant in patients reported to have a dolichovertebral artery with an abnormal course compressing both the medulla oblongata and hypoglossal rootlets [8]. This relationship is also important for completing far-lateral approaches without injury to the HN and VA [9].

The HN also traverses with its descending part very close to the ECA, OA or SCMA-V complex. The HN is the most frequently injured nerve in 2–17 % of carotid endarterectomies [2,10–13]. Most of the hypoglossal nerve injuries have been attributable to clamping, traction or stretching. The cross between the HN and the ECA, OA or SCMA-V complex may be a consequence of the close development of the hypoglossal nerve and occipital somites in staged embryos [14]. This cross should be taken into consideration in the diagnosis of peripheral paresis or paralysis of the tongue during surgery involving this area [15]. This cross may be a limiting factor during exposure of the carotid artery and the HN may be liable to injury, especially in the case of high bifurcation carotid artery lesions [16] or a low-lying HN, as well as during reconstructions of carotid kinks and elimination of aneurysms [17]. Also, some abnormalities of vascular structures including tortuous, kinked carotid arteries may caused neurological signs [18–20]. Anatomic reconstruction of the affected segments of the vascular structures may prevent progressive deterioration of the HN [21]. Otherwise, the aberrance of the anatomic position of the HN caused some clinical presentations of iatrogenic injury [22]. Especially a low-lying hypoglossal loop is vulnerable to injury during carotid artery surgery [23].

The third cross must be taken into consideration, especially in the tongue-flap surgery. The pedicle of a tongue flap must maintain an efficient venous drainage canal [24]. This venous drainage should also be protected during surgery for avoiding hypoglossal injury [25].

This anatomical study aimed to provide a better understanding about the complex anatomy of the hypoglossal nerve which traces a long intracranial and extracranial course. We have described the triple cross of the HN to serve as important landmarks of cross-compression syndromes. These three anatomic crosses between the HN and vascular structures were reported as a probable cause of cranial nerve entrapment disorders.

References

1 Gibo H, Marinkovic S, Nikodijevic I, Stimec B, Erdem A. The blood supply of the hypoglossal nerve: the microsurgical anatomy of its cisternal segment. Surg Neurol 1997; 48: 85–91

2 Ballotta E, Da Giau G, Renon L, Narne S, Saladini M, Abbruzzese E, Meneghetti G. Cranial and cervical nerve injuries after carotid endarterectomy: a prospective study. Surgery 1999; 125: 85–91

3 Meziti L, Iffenecker C, Fuerxer F, Benoudiba F, Comoy J, Lacroix C, Doyon D. XII cranial nerve pseudoneurinoma due to spontaneous transformation of an aneurysm of the vertebral artery. J Neuroradiol 1998; 25: 307–311

4 Rollnik JD, Sindern E, Mosler F, Spring B, Malin JP. Isolated peripheral hypoglossal palsy caused by a kinking of the left vertebral artery (hypoglossal vertebral entrapment syndrome). Eur Neurol 1996; 36: 324–325

5 Salvi F, Mascalchi M, Plasmati R, Tugnoli V, De Grandis D. Hypoglossal vertebral entrapment syndrome. Muscle Nerve 1999; 22: 288–289

6 Yousry I, Moriggl B, Schmid UD, Wiesman M, Fesl G, Bruckmann H, Naidich TP, Yousry TA. Detailed anatomy of the intracranial segment of the hypoglossal nerve: neurovascular relationships and landmarks on magnetic resonance imaging sequences. J Neurosurg 2002; 96: 1113–1122

7 Lang J. About a very rare variation of the course and width of the vertebral arteries and the hypoglossal nerve. Acta Neurochir (Wien) 1990; 106: 73–77

8 Morini A, Rozza L, Manera V, Buganza M, Tranquillini E, Orrico D. Isolated hypoglossal nerve palsy due to an anomalous vertebral artery course: report of two cases. Ital J Neurol Sci 1998; 19: 379–382

9 Wen HT, Rhoton AL Jr, Katsuta T, de Oliveira E. Microsurgical anatomy of the traanscondylar, supracondylar and paracondylar extensions of the far-lateral approach. J Neurosurg 1997; 87: 555–585

10 Aldoori M, Baird NR. Local neurological complication during carotid endarterectomy. J Cardiovasc Surg 1988; 29: 432–436

11 Bejjani G, Sullivan B, Lopez ES, Abello J, Wright D, Jurjus A, Sekhar L. Surgical anatomy of the infratemporal fossa: the styloid diagram revisited. Neurosurgery 1998; 43: 842–853

12 Forsell C, Kitzing P, Berqvist D. Cranial nerve injuries after carotid artery surgery. A prospective study of 663 operations. Eur J Vasc Endovasc 1995; 10: 445–459

13 Maniglia A, Han P. Cranial nerve injuries following carotid endarterectomy: an analysis of 336 procedures. Head & Neck 1991; 13: 121–124

14 O'Rahilly R, Muller F. The early development of the hypoglossal nerve and occipital somites in staged human embryos. Am J Anat 1984; 169: 237–257

15 Nathan H, Levy J. The course and relations of the hypoglossal nerve and the occipital artery. Am J Otolaryngol 1982; 3: 128–132

16 Hans SS, Shah S, Hans B. Carotid endarterectomy for high plaques. Am J Surg 1989; 157: 431–435

17 Imparato A, Bracco A, Kim GE, Bergmann L. The hypoglossal nerve in carotid arterial reconstructions. Stroke 1972; 3: 576–578

18 Radonic V, Baric D, Giuino L, Buca A, Sapunar D, Marovic A. Surgical treatment of kinked internal carotid artery. J Cardiovasc Surg (Torino) 1998; 39: 557–563

19 Scotti G, Melancon D, Olivier A. Hypoglossal paralysis due to compression by a tortuous internal carotid artery in the neck. Neuroradiology 1978; 17: 263–265

20 Takase K, Kohyama Y, Ueda S. Surgical management of peripheral hypoglossal nerve palsy caused by abnormal external carotid artery. No Shinkei Geka 1983; 11: 1313–1318

21 Bademci G, Batay F, Tascioglu AO. Non-traumatic elevation techniques of the hypoglossal nerve during carotid endarterectomy: a cadaveric study. Minim Invas Neurosurg 2005; 48: 108–112

22 Kim DD, Caccamese JF, Ord RA. Variations in the course of the hypoglossal nerve: a case report and literature review. Int J Oral Maxillofac Surg 2003; 32: 568–570

23 Bademci G, Batay F, Vural E, Avci E, Al-Mefty O, Yasargil MG. Microsurgical anatomical landmarks associated with high bifurcation carotid artery surgery and related to hypoglossal nerve. Cerebrovasc Dis 2005; 19: 404–406

24 Shangkuan H, Xinghai W, Shizhen Z, Zengxing W, Shiying J, Jiasong G. Morphologic studies of the venous drainage of the tongue. Surg Radiol Anat 1998; 20: 89–92

25 Skandalakis J, Gray S, Rowe J. Surgical anatomy of the submandibular triangle. Am Surg 1979; 590–596

Original Article

Outcome Prediction of Third Ventriculostomy: A Proposed Hydrocephalus Grading System

U. Kehler[1]
J. Regelsberger[2]
J. Gliemroth[3]
M. Westphal[2]

Abstract

An important factor in making a recommendation for different treatment modalities in hydrocephalus patients (VP shunt versus endoscopic third ventriculostomy) is the definition of the underlying pathology which determines the prognosis/outcome of the surgical procedure. Third ventriculostomies (3rd VS) are successful mainly in obstructive hydrocephalus but also in some subtypes of communicating hydrocephalus. A simple, easily applicable grading system that is designed to predict the outcome of 3rd VS is proposed. The hydrocephalus is graded on the basis of the extent of downward bulging of the floor of the third ventricle, which reflects the pressure gradient between the 3rd ventricle and the basal cisterns, presence of directly visualised CSF pathway obstruction in MRI, and the progression of the clinical symptoms resulting in five different grades. In this proposed grading system, grade 1 hydrocephalus subtype shows no downward bulged floor of the 3rd ventricle, no obstruction of the CSF pathway, and no progressive symptoms of hydrocephalus. There is no indication for 3rd VS. Grades 2 to 4 show different combinations of the described parameters. Grade 5 subtype shows a markedly downward bulged floor of the 3rd ventricle and direct detection of the CSF pathway obstruction (i.e., aqueductal stenosis) with progressive clinical deterioration. Retrospective application of this grading scheme to a series of 72 3rd VS has demonstrated a high correlation with the outcome: The success rate in grade 3 reached 40 %, in grade 4: 58 %, and in grade 5: 95 %. This standardised grading system predicts the outcome of 3rd VS and helps in decision making for 3rd VS versus VP shunting.

Key words

Third ventriculostomy · hydrocephalus · grading system · prognosis

Introduction

The endoscopic treatment of hydrocephalus shows various advantages in contrast to the ventriculoperitoneal shunts. However, 3rd ventriculostomy (3rd VS) is not successful in all forms of hydrocephalus. In various aetiologies of hydrocephalus as well as in young children there exist controversies in indication and 3rd VS is not without risks. Therefore 3rd VS should be performed only in selected cases when success is anticipated. So far no hydrocephalus classification is available to adequately predict the success rate of 3rd VS. As 3rd VS has become a widespread therapy, an objective method – a grading system – is required to predict the outcome of 3rd VS and to help in selecting the appropriate therapy.

An ideal grading system would allow a reliable estimation of the procedural success for each individual case. A grading system considering all possible factors which may influence the outcome of 3rd VS (patient age, duration and progression of symptoms, cause of hydrocephalus, co-morbidity, MRI signs, etc.) is very complex and difficult to apply in daily routine. Therefore a simple system that considers the important parameters of an individual hydrocephalus and thus arrives at a grading of the

Affiliation
[1]Neurosurgical Department, Asklepios Clinic Altona, Hamburg, Germany
[2]Neurosurgical Department, University Hospital Hamburg Eppendorf, Germany
[3]Neurosurgical Department, Medical University Schleswig-Holstein, Lübeck, Germany

Correspondence
Prof. Dr. Uwe Kehler · Department of Neurosurgery · Asklepios Clinic Altona · Paul-Ehrlich-Str. 1 · 22763 Hamburg · Germany · Tel.: + 49/40/18 18 81/1671 · Fax: + 49/40/18 18 81/4911 · E-mail: uwe.kehler@ak-altona.lbk-hh.de

Bibliography
Minim Invas Neurosurg 2006; 49: 238 – 243 © Georg Thieme Verlag KG · Stuttgart · New York
DOI 10.1055/s-2006-950382
ISSN 0946-7211

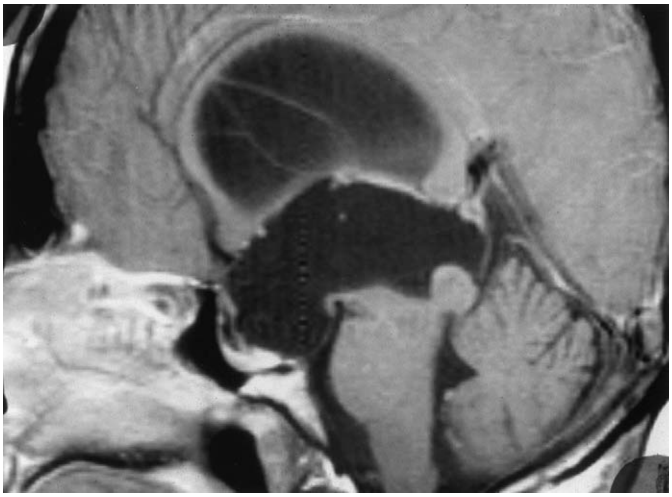

Fig. **1** Direct visible obstruction of the CSF-pathway: a tumour of the quadrigeminal plate with complete compression of the aqueduct. NMR of a young female patient with progressive clinical signs. Hydrocephalus grade 5.

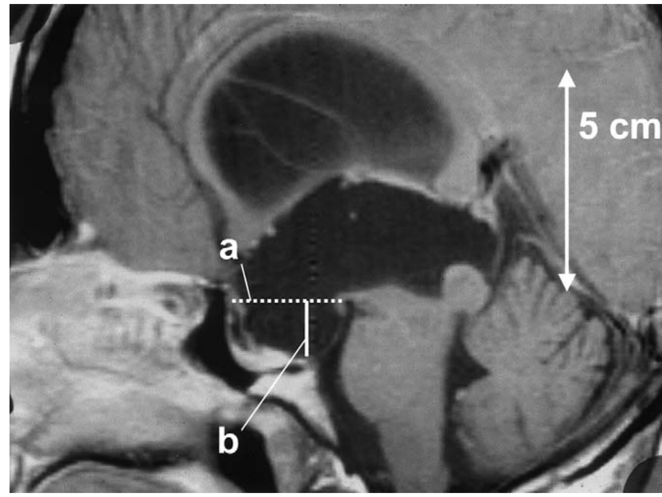

Fig. **3** Degree of downward bulging of the floor of the 3rd ventricle: The line between the chiasma and the mamillary bodies represents the normal position (a). The distance from this line to the deepest point of the floor is measured (b). If b is up to 5 mm, it is pointed with 1, if it is more it is pointed with 2.

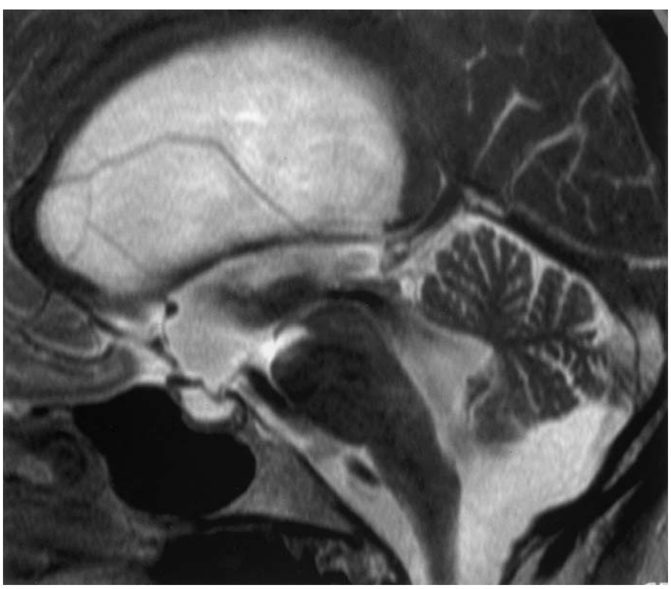

Fig. **2** No direct obstruction of the CSF-pathway is visible, however, indirect signs are visible: a, a downward bulged floor of the 3rd ventricle; b, discrepancy of the sizes of the great and prepontine cistern – suggesting that an obstruction is present between these cisterns. NMR of a 59-year-old female with progressive symptoms of normal pressure hydrocephalus. Hydrocephalus grade 4.

hydrocephalus is proposed to select the appropriate, most beneficial therapy. The aim is also to detach the indication of 3rd VS from controversial criteria as age, posthaemorrhagic and postmeningitic aetiologies etc.

Materials and Methods

Description of grading system

Experience with endoscopic hydrocephalus treatment has shown that many of the parameters which might influence the outcome of 3rd VS are interrelated, allowing us to simplify the grading to 3 features: 1) directly visible cause of obstruction, 2) downward bulging of the floor of the 3rd ventricle, and 3) progression of clinical symptoms.

Direct visibility of CSF pathway obstruction

MRI scans are analysed for an obstruction of the CSF pathways. A visible obstruction like an aqueductal stenosis, a space-occupying lesion in the 3rd ventricle or in the pineal region or a posterior fossa tumour, is scored with 1 point (Fig. **1**). If there is no clearly detectable obstruction (Fig. **2**), this is scored with 0. Also a relative stenosis of the aqueduct with present flow void was scored with 0.

The direct demonstration of the obstruction classifies the hydrocephalus to an obstructive hydrocephalus, which corresponds to the classical indication for 3rd VS as it bypasses this obstruction.

Downward bulging of the floor of the 3rd ventricle

In normal non-hydrocephalic cases the floor of the 3rd ventricle is within the line from the chiasma to the mamillary bodies. On MRI scans the downward displacement is measured from this line to the deepest point of the floor (Fig. **3**). A normal position of the floor is scored with 0 (Fig. **4**), a slight downward bulging of up to 5 mm with 1, and an marked downward bulging of more than 5 mm with 2 (Figs. **1** and **3**).

The downward bulging of the floor of the 3rd ventricle reflects the pressure gradient between the 3rd ventricle and the interpeduncular/prepontine cistern. The more it is bulged downward the more the pressure difference is between the pre- and post-stenotic spaces, which seems from the mechanical point of view to be a favourable predictor for 3rd VS [1–3].

The measurements were intentionally not scaled to the patient size in spite of the treated patients being from 7 days to 76 years of age: The relatively more extended bulging of the floor in very small infants, which reflects a higher pressure gradient, should

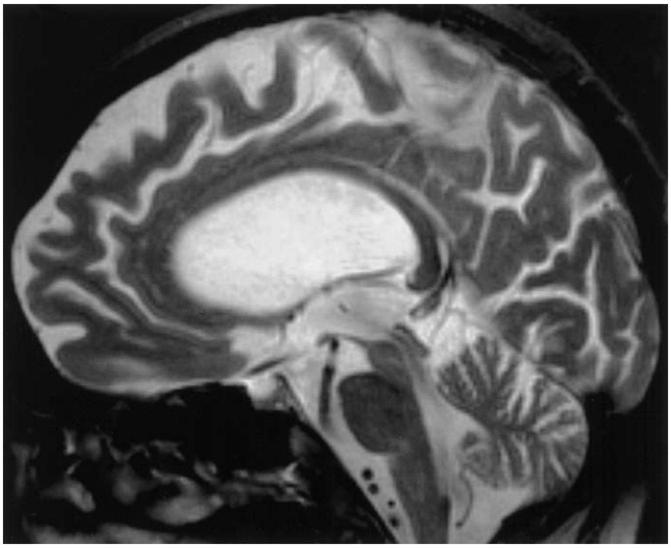

Fig. **4** A malresorptive hydrocephalus with normal position of the floor of the 3rd ventricle. No direct visible obstruction (0 points), no downward bulging of the floor (0 points) but clinical progressive symptoms (2 points). Hydrocephalus grade 2.

compensate the experienced lower success rate in these small patients.

Progression of clinical symptoms

Clinical symptoms of hydrocephalus with no progression at all in the last 12 months are assigned with 1 point, progressive symptoms are assigned with 2 points. If no clinical progression exists we might be dealing with an arrested hydrocephalus. A clinical improvement does not seem very likely.

The grade of hydrocephalus (Table **1**) is derived by summing the points achieved for each parameter. The lowest possible grade is grade 1: constant clinical symptoms, no detectable obstruction of the CSF pathway and normal position of the floor of the 3rd ventricle. The authors do not see an indication for 3rd VS in grade 1 hydrocephalus. The highest grade would be grade 5: progressive symptomatology, direct visualisation of an obstruction and a markedly downward bulged floor of the 3rd ventricle. From the theoretical point of view the Grade 5 hydrocephalus has the best chance to be treated successfully with 3rd VS.

Application of the grading system

In order to test the predictive value of this system, all the 3rd VS performed by the first author (U. K.) or under his supervision were analysed. One hundred and nine 3rd VS were performed from September 1994 to February 2003. The follow-up had to be a minimum three months. Patients who died of an unrelated problem but had until then shown good clinical recovery from the hydrocephalus ($n = 3$) were included. In cases of failed 3rd ventriculostomy, the follow-up period ended with the shunt implantation ($n = 16$). Fifteen patients had no MRI preoperatively and could not be graded. Twenty-two patients did not fulfil the follow-up criteria and were excluded as well, leaving 72 patients for the evaluation. Included were children and adults, the age ranged from 7 days to 76 years (mean: 28.6 years). The sex distribution was exactly equal. The medium follow-up time was 10.6 months with a range from 1 week (implantation of a VP shunt because 3rd VS failed) to 66 months.

Table **1** Determination of hydrocephalus grade*

Graded parameters		***Points assigned***
Cause of obstruction		
	not directly visible	0
	directly visible	1
Downward bulging of the floor of the 3rd ventricle		
	none	0
	slightly (≤5 mm)	1
	markedly (>5 mm)	2
Course of symptoms of hydrocephalus		
	steady	1
	progressive	2

*Grade: sum of points reached for every parameter.

Table **2** Correlation of hydrocephalus grade with result of 3rd ventriculostomy

Grade/Results	***Successful (n =)***	***Failed (n =)***	***Success Rate***
1	no indication for 3rd VS		
2	no indication for 3rd VS		
3	4	6	40 %
4	11	8	58 %
5	41	2	95 %
Total (n =)	56	16	72

Difference of success rate: $p < 0.001$.

The results of the procedure were analysed by dividing the successful treated patients (clinical improvement and shunt independence) from the failed ones (no clinical improvement or deterioration or shunt dependence).

Statistical analyses were performed using Fisher's exact test.

Results

The hydrocephalus was divided on the basis of presurgical MRI and clinical symptoms by allocating the patients into 5 grades. 72 patients operated with 3rd VS were included for the evaluation of this grading scheme.

There were no 3rd VS performed in grades 1 and 2 where a VP shunt (grade 2) or only observation (grade 1: stable clinical symptoms) was performed. In patients with a grade 3 hydrocephalus ($n = 10$) 3rd VS was successful in 40 %, grade 4 ($n = 19$) in 58 %, and in grade 5 ($n = 43$) in 95 %. This difference was highly significant ($p < 0.001$) (Table **2**).

In grades 1 and 5 the constellation is explicitly determined: grade 1: no downward bulged floor, no detectable obstruction and stable symptoms; grade 5: markedly downward bulged

Table **3** Frequency of different parameter constellations in grades 3 and 4

Grade	Downward bulging of the floor of the 3rd ventricle (points)	Directly visible obstruction (points)	Stable or progressive symptoms (points)	Frequency/No. of patients
3	> 5 mm (2)	no (0)	stable (1)	0
3	≤5 mm (1)	no (0)	progressive (2)	7
3	≤5 mm (1)	yes (1)	stable (1)	1
3	normal (0)	yes (1)	progressive (2)	2
4	> 5 mm (2)	yes (1)	stable (1)	2
4	> 5 mm (2)	no (0)	progressive (2)	15
4	≤5 mm (1)	yes (1)	progressive (2)	2

floor, direct visible obstruction and progressive symptoms. For grades 2 and 4 three different combinations and for grade 3 four different combinations of the parameters exist. For the endoscopic cases (grades 3 and 4) most often a marked downward bulged floor of the 3rd ventricle was present (Table **3**).

Regarding every subscale independently the differences are less pronounced. The downward bulging of the floor of the 3rd ventricle of more than 5 mm shows a success rate of 83 % (n = 50 of 60), up to 5 mm of 50 % (n = 5 of 10) and in normal position of "50 % "(n = 1 of 2) as well.

The directly observed obstruction of the CSF pathway is correlated with a success rate of 80 % (n = 48 of 60), its lack with a success rate of 67 % (n = 8 of 12).

The clinical progression of symptoms was paired with a success rate of 80 % (n = 55 of 79), the lack of progression with one of "33 %" (n = 1 of 3).

A directly visible obstruction (n = 50) was caused by aqueductal stenosis (n = 31), pineal region tumour (n = 8), tumour of the 3rd ventricle (n = 3), posterior fossa tumour (n = 3), outlet obstruction of the 4th ventricle (n = 4), and isolated 4th ventricle (n = 1).

Postoperatively the floor of the 3rd ventricle reverted generally into the normal position as seen in Fig. **5**.

Complications and difficulties

In the 72 3rd VS, 3 fornix lesion occurred but remained clinically uneventful. In three cases the ventricle puncture was not successful with the first attempt. One case of meningitis and one CSF fistula without meningitis were detected. One subdural effusion was seen but resolved spontaneously. One temporary oculomotor nerve palsy occurred in a six-month-old child.

In the remaining 37 3rd VS which did not enter in the evaluation, 3 more clinically uneventful fornix lesions and one meningitis occurred. One procedure had to be abandoned due to a too small foramen of Monro which could not be passed with the endoscope.

Discussion

An indication for 3rd VS is generally seen in obstructive hydrocephalus [1, 4–11]. In addition there are other forms of hydrocephalus where the indication of 3rd VS is discussed [2, 3, 12, 13, 19]. One problem of planning 3rd VS is that it is difficult to predict its clinical effectiveness and whether the hydrocephalus has a malresorptive component as well. Whereas the VP shunt will treat successfully both the obstructive and the malresorptive hydrocephalus, the 3rd VS will fail when there is a substantial malresorptive component.

On the other hand the advantages of 3rd VS with shunt independence, physiological CSF reabsorption, and low costs [5, 6, 10, 15] are such convincing factors that a 3rd VS should be chosen, if the chance of success is high. Nevertheless there are also surgical risks of 3rd VS [17–21] which should not be neglected, and therefore no 3rd VS should be performed when there is no likelihood of it being effective. Considering these factors, strict criteria are required to guide the differential indication for 3rd VS and VP shunt.

The presented grading system has the potential of being a very good help in this dilemma as it reliably predicts the success rate of 3rd VS. It detaches the indication from the controversy (age, Chiari malformations, posthaemorrhagic or postmeningitic aetiology, etc.) and accentuates morphological and clinical features, helping the clinician to choose an individual and adequate therapy: With a success rate of more than 90 % in grade 5 hydrocephalus of course 3rd VS performed by an experienced neuroendoscopist is the therapy of choice. In grade 4 with still

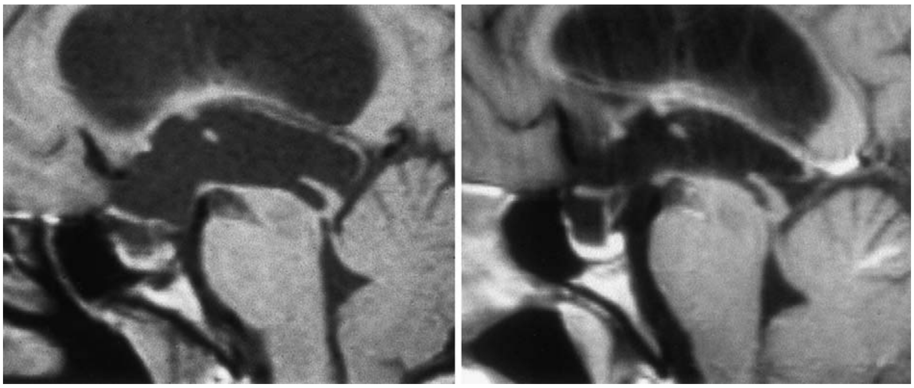

Fig. **5** Pre- and postoperative views of the floor of the 3rd ventricle. The floor was markedly bulged downward (*left*) in a case of aqueductal stenosis and has reverted to its normal position after 3rd VS (*right*).

Table **4** Authors recommendation for differential therapy of hydrocephalus (indication for 3rd VS is seen if the success rate is very high)

Grade	***Success rate of 3rd VS***	***Recommended therapy***
1	not applicable	observation or VP shunt
2	not applicable	VP shunt
3	40 %	VP shunt, exceptionally 3rd VS
4	58 %	3rd VS or VP shunt
5	95 %	3rd VS

almost a 60 % success rate the patient should have at least the 3rd VS offered as a potential treatment. If the success rate goes below the 50 % margin (grade 3 hydrocephalus) a VP shunt should be favoured. Only in cases with a history of a series of repeated shunt complications is one attempt of 3rd VS permissible. In grade 1 and grade 2 hydrocephalus the authors never see an indication for 3rd VS, because MRI gives no hint at all that there is an obstructive hydrocephalus. The authors' recommendations for differential therapy of hydrocephalus are summarised in Table **4** .

The parameters chosen for this grading are based on clinical experience and pathological and mechanical considerations:

– *Symptoms of hydrocephalus*: only patients with symptomatic hydrocephalus are treated. An asymptomatic ventriculomegaly cannot be improved at all by surgery. In slightly symptomatic patients without clinical progression, an arrested hydrocephalus may be suspected and the potential of recovery seems to be low or even absent. Therefore it is valued only with 1 point, whereas a progressive clinical symptomatology has a larger potential of recovery due to the absence of irreparable brain tissue damage.
– *Obstruction visualization*: The direct visualization of the obstruction (e.g., aqueductal stenosis, tectal tumour, brainstem tumour) proves the obstructive form of hydrocephalus. If no obstruction is detected, indirect signs like the downward bulging of the floor of the 3rd ventricle have to be checked for. Because there might be a higher mistake differentiating obstructive and communicating hydrocephalus, direct visualization was valued higher (1 point) than no direct visualization (0 point).
– *Downward bulging of the floor of the 3rd ventricle:* The downward bulging of the floor of the 3rd ventricle towards the interpeduncular/prepontine cistern reflects the pressure difference between the 3rd ventricle and the prepontine cistern, that means the pressure difference between the ventricular system and the subarachnoid space. If the downward bulged floor of the 3rd ventricle is fenestrated pressure equalisation between the prestenotic high pressure compartment and the poststenotic lower pressure compartment is accomplished [2].
  From the mechanical point of view the extent of downward bulging depends on the pressure difference as well as on its duration: A slight downward bulging reflects a low pressure difference or a short duration of a pressure difference. A marked downward bulging might be caused by an high pressure difference or by a long-standing pressure difference. A slight downward bulging (< 5 mm) might be easier misinterpreted therefore it was valued with 1 point, whereas a marked downward bulging was valued with 2 points. If the floor of the 3rd ventricle is normal, no pressure difference is present (valued with 0 points) and a fenestration will be of no use. The authors see generally no indication of 3rd VS if the floor is in a normal position. The grading system reflects this situation very well. As a normal positioned floor may reach maximally grade 3 (2 points for progressive symptoms and 1 point for direct visualization of an obstruction) such a situation would translate into a 40 % chance of success for 3rd VS. Because a normal floor excludes direct visualisation of an obstruction, the grading will only reach grade 2. A directly visible obstruction without a downward bulging floor may be seen extremely rarely, and is explicable through an existing atypical (spontaneous and undetected) 3rd VS at an other site (i.e., lamina terminalis) or through an extremely rigid and fixed floor of the 3rd ventricle (i.e., postsurgical, posthaemorrhagic, postmeningitic) which hinders the downward bulging. In such rare cases, of course, a 3rd VS might be reasonable in spite of the "normal" position of the floor.

The evaluation of success (clinical improvement and shunt independence) and failure (no clinical improvement or deterioration or shunt dependence) is simple. An assessment of the quality of life would be more desirable. However, no homogeneous scale for all age groups exists.

The conventional hydrocephalus classification of communication or non-communication has shortcomings in guiding the differential indication of 3rd VS and VP shunt. Clinical status (progressive or stable disease) is not reflected at all, however, this is an important factor from the clinical point of view. The classification of communicating hydrocephalus (which means communication between the ventricles and the subarachnoid space) does not reflect obstructions inside the subarachnoid space proximal to the side of 3rd VS (the so-called proximal extraventricular intracisternal obstructive hydrocephalus EIOH) which can be treated successfully with 3rd VS as well [2]. Also, the amount of pre-/poststenotic pressure difference is not reflected in the classical classification, it is considered in the grading with the extent of downward bulging of the floor of the 3rd ventricle. From the mechanical point of view a successful 3rd VS is rather expected in high pressure differences. These parameters are integrated in the proposed grading system.

This grading system is simple, easy to learn and easy to apply, even if no simple grading system will accurately classify all varieties of different hydrocephalus cases.

This grading system is designed to be predictive to 3rd VS outcome detached from the conventional criteria. The possibility of grades 1 and 2 opens this grading to all hydrocephalus types and does not restrict it to any subgroup even if it was designed at the beginning only for potential candidates for 3rd VS. This grading system requires for each hydrocephalus patient an MRI instead of a CT scan, but this effort is justified by the advantages in the decision making process in choosing the adequate therapeutic modality.

A prospective application of this grading system is currently underway. If this grading in its simplicity proves to predict the success rate of 3rd VS, it will provide a useful tool for decision making in differential therapy of hydrocephalus whether to perform a 3rd VS or a VP shunt.

Conclusions

The proposed grading system classifies the hydrocephalus by considering the amount of downward bulging of the floor of the 3rd ventricle, the visibility of CSF pathway obstruction and the course of clinical symptoms. A high correlation between the grading and the outcome of 3rd VS is demonstrated. Thus, this grading helps in decision making in the dilemma of how to treat a hydrocephalus: with ventriculoperitoneal shunting or with 3rd VS.

References

1. Cohen AR. Cranial endoscopy illustrative case. Techniques in Neurosurg 1995; 1: 144–147
2. Kehler U, Gliemroth J. Extraventricular intracisternal obstructive hydrocephalus–A hypothesis to explain successful 3rd ventriculostomy in communicating hydrocephalus. Pediatric Neurosurg 2003; 38: 98–101
3. Kestle J, Cochrane D, Alisharan R. The initial treatment of hydrocephalus: an assessment of surgeons' preference between third ventriculostomy and shunt insertion. Neurol Res 2000; 22: 65–68
4. Drake JM. Ventriculostomy for treatment of hydrocephalus. Neurosurg Clin North Am 1993; 4: 657–666
5. Hirsch JF. Percutaneous ventriculocisternostomies in non-communicating hydrocephalus. Monogr Neurol Sci 1982; 8: 170–178
6. Hopf NJ, Grunert P, Fries G, Resch KDM, Perneczky A. Endoscopic third ventriculostomy: outcome analysis of 100 consecutive procedures. Neurosurg 1999; 44: 795–806
7. Jones RFC, Teo C, Stening WA, Kwok BCT. Neuroendoscopic third ventriculostomy. In: Manwaring KH, Crone KR (eds): Neuroendoscopy. Mary Ann Liebert, Inc., Publishers, New York, Vol 1, 1992; 63–77
8. Kelly PJ. Stereotactic third ventriculostomy in patients with nontumoral adolescent/adult onset aqueductal stenosis and symptomatic hydrocephalus. J Neurosurg 1991; 75: 865–873
9. Kunz U, Goldmann A, Bader C, Waldbaur H, Oldenkott P. Endoscopic fenestration of the 3rd ventricular floor in aqueductal stenosis. Minim Invas Neurosurg 1994; 37: 42–47
10. Sainte-Rose C. Third ventriculostomy. In: Manwaring KH, Crone KR (eds): Neuroendoscopy. New York: Mary Ann Liebert, Vol 1, 1992; 47–62
11. Teo C. Third ventriculostomy in the treatment of hydrocephalus: experience with more than 120 cases. In: Hellwig D, Bauer BL (eds): Minimally Invasive Techniques for Neurosurgery. Springer Verlag, Berlin, Heidelberg, Berlin, 1998; 73–76
12. Korinth M, Bertalanffy H, Rhode V, Bassiouni H, Glisbach JM. Reduzierung der Shuntpflichtigkeit durch Eröffnung der Lamina terminalis bei Patienten mit rupturierten intrakraniellen Aneurysmen. Zentralbl Neurochir 1996; 70 (Suppl): (abstract)
13. Meier U, Zeilinger FS, Schonherr B. Endoscopic ventriculostomy versus shunt operation in normal pressure hydrocephalus: diagnostics and indication. Minim Invas Neurosurg 2000; 43: 87–90
14. Tomasllo F, d'Avella D, de Divitiis O. Does lamina terminalis fenestration reduce the incidence of chronic hydrocephalus after subarachnoid hemorrhage? Neurosurgery 1999; 45: 827–831
15. Barlow P, Ching HS. An economic argument in favour of endoscopic third ventriculostomy as a treatment for obstructive hydrocephalus. Minim Invas Neurosurg 1997; 40: 37–38
16. Kehler U, Gliemroth J, Wagner R, Arnold H. 3rd ventriculostomy versus ventriculoperitoneal shunt. An analysis of results, complications, and costs. Zentralbl Neurochir 1996; 84 (Suppl): (abstract)
17. Handler MH, Abbott R, Lee M. A near-fatal complication of endoscopic third ventriculostomy: case report. Neurosurg 1994; 35: 525–527
18. McLaughlin MR, Wahlig JB, Kaufmann AM, Albright AL. Traumatic basilar aneurysm after endoscopic third ventriculostomy: case report. Neurosurgery 1976; 41: 1400–1403
19. Benabarre A, Ibánez J, Boget T, Obiols J, Martinéz-Aran A, Vieta E. Neuropsychological and psychiatric complications in endoscopic third ventriculostomy: a clinical case report. J Neurol Neurosurg Psychiatry 2001; 71: 268–271
20. Schroeder HW, Niendorf WR, Gaab MR. Complications of endoscopic third ventriculostomy. J Neurosurg 2002; 96: 1032–1040
21. Schroeder HW, Warzok RW, Assaf JA, Gaab MR. Fatal subarachnoid hemorrhage after endoscopic third ventriculostomy. Case report. J Neurosurg 1999; 90: 153–155

Endoscopic Removal of Ethmoido-Sphenoidal Foreign Body with Intracranial Extension

L. Presutti
D. Marchioni
M. Trani
A. Ghidini

Abstract

We describe the case of a foreign body lodged into ethmoidal labyrinth and sphenoidal sinus with fracture of the clivus and consequent rhinoliquorrhea removed by an endoscopic technique. We performed a skull base plasty to close the rhino-liquoral fistula with resolution of the rhinoliquorrhea. There were no postoperative complications and there was a good therapeutic result at long-term follow-up.

Key words

Foreign body · rhino-liquoral fistula · sphenoid sinus · skull base plasty

Introduction

According to a literature review foreign body retention into the sphenoidal sinus is a very rare event [1] that is often associated with orbital trauma and intracranial lesions [2–5]. From our review the most frequent foreign bodies are metallic or vegetable ones (arrowhead, pellets, bamboo stick, etc.) [1–19].

The removal of these objects usually requires a surgical endoscopic approach [1, 6, 7, 8, 10, 12] and only in some selected cases an open surgical approach if the foreign body is completely intracranial [2, 5, 7, 17]. The endoscopic approach demands a well-founded anatomy of the spheno-ethmoidal region because of the presence of important and vital structures such as the ICA, the 2nd cranial nerve and the ethmoidal arteries. In this region the foreign body, once it has entered the posterior wall of the sphenoidal sinus, can break into the dura leading also to an important rhinoliquorrhea that needs a skull base plasty that is feasible at the same surgical session.

Case Report

A 47–year-old man, diabetic and hypertensive, while he was using a mowing machine, as consequence of an explosion, suffered a profound wound in the right orbito-nasal region. After an accurate washing, the wound was sutured; an X-ray scan (Fig. **1**) of the head was performed and it showed the presence of radio-opaque material in the ethmoido-sphenoidal region.

So we performed a CT scan of brain and paranasal sinuses (Fig. **2**) that confirmed the presence of the foreign body of probable metallic nature 5-cm long that had fractured the right ethmoidal labyrinth and the intersphenoidal septum, inflicted itself into the posterior wall of the sphenoidal sinus, pierced it and reached the prepontine cistern next to the basilar artery. There was also pneumocephalus.

The patient, clear-headed and co-operative, had rhinoliquorrhea from the left nasal fossa. There were no neurological deficits and, in particular, no visual ones. The traditional and endoscopic ENT examinations showed blood clots in right nasal fossa but no visible foreign body. So we decided to perform an ethmoidectomy with the endoscopic technique.

After sacrifice of the right middle turbinate, using a rigid nasal endoscope with an optic of 0° or 30°, linked with the digital

Affiliation
Department of Otorhinolaryngology, Polyclinic of Modena, Italy

Correspondence
Daniele Marchioni · Clinica Otorinolaringoiatrica · Azienda Policlinico · Via del Pozzo 71 · 41100 Modena · Italy · Tel.: +39/059/422/24 02 · Fax: +39/059/422/42 49 · E-mail: marchionidaniele@yahoo.it

Bibliography
Minim Invas Neurosurg 2006; 49: 244–246 © Georg Thieme Verlag KG · Stuttgart · New York
DOI 10.1055/s-2006-948302
ISSN 0946-7211

Fig. **1** X-ray scan of the paranasal sinuses. The radio-opaque material is the foreign body.

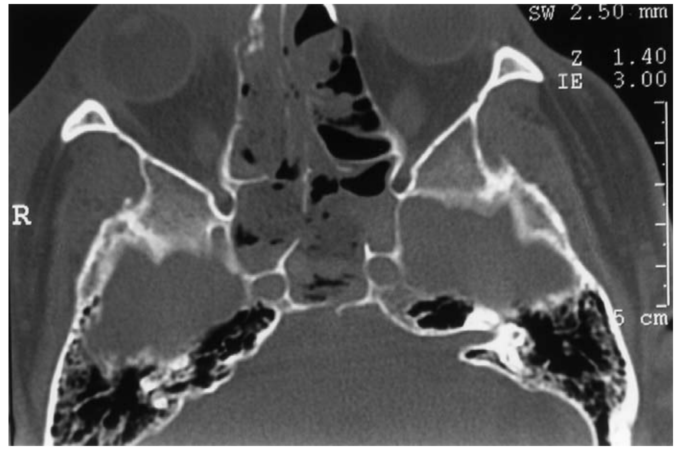

Fig. **3** Post-operative CT scan of the paranasal sinuses. Reduction of the pneumocephalus.

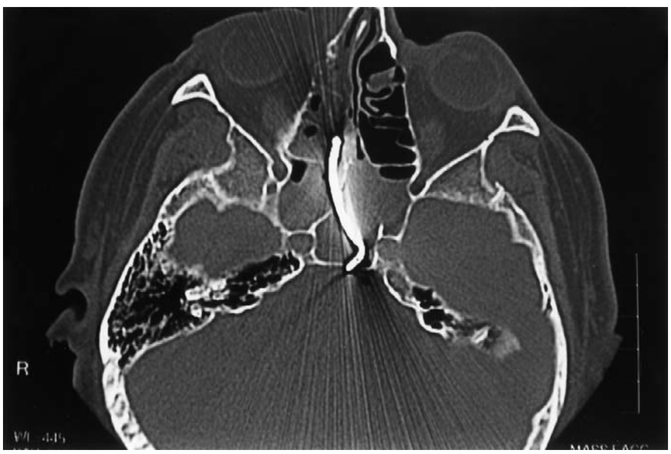

Fig. **2** CT scan of the paranasal sinuses. The foreign body in the sphenoidal sinus has pierced the clivus. The tip of the foreign body is next to the basilar artery.

camera and with a xenon light source of 300 W, we performed a complete ethmoidectomy, anterior and posterior. The foreign body was, as already shown by the CT scan (Fig. **2**), 5 cm long and lodged from the posterior ethmoidal labyrinth into the sphenoidal sinus after having fractured the anterior wall of the sphenoidal sinus and the intersinusal septum reaching the left half of the sinus. And moreover, the tip of the foreign body had pierced the posterior wall of the sinus on the left immediately medial to the ICA. From the bony breach there was an important liquorrhea. After having removed the septal rostrum, the intersinusal septum and the complete, right and left, anterior wall of the sphenoid sinus, with extreme caution, we took out the foreign body, and then demucosized the sphenoidal sinus walls. Then we performed a skull base plasty taking a big mucoperiosteum flap from the left side of the septum closing in this way the bony fracture of the skull base. The sphenoidal sinus then was sealed with tabotamp, spongostan and fibrin glue; the nasal packing was performed with 2 stripes of Lyofoam. The postoperative CT scan of the paranasal sinuses (Fig. **3**) showed the results of surgery and a reduction of the pneumocephalus noted before. There was also a small fracture in the clivus near the basilar artery with a little bony fragment where the foreign body tip had been. The basilar artery was safe and sound. The patient was instructed to remain in bed for 4 days, received antibiotic therapy with Ceftriaxone 2 g *i.v.*/die, lowered to 1 g *i.v.*/die after the removal of the nasal packing.

The nasal packing was removed on the 4th day and a CT scan was performed that showed pneumocephalus resolution and confirmed the presence of the small bony fragment next to the basilar artery. The patient never had fever or meningism signs.

The 3rd day after the removal of nasal packing the patient presented with sporadic rhinorrhea so he was obligated to remain again in bed. The CT scan was similar to the preceding one and nasal endoscopy did not show any sign of sure rhinoliquorrhea. After a forced rest in bed of 4 days the patient was free from rhinoliquorrhea. The endoscopic examination was always negative and, 14 days, after surgery the patient was discharged. The endoscopic follow-up, until 1 year, has shown a good condition of the flap and no signs or symptoms of rhinoliquorrhea.

Discussion

Foreign body retention into the sphenoidal sinus is an extremely rare event; from a literature review the majority of cases is due to metallic bodies that, upon entering the orbital medial canthus, fracture the paranasal sinuses so reaching the sphenoidal sinus. Usually this event is surrounded by sudden intracranial complications such as subarachnoidal and intraparenchymal cerebral hemorrhages; rhinoliquorrhea and pneumocephalus. And, moreover, late severe complications are possible like the meningitis or cerebral abscess. The traditional ENT and endoscopic examinations do not always show the presence of the foreign body; this underlines the importance of CT scans of the brain and paranasal sinuses in the evaluation of the position of a foreign body that can be very near to vital structures like basilar artery and ICA. Only in some selected cases when the foreign body is not radio-opaque, like bamboo sticks, is MRI useful [4, 8].

The patient's symptoms, if there are no early intracranial complications, are often soft, less important; the neurological examination is perfectly normal and the general conditions is good.

The surgical approach for foreign body removal should be evaluated after radiological imaging. In patients with a risk of intracranial hemorrhage (like when the foreign body is in contact with big vessels) should a combined approach, open and endoscopic, be preferred to more easily control the possible hemorrhage. In all other cases with the only endoscopic approach in experienced hands, it is possible to remove the foreign body and resolve the eventual rhinoliquorrhea by performing a skull base plasty.

The post-surgical period contemplates asystemic antibiotic therapy and a forced prolonged bed rest. The nasal packing is removed 4 days after the operation and the post-surgical endoscopic follow-up evaluates the results of the skull base plasty and the rhinoliquorrhea resolution. A early post-operative and a CT scan 7 days after intervention are always performed to evaluate the course of the eventual pneumocephalus that is often associated with this type of lesion.

References

1 Krause HR, Rustemeyer J, Grunert RR. Foreign body in paranasal sinuses. Mund Kiefer Gesichtschir 2002; 6: 40–44

2 Zaets VN, Marchenko LV. Combined penetrating injury of left orbit, ethmoidal labyrinth and sphenoid sinus. Vestn Otorinolaringol 2000; 38

3 Shaparenko BA, Plakhotnik LS. Foreign body of the ethmoidal labyrinth penetrating into the sphenoid sinus. Zh Ushn Nos Gorl Bolezn 1978; 103–104

4 Datta H, Sarkar K, Chatterjee PR, Kundu A. An unusual case of a retained metallic arrowhead in the orbit and sphenoidal sinus. Indian J Ophthalmol 2001; 49: 197–198

5 Mori S, Fujieda S, Tanaka T, Saito H. Numerous transorbital wooden foreign bodies in the sphenoid sinus. ORL J Otorhinolaryngol Relat Spec 1999; 61: 165–168

6 Kitajiri S, Tabuchi K, Hiraumi H. Transnasal bamboo foreign body lodged in the sphenoid sinus. Auris Nasus Larynx 2001; 28: 365–367

7 Kayikcioglu A, Karamusel S, Mavili E, Erk Y, Benli K. Intrasphenoidal migration of a premaxillary Kirschner wire. Cleft Palate Craniofac J 2000; 37: 209–211

8 LaFrentz JR, Mair EA, Casler JD. Craniofacial ballpoint pen injury: endoscopic management. Ann Otol Rhinol Laryngol 2000; 109: 119–122

9 Alsarraf R, Bailet JW. Self-inserted sphenoid sinus foreign bodies. Arch Otolaryngol Head Neck Surg 1998; 124: 1018–1020

10 Bhattacharyya N, Wenokur RK. Endoscopic management of a chronic ethmoid and sphenoid sinus foreign body. Otolaryngol Head Neck Surg 1998; 118: 687–690

11 O'Connell JE, Turner NO, Pahor AL. Air gun pellets in the sinuses. J Laryngol Otol 1995; 109: 1097–1000

12 Mladina R. Endoscopic sinus surgery: a metallic foreign body at the sphenoethmoidal junction. J Laryngol Otol 1992; 106: 998–999

13 Dimitriou C, Karavelis A, Triaridis K, Antoniadis C. Foreign body in the sphenoid sinus. J Craniomaxillofac Surg 1992; 20: 228–229

14 Shaikhov ZSh, Ivanova NB, Ermekbaeva BA. Foreign body in the sphenoidal sinus. Vestn Otorinolaringol 1991; 49–50

15 Grevers G, Reiterer A. Traumatically-induced foreign bodies of the paranasal sinuses. Laryngorhinootologie 1990; 69: 155–157

16 Megele R, Dittmann W, Mandl L. Trans-sphenoid gunshot injury of the head. Anatomic viewpoints. Aktuelle Traumatol 1990; 20: 44–47

17 Khil'ko VA, Revskoi luK, Kiselev AS. Removal of a foreign body from the sphenoid sinus and the clivus. Zh Vopr Neirokhir Im N N Burdenko 1986; 52–53

18 Starokha AV. Foreign body in the ethmoid labyrinth, sphenoid sinus and orbit. Vestn Otorinolaringol 1985; 72–73

19 Ogale SB, Wagh SP, Karnik PP. Air gun pellet in the sphenoid sinus. (A case report). J Postgrad Med 1983; 29: 45

D. Boscherini[1]
M. Pintucci[1]
L. Mazzucchelli[2]
R. Renella[1]
G. Pesce[3]

Neuroendoscopic Management of a Solitary Pineal Region Tumor. Case Report of an Adenocarcinoma Metastasis

Abstract

The present case describes a two-step endoscopic management of hydrocephalus and diagnosis of a single pineal region metastasis arising from a gastric adenocarcinoma. A 62-year-old man presenting with signs of subacute obstructive hydrocephalus from a pineal region mass had at first been treated with an endoscopic third ventriculostomy. As cerebrospinal fluid tumor markers (alpha-fetoprotein, beta-human chorionic gonadotropin) were negative, an endoscopic biopsy of the pineal region tumor was performed through a more anterior frontal burr hole. Pathology showed an adenocarcinoma and primary tumor work-up revealed an unsuspected gastric tumor, the pathology of which matched with the intracranial metastasis. The present report emphasizes the role of neuroendoscopy in pineal region tumors and reports a rare case of a solitary gastric adenocarcinoma metastasis in this location.

Key words

Minimally invasive · neuroendoscopy · pineal region · metastasis

Introduction

The diversity of tumor types present in the pineal gland region and their potential curability have prompted surgeons to maximize the surgical technique in order to obtain, as a main objective, the most accurate pathological diagnosis [1, 2]. Also, the detection of the tumor markers alpha-fetoprotein (αFP), beta-human chorionic gonadotropin (βHCG) has become an essential aid to diagnosis and management by avoiding, if high levels in cerebrospinal fluid (CSF) are detected, tissue sampling that might be unnecessary [3]. Neuroendoscopic surgery presents clear advantages in dealing with tissue sampling, gross morphological analysis of tumor and treating obstructive hydrocephalus.

38 cases of solitary pineal masses as the only sites of intracranial metastases have been reported in the literature [4–6]. Although rare, single metastasis to the pineal region, mimicking a primary pineal region lesion on imaging studies, is a diagnosis one might also consider upon encountering a pineal region mass in the elderly. Here we describe our algorithm that led to hydrocephalus treatment, accurate diagnosis and consequent targeted oncological treatment.

Case Report

A 62-year-old man with a medical history of hepatic disease, but no known tumor disease was admitted to our institution with a 3-months progressive deterioration of cognitive functions, gait disturbance and urinary incontinence. A few days before admission, the patient could not walk anymore, was unresponsive and presented episodes of vomiting. A head CT scan was performed before admission and showed a triventricular hydrocephalus with a pineal region lesion, he was consequently referred to our department for the management of the case. At admission

Affiliation
[1]Servizio Cantonale di Neurochirurgia, Ospedale Regionale Lugano, Lugano, Switzerland
[2]Servizio Cantonale di Patologia, Locarno, Switzerland
[3]Istituto Oncologico della Svizzera Italiana, Bellinzona, Switzerland

Correspondence
Dr. med. Duccio Boscherini · c/o Servizio Cantonale di Neurochirurgia · Ospedale Regionale Lugano · Via Tesserete 46 · 6900 Lugano · Switzerland · Tel.: +41/91/811/64 55 · Fax: +41/91/811/64 64 · E-mail: duccio.boscherini@eoc.ch

Bibliography
Minim Invas Neurosurg 2006; 49: 247–250 © Georg Thieme Verlag KG · Stuttgart · New York
DOI 10.1055/s-2006-948301
ISSN 0946-7211

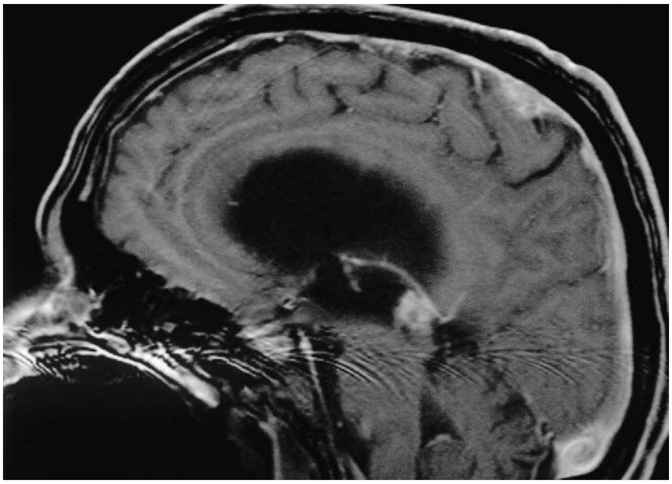

Fig. 1 Pre-operative T_1-weighted gadolinium-enhanced sagittal MRI of the lesion.

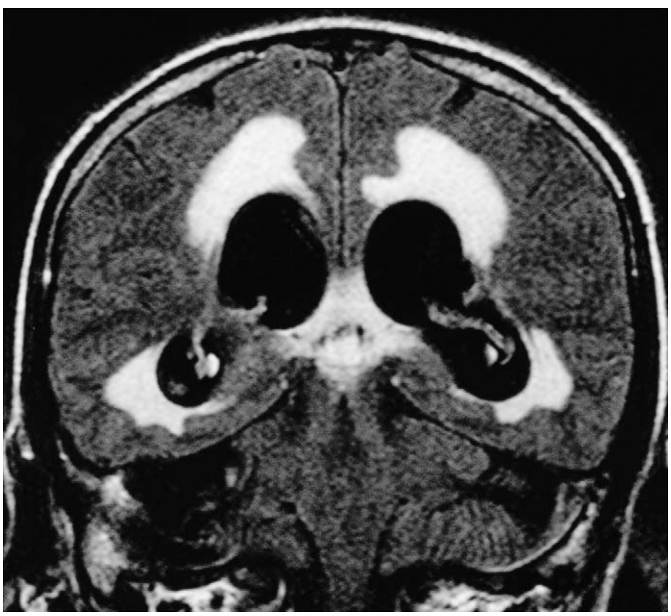

Fig. 2 Pre-operative FLAIR coronal MRI of the lesion.

Fig. 3 Post-operative endoscopic biopsy CT scan. Note the presence of a small quantity of blood in the occipital horns and the ventricular size reduction.

neurological examination showed an MMSE equal to 12/30, bilateral Babinski sign, bilateral clonus and spastic tetraparesis. Standard blood work-up was normal. Standard chest X-rays did not demonstrate any abnormality. Cerebral MRI with a CSF study showed a triventricular obstructive hydrocephalus with signs of transependymal reabsorbtion (see Figs. **1**–**3**) and a pineal gland lesion measuring 12 mm with heterogeneous contrast enhancement. We decided to perform a third ventriculostomy with a tumor markers study. Our preoperative diagnosis was oriented towards a pineal primitive tumor. Ventriculostomy through a precoronal right burr hole was uneventful. CSF was taken once the ventricle was penetrated and sent to the laboratory for a complete study. The lesion was visualized endoscopically and looked like being very vascularized. At 48 hours, patient presented a neurological improvement with a normal consciousness status, disoriented for time and space, but gait was unstable.

Tumor marker tests resulted to be negative for αFP and βHCG, CSF cytology was also negative. It was considered at this stage that a histological diagnosis would be mandatory to treat the patient optimally. Our surgical choice was oriented towards an endoscopic biopsy. This second procedure was performed 8 days later. A more frontal burr hole in the axis of the pineal region tumor was performed. As expected the tumor was hemorrhagic but irrigation and focal bipolar coagulation controlled the bleeding. The ventriculostomy was permeable. The tissue samples were considered to be representative and an external ventricular drainage was left in place at the end of the procedure. The postoperative course was marked by neurological stability.

The external ventricular drainage was removed at the second day after a CT scan showed no complications. A small quantity of blood appeared to lie in the occipital horns and third ventricle. Ventricular sizes were reduced compared to preoperative status. Histopathological analysis demonstrated a single atypical gland structure, consistent with metastatic adenocarcinoma (Figs. **4A** and **B**).

The search for a primary tumor revealed a gastric adenocarcinoma of the intestinal type (Fig. **4C**) that matched morphologically with the pineal region tumor. Consequently, patient was taken over by oncologist colleagues in order to start with a conventional whole brain radiotherapy and an adapted chemotherapy regimen.

Discussion

The majority of patients with pineal region tumors present with obstructive hydrocephalus of the aqueduct of Sylvius. The optimal surgical strategy for treating hydrocephalus in these pa-

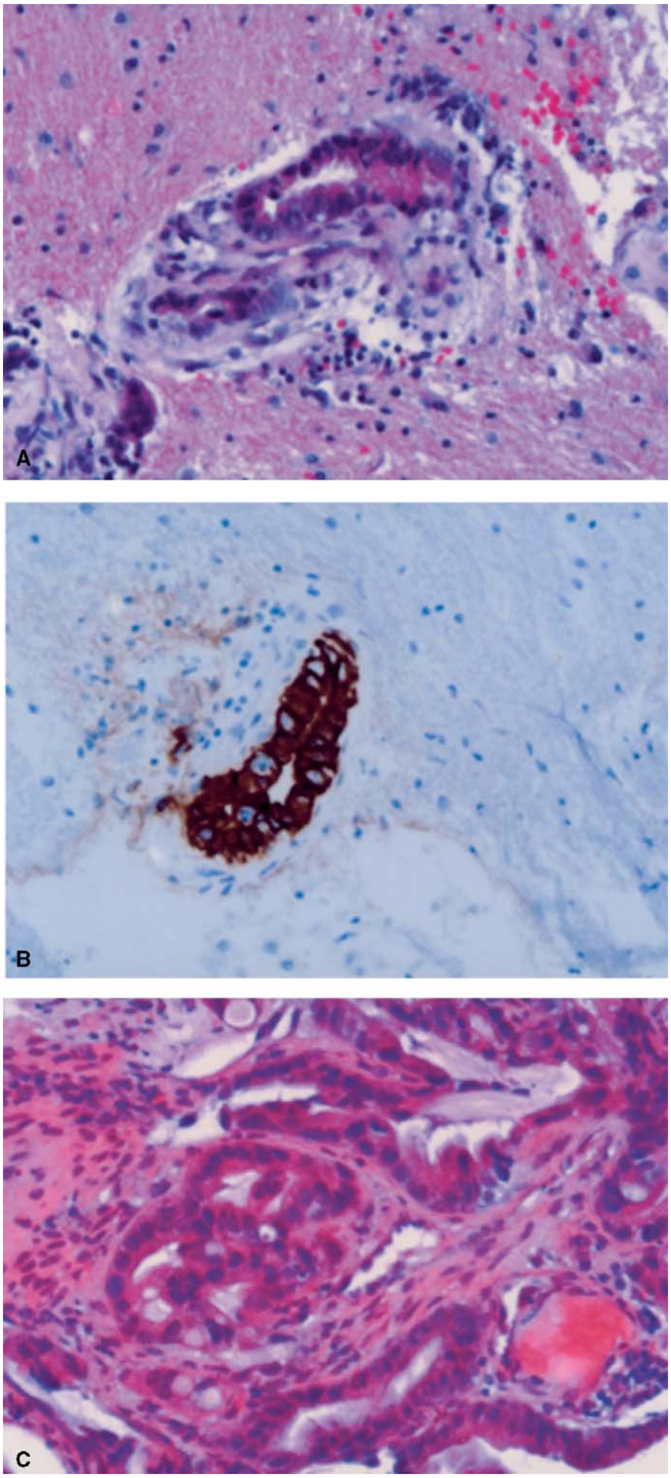

Fig. **4** Pineal biopsy showing a single atypical glandular structure (**A**). Strong pancytokeratin expression detected by immunohistochemical studies confirms the epithelial nature of the neoplasm (**B**). Gastric biopsy detected an adenocarcinoma of intestinal type with matching histopathological features (**C**).

tients involves endoscopic third ventriculostomy [7,8]. This procedure is safe, highly effective and is preferred over ventriculo-peritoneal shunting. The endoscopic procedure also allows CSF sampling precisely, before the endoscope is introduced in the frontal horn, by aspirating with a Cushing trocar a sufficient volume to obtain a complete cytological, chemical and bacteriological study. Measurements of germ cell markers, βHCG and αFP, in the CSF and serum are essential in all patients. The presence of one or both markers is pathognomonic for a malignant germ cell tumor. When markers are elevated, a tissue diagnosis might not be necessary and patients can be treated with radiation and chemotherapy. The first step of the surgical procedure in our case had two purposes: to treat the hydrocephalus and to secure a CSF sample in order to study tumor markers. As αFP and βHCG were negative the next step would be to obtain histology of the lesion. The primary objective of surgical management of pineal region tumors is the establishment of an accurate histological diagnosis. There are more than 17 different pathological tumor types in the pineal region [9] and therapeutic approach differs for each [10].

Given the variety of tumors, diagnostic accuracy is also essential for making enlightened management decisions. Neuroendoscopic procedures have clear advantages in dealing with tissue sampling of intraventricular lesions, in particular third ventricle tumors. We know that many pineal region tumors are highly vascular and obtaining satisfactory hemostasis along the tumor's ventricular surface can be hard endoscopically, although mastering the technique will allow for safe treatment of hydrocephalus with ventriculostomy and will be effective for obtaining pathological samples with the biopsy endoscopic forceps.

As previously described by Oi et al., endoscopic biopsy to the pineal region implies a low anterior frontal burr hole [11]. When this anterior approach is used the only structure that interferes with the procedure is the mass intermedia or the interthalamica adhesion and the lesion is directly visualized, anteriorly facilitating biopsy and bleeding control of the tumor.

The endoscopic procedure in this case has been preferred to stereotactic biopsy; the latter being potentially hazardous because of possible bleeding from multiple sources, including the deep venous system, choroidal vessels, and the multiple pial surfaces that must be traversed during biopsy [12,13]. The increased vascularity of many malignant pineal region tumors is an added factor.

Metastasis to the pineal region is a rare manifestation of malignancy. A literature search showed 64 such cases and among them 30 were solitary pineal mass with variable sizes [14–18]. In 18 reported cases, metastasis was found at autopsy [4]. More recently, however, pineal region metastasis have been detected on MRI. Lung carcinoma, in general small cell carcinoma, is the most frequent primary lesion [19]. Carcinomas in other organs, such as breast [20], stomach [21], esophagus, rectum and kidney [22] have been reported as primaries. Occasionally plasma cell leukemia [23], melanoma [24] and melanocytoma [25] constituted a solitary tumor mass in the pineal region. The present patient had a metastatic adenocarcinoma, and subsequently a primary gastric adenocarcinoma was histologically proven.

It is well known that germ cell tumors of the pineal gland can undergo malignant transformation into enteric-type adenocarcinoma. In such cases, glandular epithelium of enteric character may retain αFP expression. No doubt is left in the present case as to the gastric metastatic origin, considering the matching of both pineal and gastric histopathological features. If a mass is detected in the pineal region, various histological types of primary tumor arising from the pineal body should be considered. It is known that non-germinatous tumors of the pineal gland can undergo a malignant transformation into enteric-type adenocarcinoma. In such transformed regions, glandular epithelium of enteric character may express αFP. In the present case no germ-cell tumor elements or no alpha-fetoprotein-positive cells were found in the endoscopic biopsy sample obtained. No doubt is left in our case as to gastric primary origin, considering the matching of both pineal and gastric pathology results.

Conclusion

Although rare, solitary metastasis to the pineal gland is one of the possible diagnoses when dealing with a mass in this region. Solitary gastric tumor metastasis to the pineal gland is an exceptional finding. However, because of the variety of lesions and tumor pathologies arising in this region, histological diagnosis appears to be mandatory when tumor markers are negative. The unexpected pathology that emerged in our case clearly demonstrates the importance of biopsy in diagnostic management. Neuroendoscopy has proven its safety and efficacy in dealing with obstructive hydrocephalus and diagnostic biopsy of pineal region tumors.

References

1 Bruce JN. Management of pineal region tumors. Neurosurg Quart 1983; 3: 103–119

2 Stein BM, Bruce JN. Surgical management of pineal region tumors – honoured guest lecture. Clin Neurosurg 1992; 39: 509–532

3 Choi JU, Kim DS, Chung SS, Kim TS. Treatment of germ cell tumors in the pineal region. Childs Nerv Syst 1998; 14: 1–2 and 41–48

4 Kashiwagi S, Hatano M, Yokoyama T. Metastatic small cell carcinoma to the pineal body. Case report. Neurosurgery 1989; 25: 810–813

5 Brasseur P, Sukkarieh F, Dupont H, Brohee D. Pineal body metastasis. J Belge Radiol 1994; 77: 162–163

6 Bruner JM, Tien RD. Secondary tumors. In: Bigner DD, Mc Lendon RE, Bruner JM (eds). Russell and Rubinstein's Pathology of Tumors of the Nervous System Vol. 2. London, Arnold, 1998; 419–450

7 Cohen AR. Endoscopic ventricular surgery. Pediatric Neurosurg 1993; 19: 127–134

8 Bauer BL, Hellwig D. Minimally invasive endoscopic neurosurgery – a survey. Acta Neurochir Suppl 1994; 61: 1–12

9 Edwards MSB, Hudgins RJ, Wilson CB et al. Pineal region tumors in children. J Neurosurg 1988; 68: 689–697

10 Oi S, Matsuzawa K, Choi JU et al. Identical characteristics of the patient populations with pineal region tumors in Japan and in Korea and therapeutic modalities. Childs Nerv Syst 1998; 14: 36–40

11 Oi S, Shibata M, Tominaga J et al. Efficacy of neuroendoscopic procedures in minimally invasive preferential management of pineal region tumors: a prospective study. J Neurosurg 2000; 93: 245–253

12 Regis J, Bouillot P, Rouby-Volot F et al. Pineal region tumors and the role of stereotactic biopsy: review of the mortality, morbidity, and diagnostic rates in 370 cases. Neurosurgery 1996; 39: 907–912, discussion 912–914

13 Favre J, Taha JM, Burchiel KJ. An analysis of the respective risks of hematoma formation in 361 consecutive morphological and functional stereotactic procedures. Neurosurgery 2002; 50: 48–56, discussion 57

14 Keyaki A, Makita Y, Nabeshima S et al. Pineal metastatic tumor from lung cancer initially caused by neurological abnormalities of pineal body tumor. No Shinkei Geka 1989; 17: 495–499

15 Ramina R, Coelho Neto M, Mariushi WM et al. Pineal metastasis as first clinical manifestation of colorectal adenocarcinoma. Case report. Arq Neuropsiquiatr 1999; 57: 92–95

16 Schuster JM, Rostomily RC, Hahn C et al. Two cases of esophageal carcinoma metastatic to the pineal region with a review of the literature. Surg Neurol 1998; 49: 100–103

17 Vaquero J, Martinez R, Magallon R, Ramiro J et al. Intracranial metastases to the pineal region. Report of three cases. J Neurosurg Sci 1991; 35: 55–57

18 Weber P, Shepard KV, Vijayakumar S. Metastases to pineal gland. Cancer 1989; 63: 164–165

19 Halpert B, Erickson EE, Fields WS. Intracranial involvement form carcinoma of the lung. AMA Arch Pathol 1960; 69: 93–103

20 Ortega P, Malamud N, Shinkin M. Metastasis to the pineal body. Arch Pathol 1951; 52: 518–528

21 Kakita A, Kobayashi K, Aoki N, Eguchi I, Morita T, Takahashi H. Lung carcinoma metastasis presenting as a pineal region tumor. Neuropathology 2003; 23: 57–60

22 Lauro S, Trasatti L, Capalbo C, Mingazzini PL, Vecchione A, Bosman C. Unique pineal gland metastasis of clear cell renal carcinoma: case report and review of the literature. Anticancer Res 2002; 22: 3077–3079

23 Umahara T, Kikawada M, Arai H, lwamoto T, Takasaki M, Hirabayashi Y, Kudo M, Tsuchiya K, Shimada H. An autopsy case of multiple myeloma with pineal body and spinal cord dura mater infiltration. No To Shinkei 1997; 49: 655–658

24 Enriquez R, Egbert B, Bullock J. Primary malignant melanoma of central nervous system. Pineal involvement in a patient with nevus of ota and multiple pigmented skin nevi. Arch Pathol 1973; 95: 392–395

25 Czirjak S, Vitanovic D, Slowik F, Magyar A. Primary meningeal melanocytoma of the pineal region. Case report. J Neurosurg 2000; 92: 461–465

M. Izawa
M. Chernov
M. Hayashi
Y. Kubota
H. Kasuya
T. Hori

Fatal Intratumoral Hemorrhage Immediately after Gamma Knife Radiosurgery for Brain Metastases: Case Report

Abstract

Radiosurgical treatment of brain tumors is sometimes considered to be free from significant acute complications or adverse effects. A rare case of fatal intratumoral hemorrhage immediately after gamma knife radiosurgery (GKR) for brain metastasis is reported. A 46-year-old woman with lung cancer complicated by systemic dissemination experienced an acute episode of headache, speech disturbances, and right-side hemiparesis. She had no history of arterial hypertension or coagulation disorders. CT and MRI disclosed multiple brain metastases. The largest tumor, which was located in the left frontal lobe and caused a significant mass effect, was removed microsurgically without any complications. GKR for nine residual metastases was done on the fourth postoperative day. The marginal dose, which corresponded to the 50 % prescription isodose line, constituted 20 Gy. No complications were noticed during frame fixation, treatment itself, or frame removal. Fifteen minutes after the end of the GKR session the patient acutely fell into a deep coma. Urgent CT disclosed a massive hemorrhage in the left cerebellar hemisphere in the vicinity of the radiosurgically treated lesion. The patient died 4 days later and autopsy confirmed the presence of intratumoral hemorrhage. In conclusion, GKR for metastatic brain tumors should not be considered as a risk-free procedure and, while extremely rare, even fatal complications can occur after treatment.

Key words

Gamma knife radiosurgery · brain metastases · complication · intratumoral hemorrhage

Introduction

Radiosurgery, particularly gamma knife radiosurgery (GKR), is a highly effective management option for both single and multiple metastatic brain tumors. Acute adverse reactions after treatment are not uncommon, but are usually transient and generally are well controlled by medication [1–6]. Hemorrhage into intracranial tumor after radiosurgery is extremely rare, but can potentially lead to catastrophic consequences due to acute compression of the eloquent brain structures [7, 8]. Herein we report a case of fatal hemorrhage in the brain metastasis, which occurred immediately after GKR.

Case Report

A 46-year-old woman was admitted for the management of multiple brain metastases from the histologically verified lung adenocarcinoma. Previous treatment included systemic chemotherapy, radiotherapy of the primary tumor, and whole brain radiation therapy. Neurological examination at admission revealed symptoms of intracranial hypertension, papilloedema, moderate right-sided hemiparesis, and dysphasia. The Karnofsky performance scale [9] score was 60, the SIR [10] score was 3, and RPA [11] class III was defined. Ten intracranial tumors were identified radiologically. The largest one, which was located in the left frontal lobe and caused a significant mass effect, was removed surgically (Fig. **1**). Histological examination revealed a poorly differentiated tubular adenocarcinoma. The early post-

Affiliation
Department of Neurosurgery, Neurological Institute, Tokyo Women's Medical University, Tokyo, Japan

History
This case report was presented as a poster during 7th International Stereotactic Radiosurgery Society Congress, September 11–15, 2005, Brussels, Belgium

Correspondence
Masahiro Izawa, M.D. · Department of Neurosurgery · Neurological Institute · Tokyo Women's Medical University · 8-1 Kawada-cho · Shinjuku-ku · Tokyo 162-8666 · Japan · Tel.: + 81/3/33 53 81 11/26 21 6 · Fax: + 81/3/52 69 74 38 · E-mail: mizawa@nij.twmu.ac.jp

Bibliography
Minim Invas Neurosurg 2006; 49: 251–254 © Georg Thieme Verlag KG · Stuttgart · New York
DOI 10.1055/s-2006-950381
ISSN 0946-7211

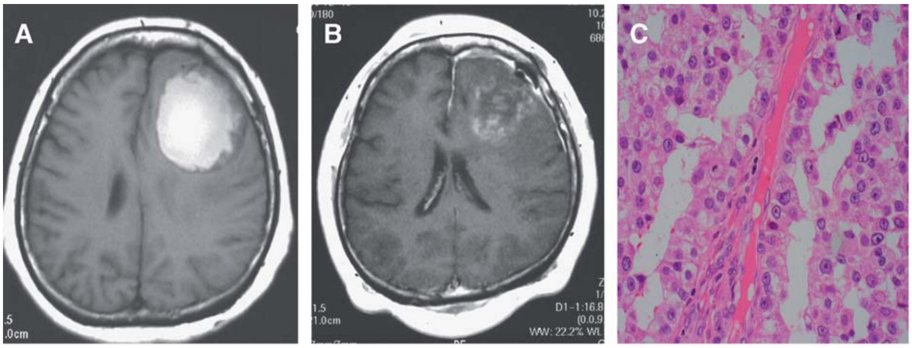

Fig. **1** The largest metastatic brain tumor, which was located in the left frontal lobe (**A**), underwent surgical resection (**B**), and histological examination confirmed the diagnosis of adenocarcinoma (**C**; H&E, ×200).

Table **1** Parameters of radiosurgical treatment of metastatic brain tumor located in the left cerebellar hemisphere which exhibited hemorrhage thereafter

Treatment characteristics	***Parameters***
Number of isocenters	One
Collimator size	14 mm
Maximal dose	40 Gy
Marginal dose	20 Gy
Prescription isodose line	50 %
Energy, delivered to tumor	85.7 mJ
Unit energy, delivered to tumor	31.7 mJ/mL
Conformity index	0.91
Selectivity index	0.78

operative course was uneventful. A significant regression of the neurological symptoms was marked.

GKR for residual intracranial tumors was done on the fourth postoperative day utilizing the Leksell Gamma Knife model C (Elekta Instruments AB, Stockholm, Sweden). Because the patient had received steroid therapy during several weeks before radiosurgery no additional dose of dexamethasone was administered on the day of treatment. After non-complicated frame fixation, which was done under local anesthesia, contrast-enhanced CT and T_1-weighted post-gadolinium MR images were obtained and transferred into the Leksell GammaPlan (Elekta Instruments AB, Stockholm, Sweden) for treatment planning and radiation dosimetry. All brain tumors were treated in a single session with a marginal dose of 20 Gy at the 50 % prescription isodose line (Fig. **2**). The total energy delivered to the skull amounted to 5.4 J. The total treatment time was 131.2 min. The radiosurgical parameters that were used for management of the metastasis in the left cerebellar hemisphere are presented in the Table **1** . Its volume was 2.7 mL and moderate peritumoral edema was presented. No complications were marked during frame fixation, pre-treatment neuroradiological investigation, the treatment session itself, and frame removal. Constant monitoring of the blood pressure during all stages of the procedure did not reveal any abnormalities.

Fifteen minutes after the end of treatment session, at the time of transportation to the ward, the patient acutely fell into deep coma, which was accompanied by cardiac arrest. Resuscitation was started immediately and led to recovery of the cardiac rhythm. An urgent CT disclosed a massive hemorrhage in the vicinity of the radiosurgically treated tumor of the left cerebellar hemisphere (Fig. **3**). The patient's family rejected surgical treatment. Intensive therapy was not effective and the patient died 4 days later. The autopsy confirmed massive intra- and peritumoral hemorrhage in the left cerebellar hemisphere.

Discussion

Early side effects after radiosurgery of intracranial lesions are encountered with an incidence of 24 – 67 %, and in 13 – 18 % of cases occur within 24 hours after treatment [1, 3, 5, 6]. These usually corresponded to swelling of the neoplasm and/or peritumoral brain, or to the irradiation of the specific structures, such as area postrema [1, 2, 5, 12]. Risk factors for clinically significant acute adverse reactions include large size of the lesion, its location in a critical brain area, prominent peritumoral edema, intracranial hypertension, and high irradiation dose [2, 3, 5, 6]. Nevertheless, the symptoms are usually mild-to-moderate and at the time of deterioration only few patients need readmission to hospital [3–6]. Periprocedural administration of dexamethasone (16 mg/day for 2 days) is considered as an effective prophylactic measure [1, 2]. At the same time a prolonged use of steroids, which was the case in our patient, probably does not have a protective effect against early adverse irradiation effects [3].

Spontaneous hemorrhage in brain tumors is encountered with an incidence of 5 %, and can be provoked by ventricular drainage, ventriculoperitoneal shunting, cerebral angiography, and head injury [7]. Intratumoral hemorrhage after radiosurgery of brain tumors is extremely rare. To the best of our knowledge only 2 such cases were reported previously. Motozaki et al. [13] described peritumoral hemorrhage 6 weeks after non-complicated radiosurgical management of the solitary metastasis of the breast adenocarcinoma in the basal ganglia. Uchino et al. [14] reported peritumoral hemorrhage 2 hours after LINAC-based radiosurgery for multiple brain metastases of the breast cancer. The authors of both case reports hypothesized that the complication resulted from the breakdown of the fragile vessels of the tumor or surrounding brain.

The cause of the complication in the present case is not clear. Both acute necrosis of the vessel wall and acute thrombosis of the vessel with subsequent local ischemia could result in hemorrhage. Apoptosis of the endothelial cells, decrease of endothelin production, increase of thromboxan, prostacyclin, and prostaglandin synthesis can occur within few hours after irradiation of

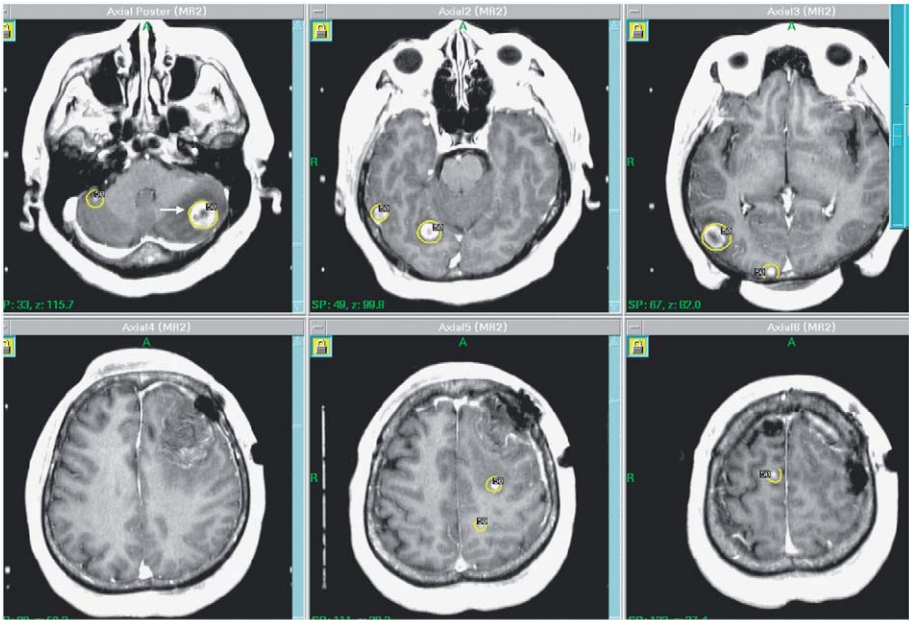

Fig. **2** Treatment plan for multiple brain metastases of the lung adenocarcinoma: nine tumors, including those which were located in the left cerebellar hemisphere (arrow) were treated using 20 Gy marginal dose at 50 % prescription isodose line (yellow circles).

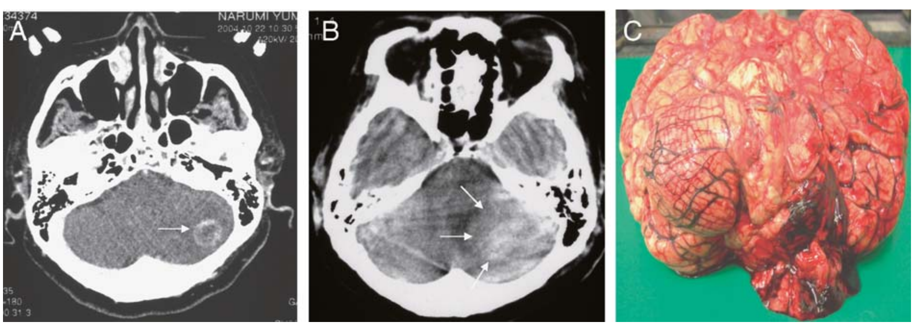

Fig. **3** Radiosurgical treatment was complicated by hemorrhage in the tumor of the left cerebellar hemisphere (**A**), which was confirmed radiologically (**B**) and, later, by autopsy (**C**).

the brain tissue and may lead to the dilatation of the vessels and local reduction of the cerebral blood flow [15]. Impairment of tissue perfusion can be facilitated by the peritumoral brain edema. The latter was present in our patient before treatment and could have been further augmented by GKR. Wolff et al. [16] showed that acute radiation-induced swelling of the cerebellum could be significant enough to cause obstruction of the CSF circulation and necessitate urgent shunt surgery.

Possible risk factors for hemorrhage in intracranial tumor include coagulopathy, arterial hypertension, and the specific histology of the neoplasm [7, 8, 17]. Our patient underwent GKR soon after microsurgical excision of another intracranial metastasis, therefore the possibility of local or systemic disturbances of coagulation could not be excluded. It is known that malignant brain tumors by themselves can cause a local increase of fibrinolytic activity, which can facilitate bleeding [17]. On the other hand, fluctuations of blood pressure seemingly did not play a role in the present case, because continuous monitoring of the blood pressure did not reveal any abnormalities. While metastatic brain tumors of a specific histology (choriocarcinoma, melanoma) have a high propensity for spontaneous hemorrhage, this is not the case in adenocarcinoma, which was present here. Finally, it could not be excluded that the spontaneous hemorrhage into brain metastasis in our patient occurred at the time of GKR just by coincidence.

In conclusion, hemorrhagic complications after radiosurgery for metastatic brain tumors are rare, but can lead to catastrophic events as is shown in the present case. Monitoring of blood pressure during all stages of the procedure and control of the coagulation status may be important for the reduction of their risk, especially in cases of neoplasms with a high propensity for intratumoral bleeding. The possibility of acute complications and their consequences have to be discussed with a patient and his or her relatives before radiosurgical treatment.

References

1 Loeffler JS, Siddon RL, Wen PY, Nedzi LA, Alexander E III. Stereotactic radiosurgery of the brain using a standard linear accelerator: a study of early and late effects. Radiother Oncol 1990; 17: 311–321

2 Plowman PN. Stereotactic radiosurgery VIII. The classification of postirradiation reactions. Br J Neurosurg 1999; 13: 256–264

3 Werner-Wasik M, Rudoler S, Preston PE, Hauck WW, Downes BM, Leeper D, Andrews D, Corn BW, Curran WJ. Immediate side effects of stereotactic radiotherapy and radiosurgery. Int J Radiat Oncol Biol Phys 1999; 43: 299–304

4 Dhanachai M, Theerapancharoen V, Laothamatas J, Pongpech S, Kraiphibul P, Chanwitayanuchit T, Pochanugool L, Dangprasert S, Sarnvivad P, Sinpornchai V, Kuonsongtum V, Pirabul R, Yongvithisatid P. Early neurological complications after stereotactic radiosurgery/radiotherapy. J Med Assoc Thai 2001; 84: 1729–1737

5 Majhail NS, Chander S, Mehta VS, Julka PK, Ganesh T, Rath GK. Factors influencing early complications following gamma knife radiosurgery: a prospective study. Stereotact Funct Neurosurg 2001; 76: 36–46

[6] George EJ, Kudhail J, Perks J, Plowman PN. Acute symptoms after gamma knife radiosurgery. J Neurosurg 2002; 97 (Suppl 5): 631–634

[7] Wakai S, Yamakawa K, Manaka S, Takakura K. Spontaneous intracranial hemorrhage caused by brain tumor: its incidence and clinical significance. Neurosurgery 1982; 10: 437–444

[8] Kalfas IH, Little JR. Postoperative hemorrhage: a survey of 4992 intracranial procedures. Neurosurgery 1988; 23: 343–347

[9] Karnofsky DA, Burchenal JH. The clinical evaluation of chemotherapeutic agents in cancer. In: MacLeod CM (ed): Evaluation of chemotherapeutic agents. Columbia University Press, New York, 1949, pp 191–205

[10] Weltman E, Salvajoli JV, Brandt RA, Hanriot R, Prisco FE, Cruz JC, Borges S, Wajsbrot DB. Radiosurgery for brain metastases: a score index for predicting prognosis. Int J Radiat Oncol Biol Phys 2000; 46: 1155–1161

[11] Gaspar L, Scott C, Rotman M, Asbell S, Phillips T, Wasserman T, McKenna WG, Byhardt R. Recursive partitioning analysis (RPA) of prognostic factors in three radiation therapy oncology group (RTOG) brain metastases trials. Int J Radiat Oncol Biol Phys 1997; 37: 745–751

[12] Tago M, Terahara A, Nakagawa K, Aoki Y, Ohtomo K, Shin M, Kurita H. Immediate neurological deterioration after gamma knife radiosurgery for acoustic neuroma: case report. J Neurosurg 2000; 93 (Suppl. 3): 78–81

[13] Motozaki T, Ban S, Yamamoto T, Hamasaki M. Peritumoral hemorrhage after radiosurgery for metastatic brain tumor: a case report. No Shinkei Geka 1994; 22: 789–793 (in Japanese)

[14] Uchino M, Kitajima S, Miyazaki C, Otsuka T, Seiki Y, Shibata I. Peritumoral hemorrhage immediately after radiosurgery for metastatic brain tumor. No Shinkei Geka 2003; 31: 911–916 (in Japanese)

[15] Nieder C, Andratschke N, Price RE, Rivera B, Ang KK. Innovative prevention strategies for radiation necrosis of the Central Nervous System. Anticancer Res 2002; 22: 1017–1024

[16] Wolff R, Karlsson B, Dettmann E, Bottcher HD, Seifert V. Pertreatment radiation induced oedema causing acute hydrocephalus after radiosurgery for multiple cerebellar metastases. Acta Neurochir (Wien) 2003; 145: 691–696

[17] Oka K, Tsuda H, Sakamoto S, Go Y, Tomonaga M. Plasminogen activator and hemorrhage in brain tumors. J Neuro-Oncol 1994; 22: 183–187